ÇUKUROVA UNIVERSITY
INSTITUTE OF NATURAL AND APPLIED SCIENCES

PhD THESIS

Zehan KESİLMİŞ

AN ARTIFICIAL NEURAL NETWORK CONTROLLED MICROELECTROMECHANICAL ACCELEROMETER

DEPARTMENT OF ELECTRICAL AND ELECTRONICS ENGINEERING

ADANA, 2011

ÇUKUROVA UNIVERSITY
INSTITUTE OF NATURAL AND APPLIED SCIENCES

AN ARTIFICIAL NEURAL NETWORK CONTROLLED MICROELECTROMECHANICAL ACCELEROMETER

Zehan KESİLMİŞ

PhD THESIS

DEPARTMENT OF ELECTRICAL AND ELECTRONICS ENGINEERING

We certified that the thesis titled above was reviewed and approved for the award of degree of Doctor of Philosophy by the board of jury on 07/07/2011.

…….....	……..	…….....
Asst. Prof. Dr. Murat AKSOY	Prof. Dr. Mehmet TÜMAY	Assoc. Prof. Dr. Ulus ÇEVİK
SUPERVISOR	MEMBER	MEMBER
…….....	……..……..	
Asst. Prof. Dr. Emin ÜNAL	Asst. Prof. Dr. Mutlu AVCI	
MEMBER	MEMBER	

This PhD Thesis is performed in Department of Institute of Natural and Applied Sciences of Çukurova University.
Registration Number:

Prof. Dr. İlhami YEĞİNGİL
Director
Institute of Natural and Applied Sciences

ABSTRACT

PhD THESIS

AN ARTIFICIAL NEURAL NETWORK CONTROLLED MICROELECTROMECHANICAL ACCELEROMETER

Zehan KESİLMİŞ

ÇUKUROVA UNIVERSITY
INSTITUTE OF NATURAL AND APPLIED SCIENCES
DEPARTMENT OF ELECTRICAL - ELECTRONICS ENGINEERING

Supervisor: Asst. Prof. Dr. Murat AKSOY
Year: 2011, Pages:138
Jury :Asst. Prof. Dr. Murat AKSOY
Prof. Dr. Mehmet TÜMAY
Assoc. Prof. Dr. Ulus ÇEVİK
Asst. Prof. Dr. Emin ÜNAL
Asst. Prof. Dr. Mutlu AVCI

In this dissertation, a neural network based Micro-Electro-Mechanical-System (MEMS) accelerometer is designed. Analog neural network controller for the MEMS accelerometer is researched and a specific hardware design is implemented. Aim of the proposed neural network controller is to improve the performance of capacitive MEMS accelerometer. The study has been performed in both MATLAB and SPICE environments. Simulation results show that, proposed neural network controller improves performance of MEMS accelerometer.

Key Words: MEMS, Artificial Neural Network, Electrostatic feedback, MATLAB, SPICE

ÖZ

DOKTORA TEZİ

YAPAY SİNİR AĞI KONTROLLÜ MİKROELEKTROMEKANİK İVMEÖLÇER

Zehan KESİLMİŞ

ÇUKUROVA ÜNİVERSİTESİ
FEN BİLİMLERİ ENSTİTÜSÜ
ELEKTRİK ELEKTRONİK MÜHENDİSLİĞİ ANABİLİM DALI

Danışman : Yrd. Doç. Dr. Murat AKSOY
Yıl: 2011, Sayfa: 138
Jüri : Yrd. Doç. Dr. Murat AKSOY
Prof. Dr. Mehmet TÜMAY
Doç. Dr. Ulus ÇEVİK
Yrd. Doç. Dr. Emin ÜNAL
Yrd. Doç. Dr. Mutlu AVCI

Bu tezde, Yapay Sinir Ağı (YSA) kontrollü bir Mikro-Elektro-Mekanik-Sistem (MEMS) ivmeölçer tasarlanmıştır. MEMS ivmeölçer için analog YSA gerçeklemesi araştırılmış ve özel donanım tasarımı gerçekleştirilmiştir. Önerilen kontrolcünün amacı, kapasitif MEMS ivmeölçerin başarısını arttırmaktır. Bu çalışma MATLAB ve SPICE benzetim ortamlarında gerçekleştirilmiştir. Sonuçlar göstermektedir ki, YSA kontrolcüsü MEMS ivmeölçerin başarısını arttırmaktadır.

Anahtar Kelimeler: MEMS, Yapay sinir ağı, Elektrostatik geri besleme, MATLAB, SPICE

ACKNOWLEDGEMENTS

I would like to express my respects and deepest gratitude to my supervisor Asst. Prof. Dr. Murat Aksoy and co-supervisor Asst. Prof. Dr. Mutlu Avcı. They have provided me with their thoughtful guidance, remarkable insights and continuous encouragement.

I also thank my committee members, Prof. Dr. Mehmet Tümay, Assoc. Prof. Dr. Ulus Çevik, Asst. Prof. Dr. Emin Ünal for their supports and valuable discussions.

I greatly appreciate my family for their invaluable supports. They are always there to take care of me and motivate me.

CONTENTS **PAGE**

LIST OF TABLES **PAGE**

LIST OF FIGURES **PAGE**

ABBREVIATIONS

ADC	:	Analog to Digital Converter
ANN	:	Artificial Neural Network
ASIC	:	Application Specific Integrated Circuit
CAN	:	Controller Area Network
CMOS	:	Complementary Metal Oxide Silicon
DAC	:	Digital to Analog Converter
DSP	:	Digital Signal Processor
ECU	:	Electronic Control Unit
FGMOS	:	Floating Gate MOS
FL	:	Fuzzy Logic
FLC	:	Fuzzy Logic Controller
FLS	:	Fuzzy Logic System
IC	:	Integrated Circuit
MEMS	:	Micro Electromechanical System
MLP	:	Multi Layer Perceptron
MOS	:	Metal Oxide Silicon
NNC	:	Neural Network Controller
PID	:	Proportional Integral Derivative
PLL	:	Phase Locked Loop
VLSI	:	Very Large Scale Integration
∑Δ	:	Sigma Delta
∑ΔM	:	Sigma Delta Modulation

1. INTRODUCTION

Modern industrial processes are controlled by complex control systems. Such controllers rely on interactions with controlled process and must react according to physical parameters such as temperature, pressure, force and acceleration. Consequently, the sensing and processing of these parameters are very important for production quality and sustainability.

The sensing devices or sensors convert the physical parameters to electrical parameters. Most of the sensors are equipped with control and interface circuitry. Interface circuits are establishing an interaction between sensor and following electronic system. Present trend of sensor technology is designing smart sensors. These sensors contain its own control and interface electronics such as inertial measurement units (IMU) of the Analog Devices Inc. These devices are solution for the automobile airbag deployment system and they can easily integrate with CAN bus to communicate Electronic Control Unit (ECU) of the vehicle (Analog, 2011).

MEMS, the acronym of "Micro Electro Mechanical Systems", are generally considered as micro systems consisting of micro mechanical sensors, actuators and microelectronic circuits. The acronym MEMS is used almost universally to refer to the entire field of all devices produced by micro fabrication except Integrated Circuits (ICs). Other names for this field of miniaturization include: Micro Systems Technology (MST), popular in Europe, and micro machines, popular in Asia (Judy, 2001).

MEMS processes are used to build three-dimensional structures and movable parts by the combination of lithography, etching, film deposition, and wafer bonding (Fujita, 2007). Also these techniques enable the integration of MEMS with transistors in the same die area. MEMS devices are built on wafers of silicon die, using micromachining technologies which adopted from IC manufacturing and batch fabrication techniques. IC production is a well-developed and matured technology and the research and development of MEMS are concentrated on the research and development of micro mechanical sensors and actuators (Bao, 2005).

Technical achievement of MEMS sensors includes multiple factors:

- The use of existing IC technology in production of MEMS devices allows these devices to be batch-manufactured; this merit converts them to almost inexpensive products.
- Using extremely pure silicon structure as a production material, excellent mechanical properties are resulting. Silicon is almost a perfect material for production of mechanical sensors.
- IC processing industry created technology infrastructure immediately available for MEMS technology, cutting-edge IC processing equipment, ultrapure low-cost materials, sophisticated diagnostic and test equipment, design and simulation tools, and high-volume IC packaging technologies.
- Also there is big potential for the integration with IC circuitry to create low-cost integrated mechanical, optical, and biological systems on a chip (Bryzek et al., 2006). This concept also named as System on Chip (SoC).

MEMS technology has enabled the production of many types of sensor, actuator and system to be reduced in size by orders of magnitude, while often even improving sensor performance. The increasing complexity and integration level of MEMS devices bring the need for advanced control technology (Bryzek et al., 2006). An integration of MEMS device with electronic controller improves the performance of the MEMS devices and reduces the cost of manufacturing.

1.1. Overview of MEMS Market

MEMS products can be classified as sensors and actuators. As seen on Figure 1.1, there are three major application areas of MEMS; first one is the actuator such as Ink Jet Printer head and others are micro mirror device for projector and pressure sensor. As for the MEMS sensors, more than 90% of sensors are commercialized in automobile applications one of these sensors are accelerometers (Tanaka, 2007).

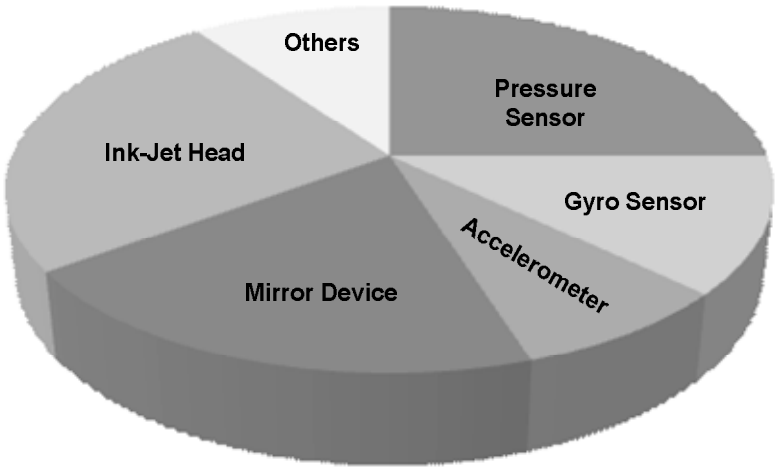

Figure 1.1. Application areas of MEMS devices

Accelerometer is an inertial sensor that measures linear or angular acceleration (IEEE, 2007). This acceleration can be static (tilt) or dynamic (vibration). These sensors have broad application potential in various commercial markets due to low cost and batch production. Primary markets of the MEMS accelerometers can be listed as follows:

- Automotive: This is the major market segment for MEMS accelerometers where the airbag control is the well known application since mid-90's. MEMS accelerometers are primer detecting element for airbag systems. As a relatively high g-level (+50g) sensor is required the emerging application in the automotive sector is for suspension and braking systems. Other application areas of MEMS accelerometers in automobile sector are active suspension control, brake control, fuel cut-off and engine knock monitoring (Spangler & Kemp, 1996).
- Industrial instrumentation: Accelerometers are widely used in machinery health monitoring of rotating equipments where the vibration data allows the user to monitor machines and detect the faults at an early stage so that preventive actions can be taken (Kumar, 2010). For this application high frequency accelerometers have to be utilized. Nowadays highest frequency response accelerometer of the market is Analog Devices Inc's ADXL001.

- Consumer electronics: MEMS accelerometers take place in cellular phone, game console controller, video camera devices (Wicht & Bouchaud, 2005). For this application area static acceleration measurement is used. For tilt measurement low frequency MEMS accelerometers can be used such as MEMSIC's MXA2100.
- Motion and inertial sensing: This is foremost application areas of accelerometers. Security systems, weapon systems, and patient movement tracking have employed with MEMS accelerometers. Devices with motion sensing ability can monitor their motions and respond to them. Consider a cell phone, handheld computer containing inertial sensors, these devices could allow detect its position or acceleration and give appropriate feedback. Also, robots, aircrafts, automobiles, and other vehicles have been sensed and measured using MEMS accelerometers (Verplaetse, 1996).

MEMS sensors are high technology products with huge commercial potential. The requirements for many applications make these sensors should be cheap, could fit into small volume. Also, their power consumption must be suitable for the battery powered operation (Beeby et al., 2004).

1.2. Operation Principle of MEMS Accelerometers

MEMS accelerometers are designed to convert linear or angular acceleration to capacitive or resistive variations as illustrated in Figure 1.2. MEMS accelerometers consist of a sensing element that converts acceleration into electrical signals. Remaining system and its electronics are designed for interface and control purposes. Signal processing electronic circuits can be found on the same chip with sensing element or send to another system to be processed (Gaura, 2000).

Accelerometers are designed for sensing acceleration along their sensitive axis. There are various MEMS accelerometers in market from one to three axis options. Basically, such sensors convert acceleration into electrical signals by means of capacitive and resistive changes. This fact shows that, designing an accelerometer requires electrical background (Kraft et al., 1998)

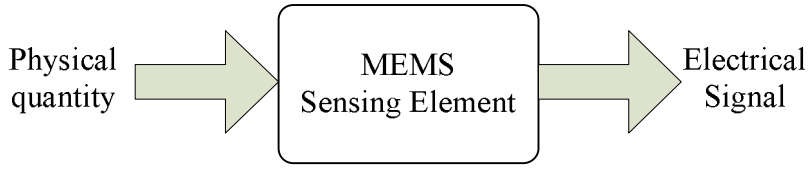

Figure 1.2. Simplified diagram of a MEMS accelerometer

Acceleration is measured in (m/s^2), and earth's gravity ($G=9.8m/s^2$) is preferred for reference. G levels of various conditions are listed in Table 1.1 (TI, 2005).

Table 1.1. Some "G" references

Description "G"	**Level**
Earth's gravity	1g
Passenger car in corner	2g
Race car driver in corner	3g
Bobsled rider in corner	5g
Space shuttle	10g

Operation of MEMS accelerometers depends on Newton's second law of motion. It states that any object undergoing acceleration is responding to a force. Newton's second law is expressed in Eq. (1.1).

$$F = ma \tag{1.1.}$$

where F is the force exerted on the accelerometer (or object) from outer environment, m is the mass of the seismic mass, and a is the acceleration of the seismic mass. All of accelerometers share a basic structure consisting of a seismic mass suspended from a spring. They differ in the sensing of relative position of the seismic mass as it displaces under the effect of an external acceleration. Illustration of basic MEMS accelerometer model is given in Figure 1.3. As seen on Figure 1.3, MEMS accelerometer is modeled as spring-mass-damper system. Seismic mass is the effective mass whose inertia transforms acceleration along an input axis into a force (Zhang, 1998).

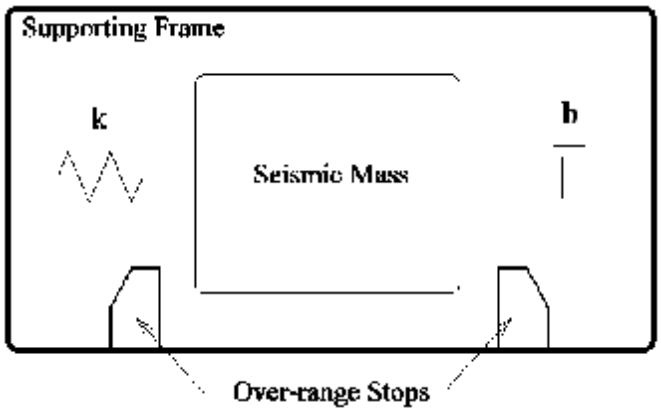

Figure 1.3. Basic accelerometer model

In Figure 1.3, k is spring constant and b is the damping factor. External acceleration displaces the seismic mass relative to the support frame. This displacement can be sensed with different transductions mechanisms. Details of these sensing mechanisms will be given in section 1.3.

1.3. Classification of MEMS Accelerometers

MEMS accelerometers can be classified by sensing mechanism and control method. Many types of MEMS accelerometers are reported with various sensing mechanism in the literature such as piezoresistive, tunneling, optical and capacitive. Piezoresistive and capacitive type MEMS accelerometers are the most popular. A few of the accelerometer types are explained below.

First MEMS accelerometer was reported by Roylance and Angell at Stanford University (Roylance & Angell, 1979). This sensor was unique with the seismic mass, supporting fingers and reference frame etched as an integrated accelerometer in silicon. Acceleration detection method was piezoresistive. The sensor was a cantilever beam-mass structure made out of a silicon wafer as seen on Figure 1.4. (Bao, 2005).

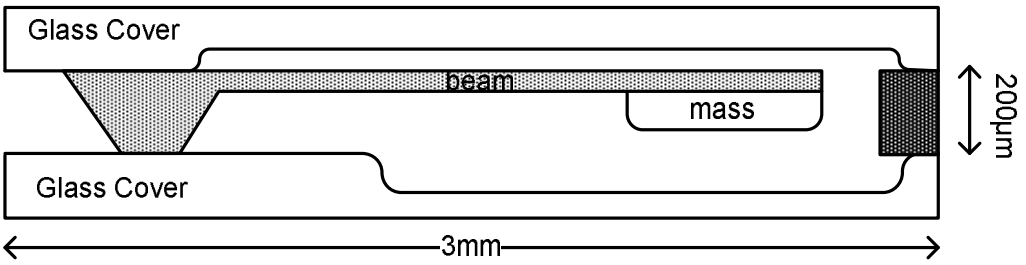

Figure 1.4. Cross section of the first silicon accelerometer

The working principle of the piezoresistive accelerometer is rather simple, when a physical force is exerted on the accelerometer the inertial force on the mass forces the beam to be bent and causes stress in the beam. The stress experienced by a piezoresistive material causes a position change in atoms of piezoresistive material, resulting in the change of its electrical resistance. By completing a Wheatstone bridge around the piezoresistor of the accelerometer, a linear relationship between acceleration and voltage can be derived.

Although, the design and operation of piezoresistive accelerometer is simple there are various drawbacks of this structure. The temperature cross-sensitivity is an obvious drawback of silicon piezoresistors. The change in resistance due to temperature often exceeds the change in the measurand. Also, obtaining high sensitivity from piezoresistive accelerometer is another issue. In addition to the difficulty in processing such a fragile structure, the beam can easily break due to a drop on to the ground or an inadvertent crash of the device onto a hard surface (Bao, 2005).

Tunneling accelerometers contain a cantilever structure with a variable gap between an integrated tunneling tip and a conducting electrode causing electron tunneling in the gap, this principle can be applied to detect extremely sensitive accelerations (Cortés-Pérez et al., 2010).

Interferometric accelerometers use optical principles for measuring acceleration. Such system forms an optical diffraction grading where the displacement of the seismic mass relative to the support substrate is measured with a standard laser diode and photo detector (Zhao et al., 2010).

Heat convection accelerometers are produced by MEMSIC Inc. Operation of this sensor is based on patented thermal MEMS technology and it is built using standard IC process. Design of the offered accelerometers is based on heat convection and requires no solid seismic mass or mechanical springs. This feature provides shock survival greater than 50.000G. Main drawback of this sensor is the limited bandwidth. Block diagram of the heat convection MEMS accelerometer is depicted in Figure 1.5 (MEMSIC, 2011).

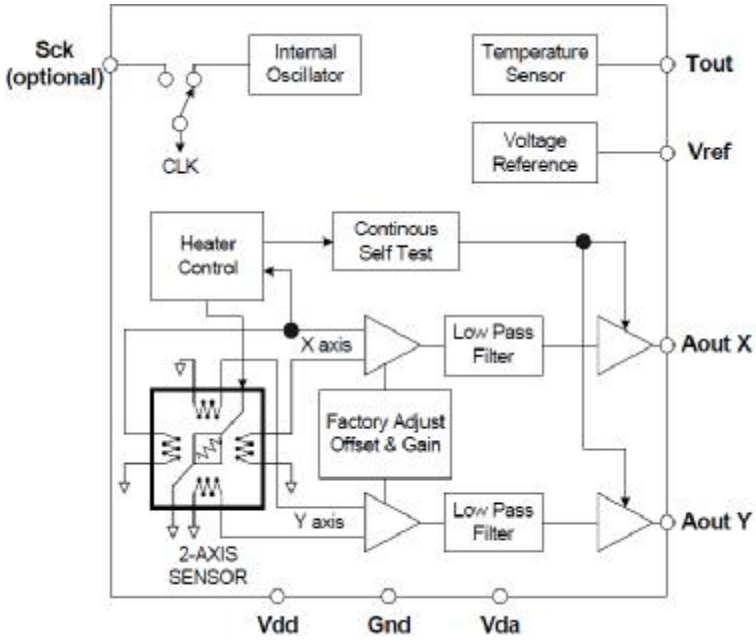

Figure 1.5. Block diagram of the heat convection accelerometer

Capacitive MEMS accelerometers contain a seismic mass that can be move freely between two fixed electrodes, each forming a capacitor with the seismic mass. The differential change in each capacitance is proportional to the deflection of the seismic mass. A built in electronic circuitry can easily measure this capacitance change. Model of capacitive MEMS accelerometer is given in Figure 1.6 (Yazdi, 1998).

Many commercial MEMS accelerometers are based capacitive sensing, such as the ADXL series by Analog Devices and LIS series by ST microelectronics. Capacitive MEMS accelerometers offer several benefits when compared with other

types. The advantages of capacitive accelerometer are low noise, easy realization with conventional processes and high sensitivity (Acar & Shkel, 2003).

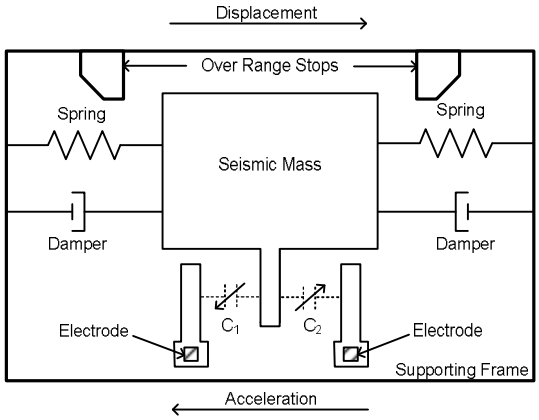

Figure 1.6. Simplified capacitive MEMS accelerometer structure

Figure 1.6 illustrates principal structure with one movable finger and two fixed fingers for demonstration purposes. As previously mentioned, when an external acceleration is applied the seismic mass it moves with respect to the supporting frame. Motion of seismic mass is resulted by increasing value of one capacitance and decreasing other one. Change in capacitance value is used to measure displacement of seismic mass. Also displacement can be easily used for measuring external acceleration.

From different types of accelerometers, capacitive sensing and actuation mechanism is chosen as the principle of the design. In this work capacitive scheme is used because of its high sensitivity, wide range of application areas and easily integration with IC process.

Fabrication methods for the capacitive accelerometers are surface, bulk and LIGA (German abbreviation for Lithografie, Galvanoformung, Abformung). In surface micromachining technique the sensor is formed by a thin poly silicon layer. Surface micro machining is fully compatible with IC process. Bulk micromachining is used for generating thick structures and bulk silicon substrate is etched with wet or dry etching technique.

LIGA is used for the design and manufacturing high aspect ratio MEMS structures. There are two types of LIGA process. These are UV-LIGA and XRAY-

LIGA however; they are very expensive process compared to the conventional IC processes. Also, integration of the LIGA products with IC components is not straightforward (Saile & Wallrabe, 2009).

Surface micro machined accelerometers emerged in the late 1980s a perceived low-cost alternative for accelerometers aimed primarily at automotive market. Both, Bosch GmbH and Analog Devices Inc. offer surface MEMS accelerometers, Analog Inc. is the market leader company that benefited from wide publicity to their ADXL family. Bosch accelerometers were firstly used in Mercedes Benz automobiles in 1982. The ADXL parts were used on Ford, General Motors and other vehicles (Maluf & Williams, 2004).

Surface micro machined accelerometers are finding widespread commercial use in automotive and industrial applications. These devices can be divided into two portions: the mechanical sensing element and the signal detection/control circuit. The sensing element formed using surface micromachining technology is schematically shown in Figure 1.7 (Bao, 2005).

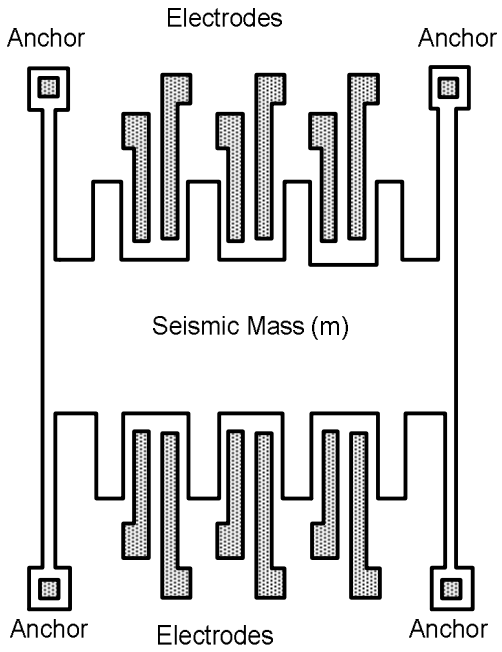

Figure 1.7. A micro mechanical capacitive sensor

The first commercial accelerometers were bulk ones. Such technology allows the production of large seismic masses that gives a greater output signal level. Main

drawback is the size of typical sensing element is about the size of a die, making it difficult to integrate the electronic circuits on same chip. Figure 1.8 shows a capacitive accelerometer made by bulk micromachining technology (Bao, 2005).

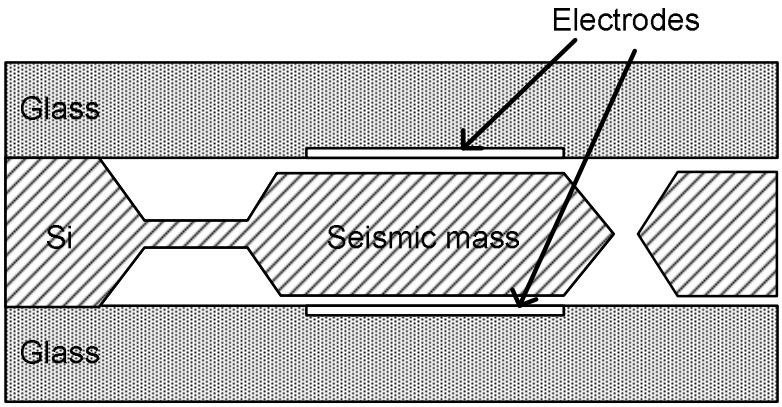

Figure 1.8. Bulk micro machining capacitive accelerometer

Bulk fabrication process was developed solely to manufacture micro machined components and allows the design of three-dimensional structures with high aspect ratios, it has much greater structural heights than other micromachining processes. However, bulk process is not directly compatible with standard IC manufacturing processes. The axis of sensitivity is parallel to the wafer (Bao, 2005).

Today, there are various producers that manufacturing MEMS products in high volumes. One of most the successfully commercialized products in market is ADXL family of MEMS accelerometers produced by Analog Devices Inc. This company uses monolithic integrating technology which allows realizing the mechanical device and electronics on the same die area to obtain better performance. Also Motorola, ST, Summit, MEMSIC, Reiker, Digisens, Silicon Design and Freescale are high volume producers of MEMS accelerometer market.

In control engineering point of view MEMS accelerometers can be classified into two groups as open and closed loop. These two concepts are briefly explained following titles, also detailed mathematical model and computer simulations are given in chapter 3.

1.3.1. Open-loop Architecture

If the electrical output signal of the position measurement interface circuit is used as directly as the output of the accelerometer, this will be called an open loop accelerometer. Some commercial micro machined accelerometers are open loop and they are simple devices such as ADL50 series (Analog Devices, 1996). The dynamics of the mechanical sensing element determine the characteristics of the sensor. This can be problematic as the mass and spring constant are usually subject to considerable manufacturing tolerances. Furthermore, second order effects for larger seismic mass deflection introduce nonlinear effects; such as the spring stiffening effect, for larger deflections (Beeby et al., 2004).

1.3.2. Closed-loop Architecture

High performance MEMS accelerometers use force balancing technique for realizing closed loop control. Force balancing techniques have been used for many years in conventional accelerometer structures to improve performance. This technique is utilized to compensate the inertial force on seismic mass due to acceleration. By generation of a counter balance force the seismic mass almost kept at its rest position. This method eliminates the disadvantages of the open looped accelerometer (Gaura, 2000).

1.4. Objectives and Contribution

The objective of this work is the designing of Artificial Neural Network (ANN) controlled capacitive MEMS accelerometer. The accelerometer and its electronics must be low cost and mass producible, which can be achieved using standard foundry fabrication processes.

1.5. Research Outline

As previously stated above, this work proposes analog neural network controlled MEMS accelerometer. The technique of electrostatic feedback is adopted to realize a high stability, high linearity accelerometer. Proposed MEMS accelerometer takes advantage of the increase in sensitivity and linearity.

Chapter 2 begins with an overview on the various proposed methods of electrostatic feedback controllers for MEMS accelerometers. Also includes comprehensive explanations of previously proposed controllers.

Chapter 3 contains the sensor structure and focuses on the mathematical model of open loop and closed loop accelerometers. It also explains the proposed electrostatic feedback controller and clarifies the components of analog neural network hardware used for electrostatic feedback controller.

Chapter 4 gives simulation results of proposed analog neural network hardware and Chapter 5 concludes the thesis with a brief summary, and outline for future work.

2. PREVIOUS STUDIES

Various control systems are proposed to MEMS accelerometers to improve the dynamical behavior and linearity of the system. These controllers can be classified into two groups, as open and closed loop controllers. Open loop accelerometers directly use displacement of seismic mass for acceleration sensing. It is well known phenomenon that for obtaining higher dynamic range from accelerometer, closed loop control is required (Yin et al., 2011).

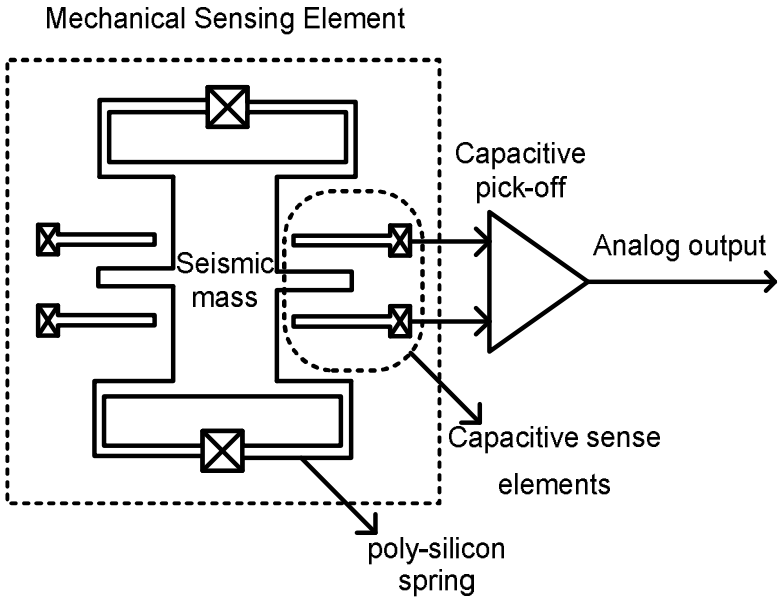

Figure 2.1. Open loop accelerometer

The force-balancing control strategy was originally developed for MEMS accelerometer control (Lu et al., 1995), where it has been successfully applied. A counter-balance force should be applied to seismic mass to limit its displacement. Since the electrostatic forces show a nonlinear function of applied voltage and mass displacement, limiting the displacement of the seismic mass can improve the performance of the accelerometer.

In closed loop MEMS accelerometers, comb fingers are used for sensing. They are also used to exert counter-balance force (Piyabongkarn, 2005).

Several control methods was suggested for closed-loop accelerometers, such as Proportional Integral Differential (PID), Sigma-Delta Modulation (∑ΔM) and phase locked loop (PLL) based techniques (Yazdi, 1998). For closed loop approach, conventional PID controllers can be implemented. Such controllers cannot limit the nonlinearities of the sensor (Yin et al., 2011).

In conventional analog controller, a bias and feedback voltages are applied to both electrodes. This generates an electrostatic force on the mass to keep it at the central position between electrodes (Kraft & Lewis, 1998). Conventional MEMS capacitive accelerometers have stable deflections limited to 1/3 of the initial gap. This problem is known as pull in. Over range or shock acceleration conditions can drive the accelerometer to its limits. This problem is resulted by pull-in and movable electrode snap to the one of the outer electrodes. Conventional accelerometers solve this problem by mechanical limit stop which is limit the displacement of the seismic mass in 1/3 range.

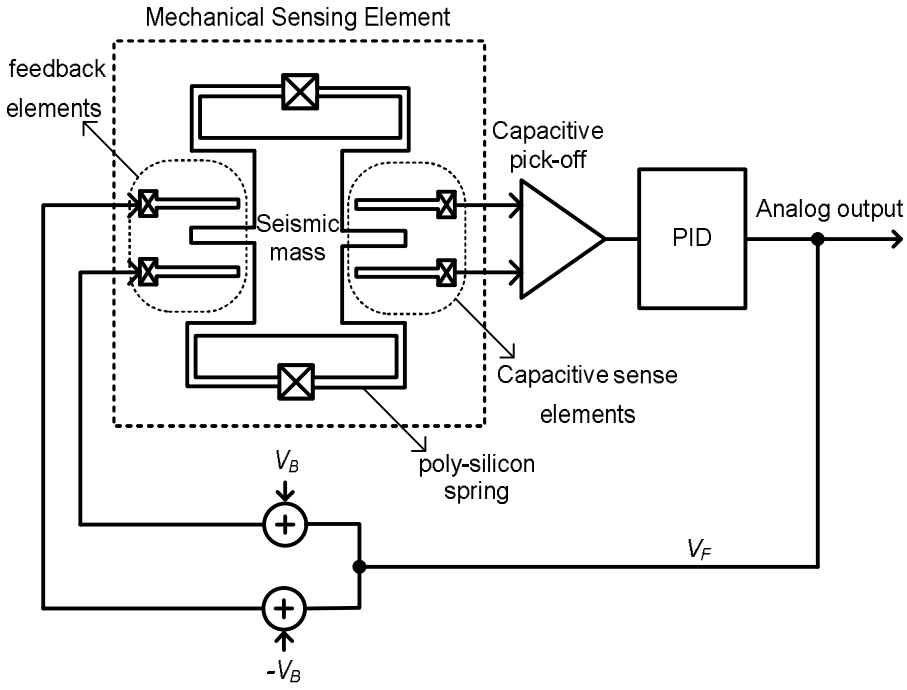

Figure 2.2. Conventional analog closed loop accelerometer

∑ΔM based controllers provide digital bit stream as output. This is a major advantage of the ∑ΔM controllers over the analog controllers. In ∑ΔM technique only the electrode further away from the seismic mass is excited, the other one is grounded. Schematic of this procedure is illustrated in Figure 2.3.

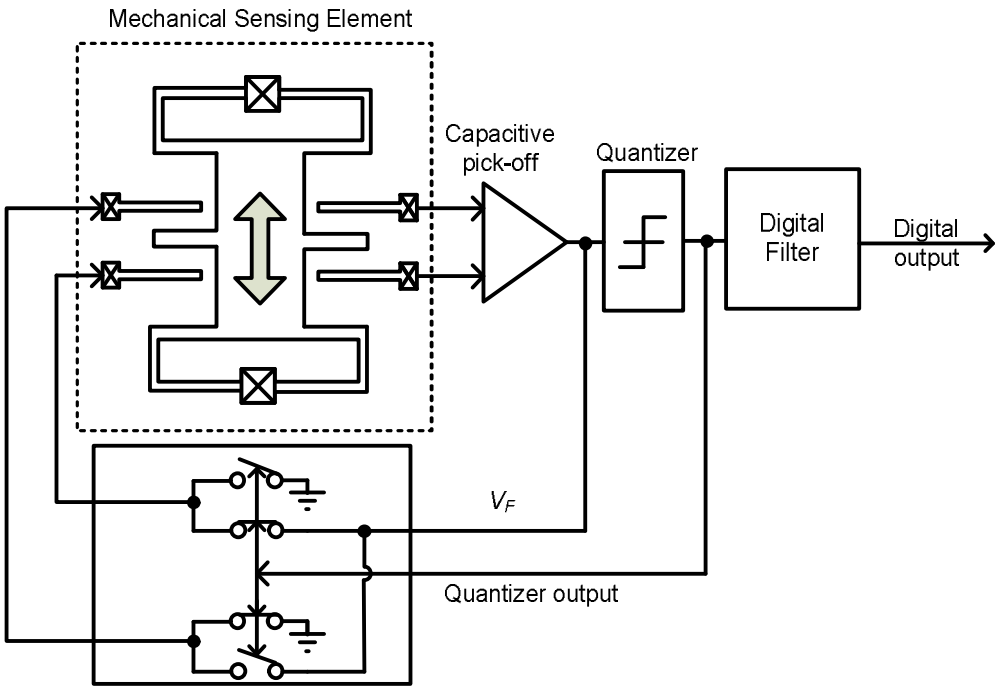

Figure 2.3. Digital ∑Δ controller

Average electrostatic force on the seismic mass is proportional to the number of voltage pulses in a given time period. ∑ΔM is alternative approach for the analog implementation. The nonlinear relationship between voltage and the force in electrostatic actuators is eliminated by quantizing the feedback to 1bit and encoding only the sign of the seismic mass displacement from rest position. Linearity is assured because only two force levels are sensed or generated (Kraft, Lewis, & Hesketh, 1998). Disadvantage of the ∑ΔM is to design high order structure of a closed loop accelerometer in order to achieve high dynamic range, which is very difficult to control the stability of the closed loop accelerometer (Yin et al., 2011).

Two works done by Hassani and Payam proposing a back stepping controller and a sliding mode controller (Hassani 2010; Payam 2007). The proposed systems are incompatible with analog Very Large Scale Integration (VLSI) techniques. Hollocher and Memishian designed force-balanced technique controller.

This technique uses 1MHz square wave with variable amplitude to excite capacitive electrode. Various commercial MEMS accelerometers use this technique such as Analog Devices Inc.'s ADXL series (Hollocher & Memishian, 2003).

Advantages of the analog accelerometer are simple signal pick-off scheme employing a capacitive half bridge technique and simple implementation with VLSI techniques. On the other hand, digital accelerometer is relatively sophisticated with a considerable number of analogue switches and a complex timing diagram (Kraft & Lewis, 1998).

The use of a neural network was firstly proposed Gaura to improve the performance of the accelerometer (Gaura, 2000). The neural network was trained to approximate the partial function as given in Eq. (2.1). Training data set contained 200 samples and back-propagation algorithm was used for the network training. The desired approximation was performed by a one hidden layer with 6 neurons. However, this work does not propose any neural network circuitry.

$$output_1 = \begin{cases} \sqrt{input} & if \quad input \rangle 0 \\ 0 & if \quad input \le 0 \end{cases}$$
$$output_2 = \begin{cases} \sqrt{|input|} & if \quad input \langle 0 \\ 0 & if \quad input \ge 0 \end{cases} \qquad (2.1.)$$

where ***input*** is the output voltage of the capacitive pick-off circuit and $output_1$ and $output_2$ are top and bottom electrode voltages, respectively. Aim of this controller is mimic the behavior of the ∑ΔM controller by using ANN. As seen on Eq. (2.1) such controller exerts excitation voltage only one electrode at a time, the other electrode is grounded. Applied voltages to the electrodes eliminate the nonlinear effects of electrostatic characteristics.

In the literature first neural network circuitry for MEMS sensor is proposed by Futene et al. This work presents an ASIC based scheme to compensate the temperature error of high resolution MEMS piezoresistive pressure sensor. The scheme under consideration is based on a CMOS ASIC realization of a feed forward artificial neural network (Futane et al., 2010).

Fuzzy logic is an attractive technique when the plant model is complex or ill defined. The main disadvantage with fuzzy control system is the heavy computation burden in translating the linguistic control rules into the corresponding control actions. A trained neural network is promising as it requires very less computation time and memory. It is therefore reasonable to combine the merit of fuzzy systems and neural network namely for the pattern recognition ability of neural network and adaptive ability of fuzzy systems (Kumar et al., 2008).

This work focuses on the development of an NNC for analog MEMS accelerometer. The proposed NNC is to overcome the pre-mentioned drawbacks. A Fuzzy Logic System (FLS) is utilized to obtain training data set of NNC. The training data set includes a number of cases, where each contains different values in a range of input and output variables. Proposed controller has also additional contributions: preventing occurrence of pull-in problem and achieving negative electrostatic feedback force.

3. MATERIALS AND METHODS

In this study, a neural network based control of MEMS accelerometer is proposed. This method employs and extends techniques of artificial neural networks and fuzzy logic. Before introducing the method, mathematical background of open and closed loop MEMS accelerometers are explained. Presented mathematical models include damping, electrostatic and the capacitive pick-off interface.

MEMS accelerometers can be classified in two groups as open and closed loop. Open loop accelerometers directly use output of the capacitive pick-off circuit as output however; this method shows limited performance. Closed loop control brings several advantages. It reduces some recurrent problems in open loop method, such as signal distortion due to nonlinear elements.

In this work capacitive sensing method is used for sensing element. At the same time, closed loop control method is employed. Proposed controller executes a decision mechanism with feedback voltage to generate counter balance force. Details of these control methods are given in following titles.

3.1. Mathematical Modeling of MEMS Accelerometer

MEMS accelerometers provide a measure of acceleration in form of an electrical output signal. Accelerometer can also provide a measure of velocity and position by integration of output signal. Since the accelerometers measure the earth's gravity, they can be used to detect a change in tilt. MEMS accelerometers are utilized in various video game controllers and camera image stabilizers as a tilt sensor. A MEMS accelerometer consists of sensing element and interface/control circuitry. Details of these parts will be given in following titles.

3.1.1. The MEMS capacitive sensing element

Sensing element is central part of the accelerometer and responds to the external acceleration by mechanical displacement. Displacement of seismic mass is detected by measuring the capacitance change between the seismic mass and adjacent fixed electrodes. The capacitive MEMS sensing element used in this research is surface micro-machined and it has capacitive signal pick-off circuit. Movable comb fingers are attached to the seismic-mass, and fixed fingers are attached to the reference frame form the sensing element as illustrated in Figure 3.1.

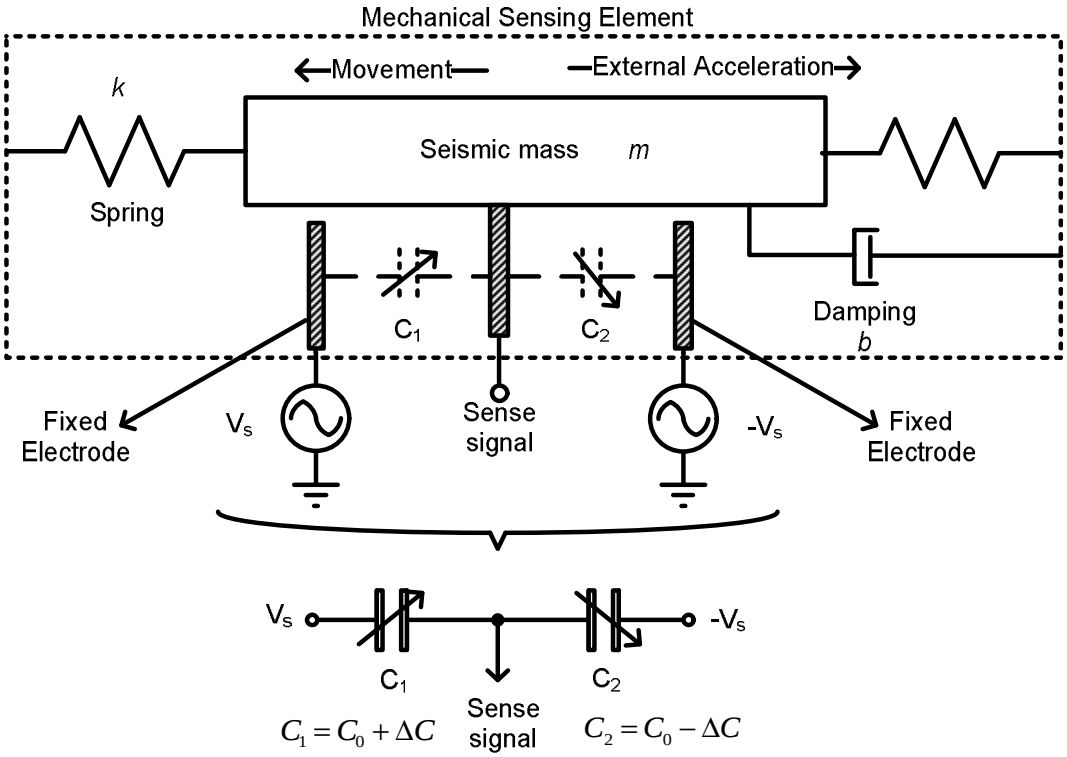

Figure 3.1. Schematic of capacitive sensing element

Under external acceleration condition sensing element moves with respect to reference frame. Consequence of this motion value of the sensing capacitances (C_1 and C_2) increases while other decreases.

Relative displacement of the seismic-mass is detected by measuring this capacitance change. In this thesis, single ended half bridge capacitance sensing method is used. It contains a charge amplifier circuit used for measuring the imbalance in capacitances. Details of the charge amplifier circuit are given in section 3.1.2.

Sensing element of the MEMS accelerometers can be modeled as spring-mass-damper system as depicted in Figure 3.1 (Zhang, 1998). The differential equation for the displacement as a function of external acceleration defines a second-order system given in Eq. (3.1).

$$ma_{input} = m\frac{d^2x}{dt^2} + b\frac{dx}{dt} + kx \tag{3.1.}$$

where, a_{input} is external acceleration, m is seismic mass, b is damping factor, k is spring constant and x is displacement of seismic mass (Acar & Shkel, 2003). Dynamic performance of accelerometer can be formulated in Laplace domain as Eq. (3.2).

$$\frac{x(s)}{a(s)} = \frac{1}{s^2 + \frac{b}{m}s + \frac{k}{m}} \tag{3.2.}$$

Block diagram of MEMS sensing element is depicted in Figure 3.2. This diagram contains saturation block that mechanically limits the displacement of the seismic mass. Most of the MEMS accelerometers contain mechanical stop element to limit the displacement. Input to the given model is external acceleration and the output is displacement of the mass.

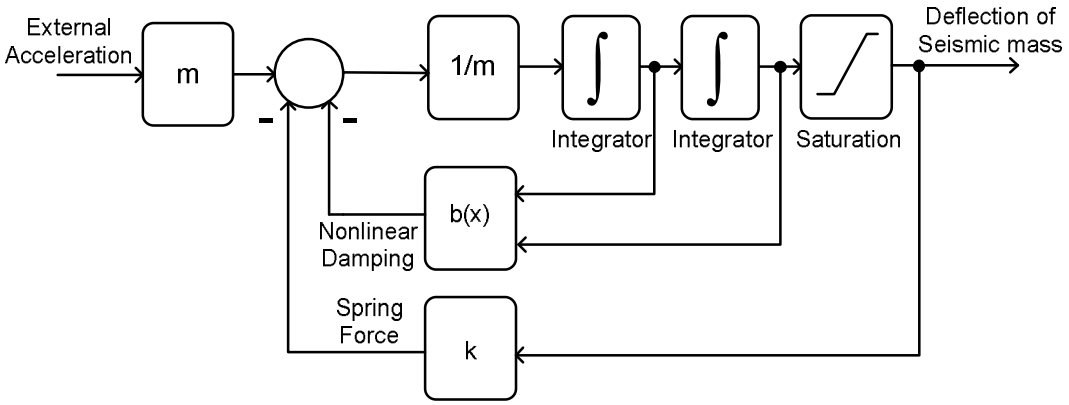

Figure 3.2. Block diagram for the MEMS sensing element model

A top view of sensing element is illustrated in Figure 3.3. The mechanical structure of the sensor is made of a layer of poly silicon material about 2μm thick. A central mass plate with fingers on both sides is suspended over the substrate by suspension beams. This device is similar to ADXL 150 accelerometer developed by Analog Devices Inc. (Analog Devices, 1996). The movable part of the MEMS accelerometer consists of two folded beam: a seismic mass and some movable fingers. The fixed parts include two anchors and some top/bottom fixed fingers. The central mass plate (working as the seismic mass of accelerometer) can be displaced by an inertial force in the surface plane and in perpendicular to the beam flexures (Bao, 2005).

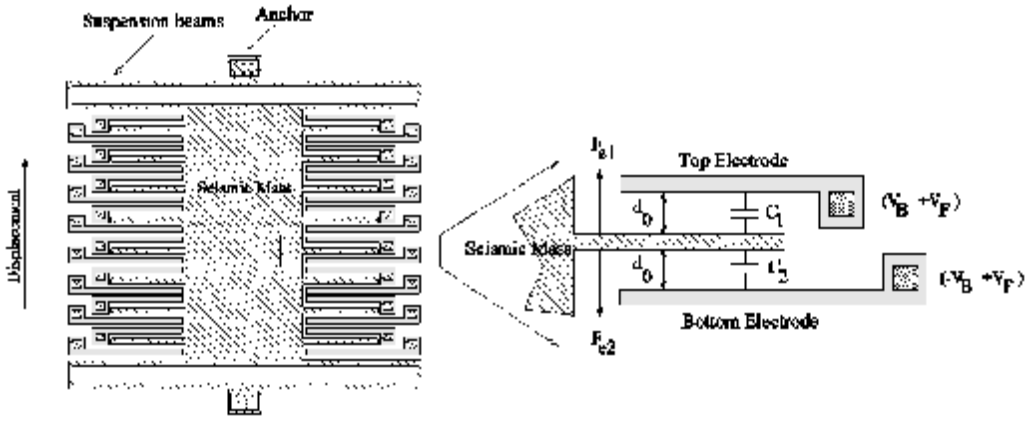

Figure 3.3. Top view of sensing element of accelerometer

As can be seen in the Figure 3.3, sensing element has a lot of capacitor pairs. All upper capacitors are wired parallel for an overall capacitance C_1 and likewise all

lower ones for overall capacitance C_2. As an example, Analog Devices accelerometer ADXL05 has 46 pairs of capacitors (Analog Devices, 1996). Figure 3.4 illustrates the measurement setup used to measure the difference between the two capacitances.

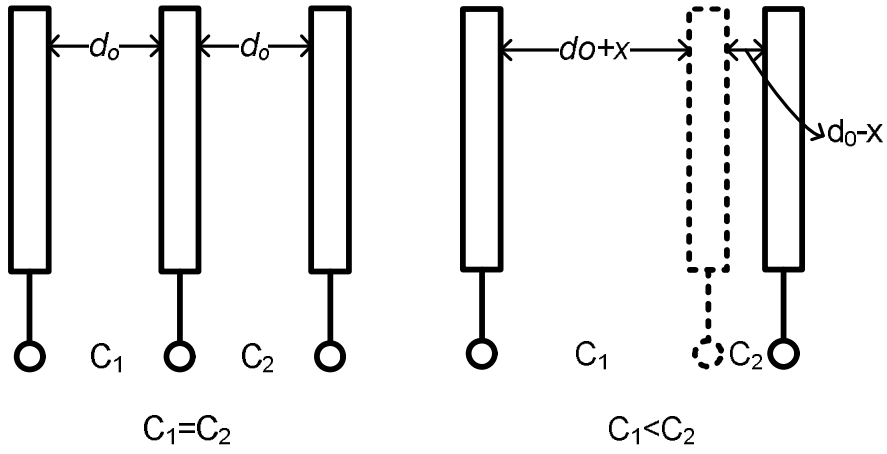

a) Capacitances in rest position b) Capacitances in deflection

Figure 3.4. Differential capacitors in different conditions

Determination of the capacitances with respect to displacement is given in Eq. (3.3). The analysis below only is given for a single capacitor pair, one of the multi copies. The capacitances of two pairs of parallel conductive plates of cross section area A separated by nominal capacitance gap under static condition d_0 with ε as dielectric permittivity of air are given in Eq.(3.3).

$$C_1 = \frac{eA}{d_0 - x}, C_2 = \frac{eA}{d_0 + x} \tag{3.3.}$$

Area of this capacitance can be defined as $A=lt$. where t is thickness of poly-silicon material, l is the length of fingers. The seismic mass and electrodes are made of poly silicon material and electrically the seismic mass acts as the common electrode for two capacitors C_1 and C_2 in series. With a lateral acceleration, the plate is displaced and the capacitances C_1 and C_2 change in a push-pull way.

The differential capacitance C_1 and C_2 can be used as a measure of the acceleration. When there is no acceleration, the movable fingers rest in the middle of the fixed electrodes. In this way, C_1 and C_2 capacitances are equal. Under external acceleration, the seismic mass, *m*, experiences an inertial force. As a result the seismic mass deflects from its rest position for a certain displacement, *x*, hence the C_1 and C_2 capacitances are changed. By measuring this small capacitance change one can easily measure the value and direction of the external acceleration. This is the working principle of the capacitive MEMS accelerometer.

According to their different action in the system, these differential capacitors are divided as sense and feedback elements. In conventional closed loop MEMS accelerometers the feedback capacitors have preloaded with DC voltage $\pm V_B$ and V_F. where V_B is bias voltage and V_F is feedback voltage.

3.1.2. Capacitive Pick-off Circuit

The displacement of the seismic mass can be measured using an opposite excitation method as shown in Figure 3.5. This figure contains mechanical sensing element and a capacitive charge amplifier. The sense capacitors are supplied by the two AC signals ($+V_s$ and $-V_s$) with 180˚ phase difference. When no external acceleration occurs, C_1 and C_2 are exactly the same (nominal value C_0) hence the input voltage of the amplifier is zero. Under external acceleration condition C_1 and C_2 are different. Difference of the capacitances is represented by ΔC. Under an applied acceleration capacitances can be defined as

$$C_1 = C_0 + \Delta C \, , \; C_2 = C_0 - \Delta C \tag{3.4.}$$

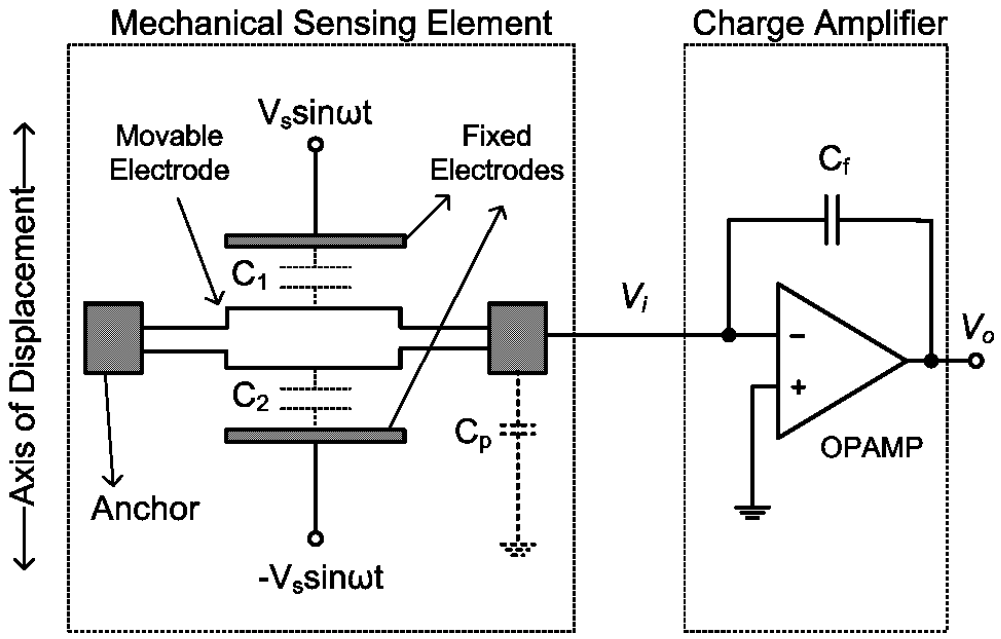

Figure 3.5. Opposite excitation sensing scheme

Detailed view of the charge amplifier is given in Figure 3.6. C1 and C2 represent the variable capacitors of the sensing element and C_f is feedback capacitor of the OPAMP. C_p represents total parasitic capacitance. Parasitic capacitance is caused by the anchors and effect of this capacitance can be eliminated since the output node (or input of the charge amplifier) is at virtual ground. To simplify the calculation, let the OPAMP have infinite input impedance, so no current flows into the amplifier input. Input charge of the charge sensitive amplifier can be determined as follows:

$$q_1 = -V_s(C_0 + \Delta C)\ ,\ \ q_2 = +V_s(C_0 - \Delta C) \tag{3.5.}$$

$$Q_i = q_1 + q_1 = -2V_s\Delta C \tag{3.6.}$$

Since no current can flow into the amplifier, all of the current must charge up the feedback capacitance, so Q_i=Q_f.

$$Q_i = Q_f = -2V_s\Delta C = V_oC_f \tag{3.7.}$$

Voltage signal at the output is defined as:

$$V_{out} = \frac{-2V_s \Delta C}{C_f} \tag{3.8.}$$

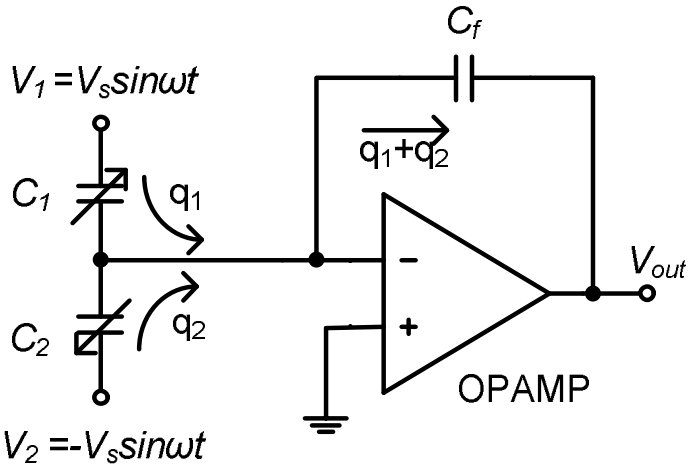

Figure 3.6. Position sensing circuit

As a result, amplitude of the V_{out} is a linear function of the displacement of the seismic mass. Parameters of the sensing element are given in Table 3.1.

Table 3.1. Parameters of proposed accelerometer

Symbol	**Explanation**	**Value**
ε	dielectric permittivity of air	$8.854 \times 10^{-14} Fcm^{-1}$
t	thickness of poly-silicon material	$5\mu m$
d_0	the gap finger to outer electrode	$2\mu m$
l	length of fingers	$50\mu m$

In order to operation of the accelerometer, the seismic mass is subjected to four forces. These are the force caused by the acceleration, the spring force of the flexure structure, the damping force and the electrostatic force. Details of these forces are given in following section.

3.1.3. Damping Force

Damping force is a counter force on the moving plates. The air between such plates generates this counter reactive force. Damping force can be neglected for a machine of conventional dimensions. It may play an important role with micro-machines and the significance of the effect becomes greater as micro-machined structures decrease in size.

For a MEMS device moving against a trapped film, air damping has been a problem of great importance affecting the system response. The dynamic behavior of accelerometers, optical switches, micro-torsion mirrors, resonators, etc. is significantly related the squeeze film air damping of the mechanical structures (Bao & Yang, 2007).

In order to develop a more realistic mathematical model of the sensing element, damping factor has to be considered. The damping characteristic of the system is a complex phenomenon, which introduces nonlinearities. There is a dependency of the damping on the deflection of the seismic mass. Formulation of the damping force is given in Eq. (3.9).

$$b(x) = \frac{1}{2} m A^2 \left(\frac{1}{(d_0 - x)^3} + \frac{1}{(d_0 + x)^3} \right) \tag{3.9.}$$

where m is the viscosity of air and A is the area of the seismic mass (Maro et al., 1993).

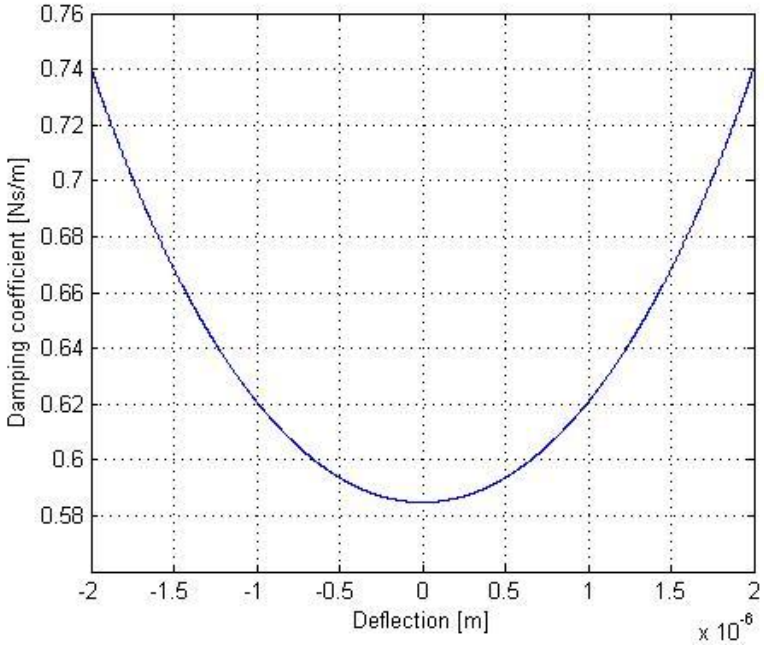

Figure 3.7. Damping coefficient as a function of the displacement

Figure 3.7 illustrates the nonlinear relation between damping force and seismic mass displacement. To minimize this effect displacement of the seismic mass must be minimized.

3.1.4. Electrostatic Force

In MEMS accelerometers electrostatic force is generated by the two means. First is the driving signal that used for capacitive sensing circuitry. It is caused by a nonlinear electrostatic force and second is the feedback system that designed for control purposes.

High performance MEMS accelerometers are equipped with feedback system. In operation of the capacitive MEMS accelerometers, the small dimensions allow the electrostatic forces to be used to provide feedback. In order to operation of the closed loop MEMS accelerometers the appropriate electrostatic force is to be applied to keep the position of the seismic mass fixed.

The electrostatic feedback method has the advantage of low power consumption with some drawbacks. Firstly, a nonlinear relation exists between the

applied voltage and the output feedback force; secondly, electrostatic forces are always attractive and negative feedback is difficult to maintain.

Block diagram of the closed loop accelerometer is depicted in Figure 3.8. The output signal of the position measurement circuit can be used together with a suitable controller, to steer an actuation mechanism that forces the seismic mass back to its rest position. The electrical signal proportional to this feedback force provides a measure of the input acceleration (Beeby et al., 2004).

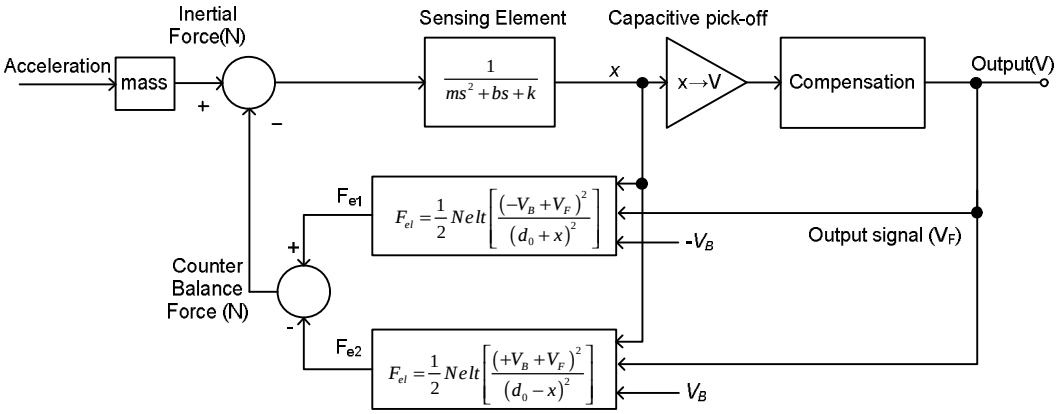

Figure 3.8. Block diagram of the closed loop accelerometer

Conventional closed loop analog MEMS accelerometers use bias voltage to improve linear region of electrostatic force. The two fixed sets of comb fingers are held at DC bias voltages, $\pm V_B$. Also feedback voltage is proportional to output voltage of the position of the seismic mass, hence $V_F=Kx$, where x is the displacement and K is the gain factor (Kraft, 1997).

The equation for the electrostatic force of attraction between two capacitor plates is formulated in Eq. (3.10) for analog accelerometer.

$$F_{el} = N(F_{e1} - F_{e2}) = \frac{1}{2} Nelt \left[\frac{(v_1 + V_B + V_F)^2}{(d_0 - x)^2} - \frac{(v_2 - V_B + V_F)^2}{(d_0 + x)^2} \right] \qquad (3.10.)$$

where, F_{el1} and F_{el2} represent electrostatic forces generated by voltage on top and bottom electrodes, respectively. N is number of parallel capacitor pairs. Voltages V_B and V_F stand for bias voltage and feedback signal, respectively. Feedback signal is

result of displacement of seismic mass. The mathematical expression of closed loop capacitive MEMS accelerometer is given in Eq. (3.11) (Kraft et al., 1998).

$$F_{el} - ma_{input} = m\frac{d^2x}{dt^2} + b\frac{dx}{dt} + kx \tag{3.11.}$$

The electrostatic force F_{el} is nonlinear, since it depends on $1/(d_0 \pm x)^2$. When the applied acceleration exceeds the specified maximum range, the displacement may increase more than one-third of the full gap between electrodes. This phenomenon known as pull-in and tends to instabilize the system.

Figure 3.9 shows the relation between displacement and resulting total electrostatic force. As seen on figure, displacement cannot exceed a certain limit. In normal operation conditions such accelerometer works linearly however in shock acceleration condition controller cannot respond linearly. In such condition polarity of the electrostatic force changes suddenly and seismic mass snaps to the outer electrode. This phenomenon is called as pull-in.

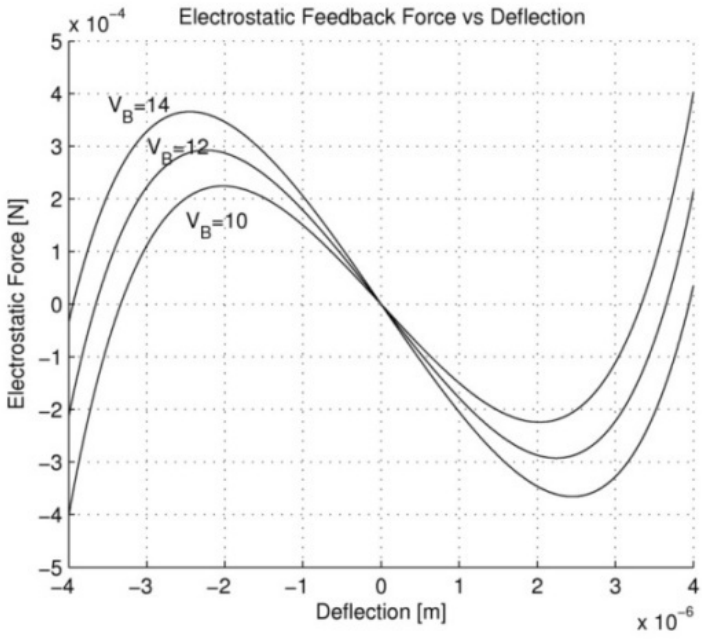

Figure 3.9. Total electrostatic force on the seismic mass

Although, conventional closed loop accelerometers utilize the linear controllers to improve the performance, such controllers cannot prevent the pull-in. This problem is independent of mechanical design parameters such as spring constant and mass (Piyabongkarn, 2005).

3.2. Open-loop Accelerometer

If the electrical output signal of the position measurement interface circuitry is directly used as the output signal of the accelerometer, this will be called an open loop accelerometer. Some commercial accelerometers are open-loop devices (Analog Devices, 1996). They are the most simple and low cost devices possible. Dynamics of the sensing element are mainly to determine the characteristics of the sensor. This can be problematic as the mass and spring constant are usually subject to considerable manufacturing tolerances.

Furthermore, second order effects for larger seismic mass deflection introduce nonlinear effects (Beeby et al., 2004). Illustration of this concept is depicted in Figure 3.10.

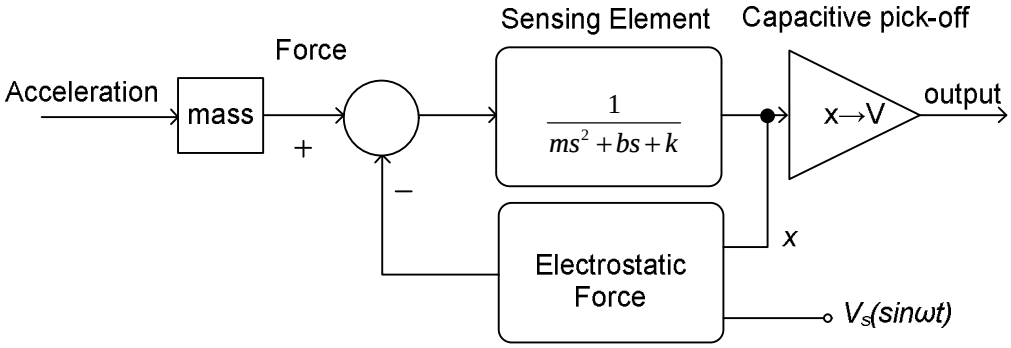

Figure 3.10. Open loop accelerometer

A high frequency voltage V_s is applied to electrodes to detect position of the seismic mass. This voltage results two electrostatic forces in open loop accelerometer. This force is not the part of the feedback system it is resulted from capacitive pick-off. If the seismic mass at its rest position, these two electrostatic forces will cancel each other. If seismic mass is deflected a positive electrostatic

force term will be occurred. Mathematical expression of the electrostatic force for the open loop accelerometer is given in Eq. (3.12).

$$F_{el} = F_{el1} - F_{el2} = \frac{e\,A\,V_s^{\,2}}{4}\left(\frac{1}{(d_0 - x^2)} - \frac{1}{(d_0 + x^2)}\right) \qquad (3.12.)$$

In order to operation of the open loop accelerometer this electrostatic force limits the performance. To minimize effect of electrostatic force in the open loop accelerometer, amplitude of the excitation voltage should be minimized.

With the considerations described above, it is possible to derive a complete mathematical model for the open loop MEMS device and its block diagram shown in Figure 3.11. The input of the system is the external acceleration, and the output is voltage produced by capacitive pick-off circuit. The saturation block models the restraint in movement of the seismic mass by the outer electrodes. This model is suitable for implementation in both MATLAB and SPICE environment (Gaura, 2000).

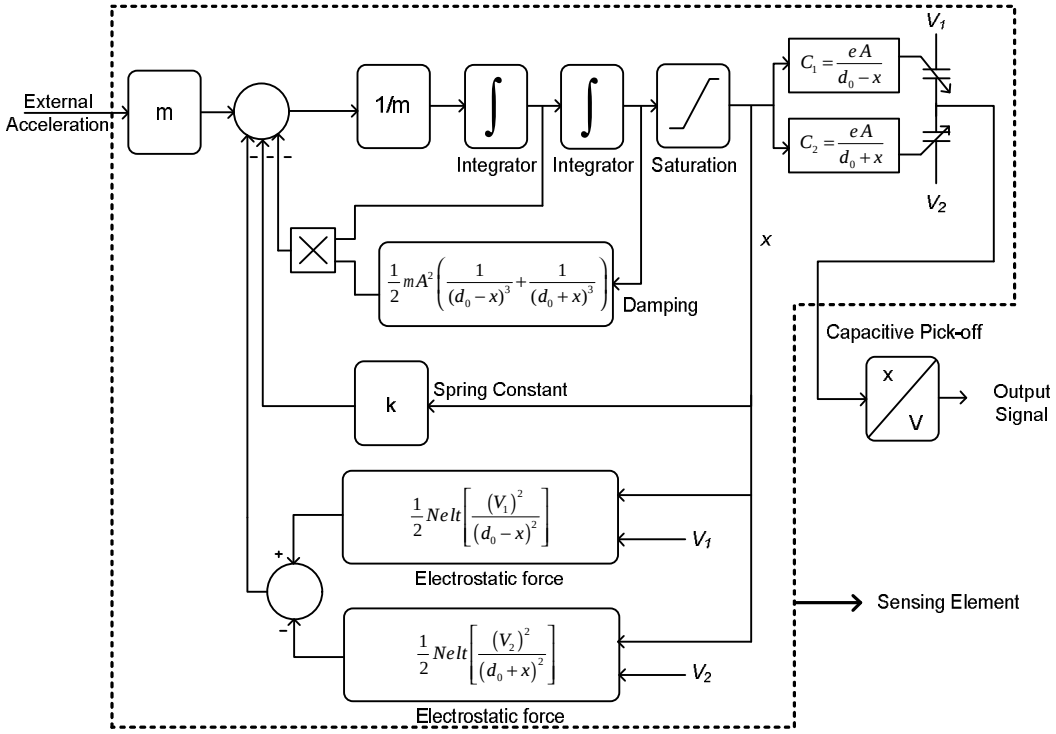

Figure 3.11. Mathematical model of the open loop accelerometer

3.2.1. Simulation Results of Open-loop Accelerometer

The MATLAB/Simulink model of the open-loop accelerometer is depicted in Figure 3.12. A number of simulations have been done with this model. The step like acceleration signal used for first simulation. Amplitude of the input acceleration is 3g for this case and forces acting on the seismic mass are illustrated in Figure 3.13. Acceleration force (F_i), damping force (F_a) and spring force (F_e), electrostatic force (F_{el}) are represented with respect to time for an interval of 25ms.

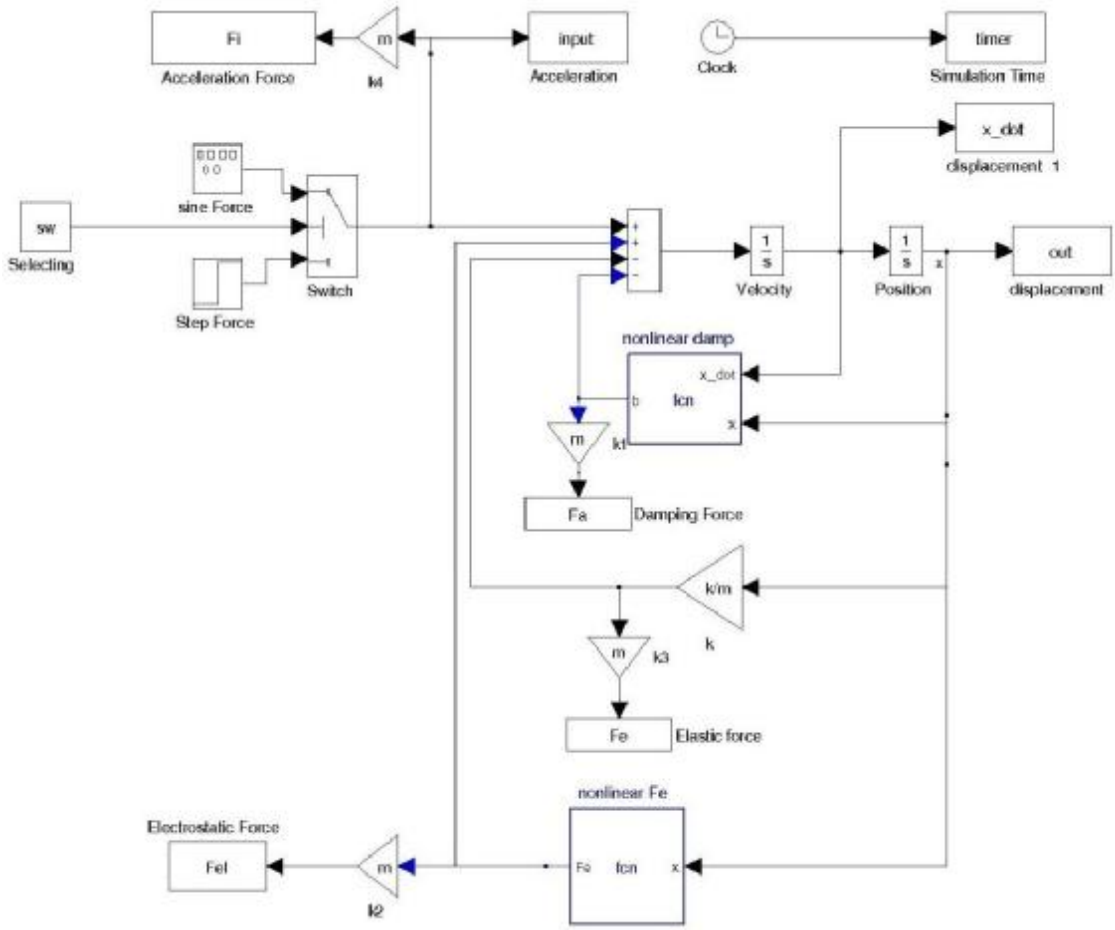

Figure 3.12. MATLAB/Simulink model of the open-loop accelerometer

As seen on Figure 3.13, electrostatic force F_{el} is 3-order smaller than the other forces and damping force presents an initial jump to its maximum value then it falls slowly and reaches zero value. Spring force raises form zero value and becomes steady.

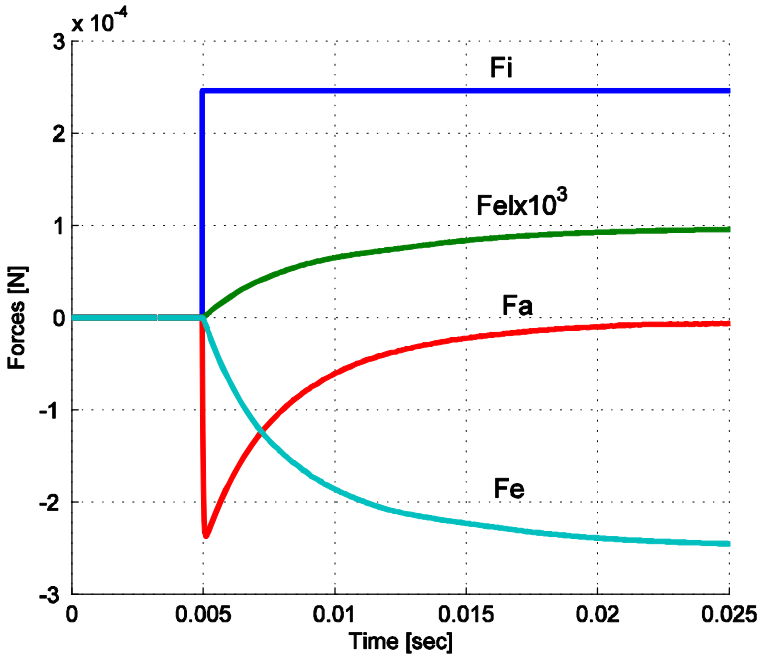

Figure 3.13. Graphics of the forces that acts on seismic mass

Step-like acceleration signals are applied at the Simulink model input and displacement of the seismic mass is obtained. The values of the step-like acceleration signals are 1g, 3g, 5g and 7g, respectively. Response of the open loop accelerometer to the step shaped acceleration signals are illustrated in Figure 3.14.

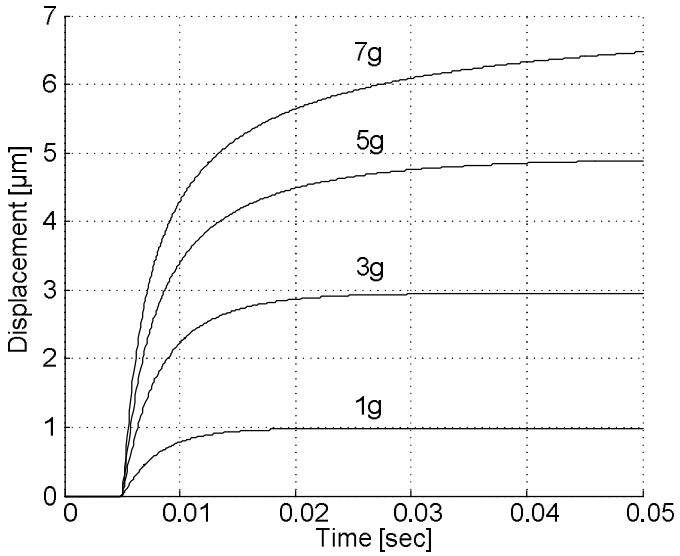

Figure 3.14. Simulated step responses of open loop system

Sine shaped acceleration signals are used for third simulation step with frequency of 40Hz and magnitudes of 1g, 3g, 5g, and 7g sequentially. Nonlinear effects of the system can be noticed on this case easily. It can be seen that the displacement of the seismic mass is a sine wave for smaller magnitudes; however for larger magnitudes like 5g and 7g, it is slightly deformed. Additionally, for larger input accelerations the phase shift occurs. These effects are due to the nonlinear damping force which increases with deflections.

Limited performance of the open loop accelerometer shows that designing of a closed loop system is not a trivial task. The drawback of the closed loop accelerometer is mainly the added complexity in interface and control electronics. There is range of possible actuation mechanisms to keep the seismic mass at its rest position such as electrostatic, magnetic and thermal.

To improve the performance of the accelerometer closed loop control is required. Closed loop operation maintains linearity, supplies high bandwidth and limits the displacement of the seismic mass. Limiting the displacement range prevents damping nonlinearities and improves the performance.

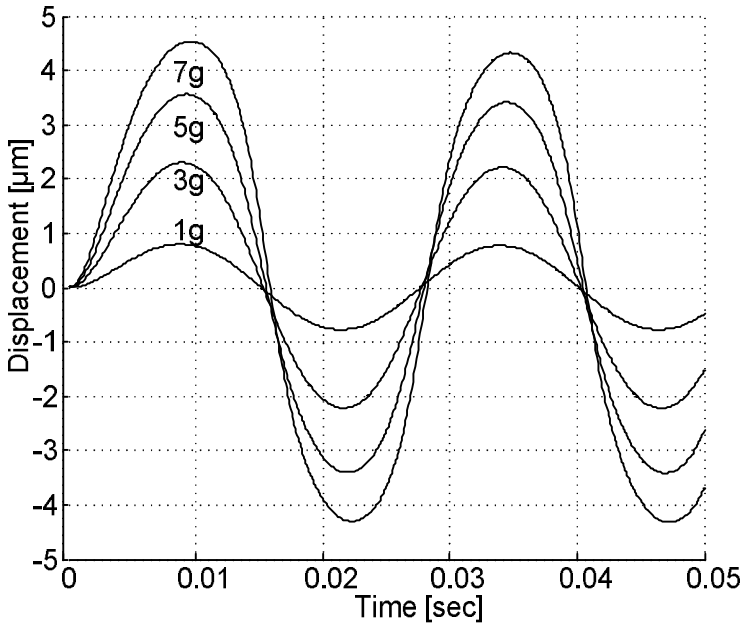

Figure 3.15. Response of the open-loop system for sine inputs

3.2. Conventional Closed Loop MEMS Accelerometer

Simulation of the open loop accelerometer shows that it can work linearly in |4g| range. Also nonlinear effects of the damping and electrostatic force are increasing with deflection of the seismic mass. To obtain higher range from the same accelerometer it is necessary to close its loop and limit the displacement of the seismic mass. For this purpose, a certain counter balance force must be applied over the seismic mass to limit its deflection. This technique is known as force balance or electrostatic feedback. Applied force balance the external acceleration force and also provides information about the acceleration applied to the system.

Components of closed loop model are the sensing element, capacitive pick-off, PID controller and electrostatic feedback force block. Sensing element is mechanical element illustrated in Figure 3.3. Detailed model of a conventional analog closed loop accelerometer is given in Figure 3.16. As stated above, the acceleration force acting on the sensing element cause the seismic mass to deflect from its rest position resulting in a differential change in capacitance proportional to the acceleration. This capacitance change is converted voltage by pick-off circuit.

The PID controller amplifies the imbalance in capacitance that is converted into an output signal. The output signal of the capacitive pick-off circuit can be used together with a suitable controller to steer an actuation mechanism that forces the seismic mass back to its rest position. This is usually referred to as closed loop or force balanced accelerometer. Output of the PID controller can be used to measure of the external acceleration.

This approach has several advantages.

- Deflection of the seismic mass is reduced considerably; hence nonlinear effects from damping and the mechanical suspension system are reduced considerably.
- Dynamics of the sensor can be tailored to the application by choosing a suitable controller (Beeby et al., 2004).

Electrostatic forces are the most commonly used type since for small gap sizes these forces are relatively large. For capacitive MEMS accelerometers the same or different set of electrodes can be used for the electrostatic actuation (Bao, 2005). General mathematical expression of such accelerometer is given in Eq. (3.10). As previously stated performance of the PID controller is limited and cannot prevent pull-in problem. Detailed simulation result for the PID accelerometer is given in next chapter.

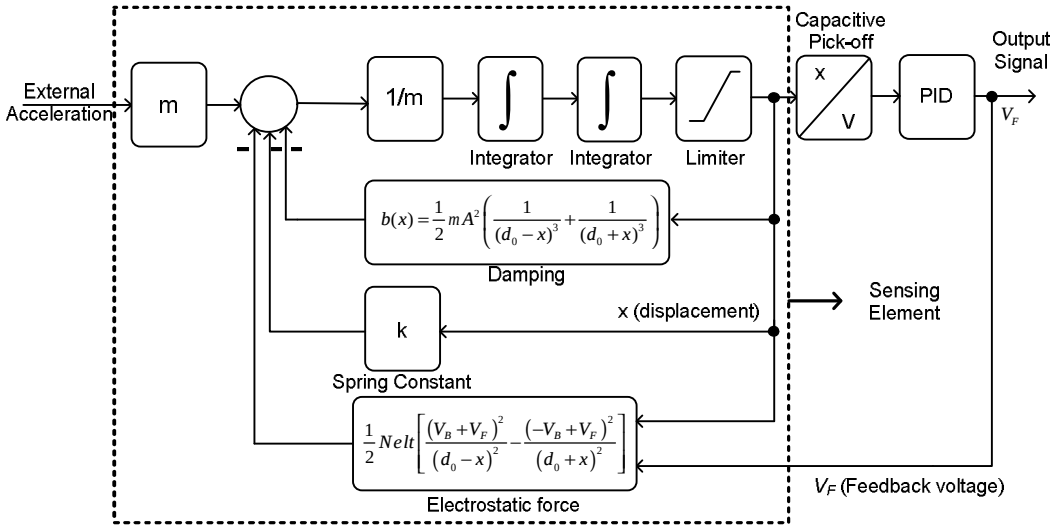

Figure 3.16. Model for the conventional closed loop accelerometer

The problems pre-mentioned above have to be addressed carefully. Nonlinear control techniques could be needed for the design of closed-loop high performance accelerometers.

3.4. SPICE modeling of MEMS Accelerometer

Computer simulation programs are widely used as tools for designing and testing the products within the different research fields of engineering. There are many simulation programs for engineering such as SPICE and MATLAB (Al-Ruwaihi & Qamber, 1999).

SPICE is a general purpose electronic circuit simulation program. Such program is equally suited to solve linear as well as nonlinear electrical circuits. Since SPICE is an electrical system simulator, its input file requires that the input should be in terms of electrical devices. The text file including the circuit information is called the netlist of the circuit. SPICE provides a sub circuit capability, which allows a user to define a subnet or a block and then instantiate it repeatedly in the overall circuit. Also SPICE has the ability to handle differential or algebraic equation.

Combining the MEMS and electronic circuits together gives more realistic simulation results. It should be noted that the simulation of the mechanical device behavior together with surrounding electronics is important for mechatronic systems.

There are various solutions for integration of SPICE netlist in MATLAB environment such as SLPS developed jointly by Cybernet Systems Company Ltd., and Cadence Design Systems, Inc. Instead of very expensive and time consuming device level simulation, efficient and free behavioral simulation becomes more acceptable. In this work behavioral simulation is preferred.

There are many approaches to modeling MEMS devices. The most widely used is to take a purely mathematical and systems level approach (Gibson & Purdy, 1999; Boser & Howe, 2002; Lo, et al., 1996). It has the advantage in system level simulators such as MATLAB or in circuit simulators such as SPICE.

Following section describes how SPICE can be used to support the design and simulation of MEMS accelerometer. The modeling of MEMS accelerometer and its controller is performed using SPICE. Each of models is implemented as behavioral model. The performance of these models is compared with MATLAB simulations. Simulation results show that the accuracy of each behavioral model is excellent and it is possible to simulate MEMS and analog circuits in SPICE environment.

3.4.1. SPICE implementation

The mechanical and electrical sections of MEMS are explicitly coupled. The goal of the simulation effort is to simulate the performance of micro electro-mechanical systems. From this point of view SPICE is right solution for MEMS simulation. Another approach is the integrating the system to a general purpose mathematical tool such as MATLAB.

There are two approaches to simulate the MEMS in SPICE; one is to use component level simulation which model is implemented with time variant, passive, electric component and system level modeling. Component level approach is illustrated in Figure 3.17 as simple RLC circuit (Boser & Howe, 2002). Equations for the given RLC model are given in Eq. (3.13-14).

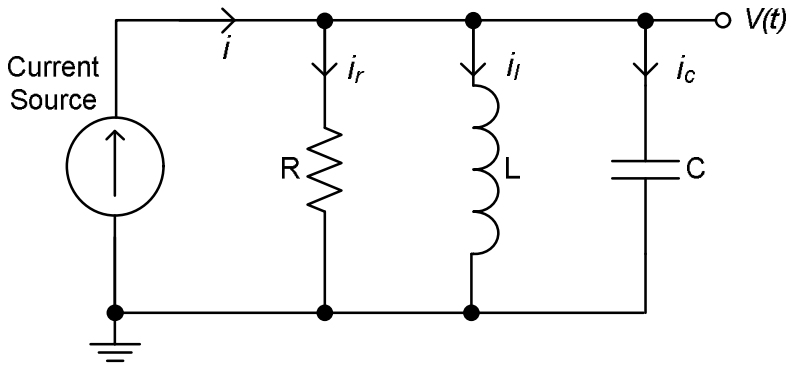

Electrial	Physical
$\frac{1}{R}$	Damping
C	Mass
$\frac{1}{L}$	Spring Constant

Figure 3.17. Equivalent electrical model of MEMS product

$$i = i_r + i_l + i_c \tag{3.13.}$$

$$i = C\frac{dV}{dt} + \frac{1}{R}V + \frac{1}{L}\int V(t)\,dt \tag{3.14.}$$

As seen on Eq. (3.14-15), mechanical coefficients mass, spring constant and damping can be modeled by passive electrical components. This kind of modeling implies that force is analogous to current, mass to capacitor, spring constant to resistor and damping to inductor (Lo, et al., 1996). Also, in electrical equivalent circuit, current represent forces, and voltage corresponds to velocity (Boser & Howe, 2002).

In this work, a behavioral modeling library is developed for realizing system level modeling approach. Such library is intended for use in creating custom components that can be described mathematically. Nearly any mechatronic system can be simulated with designed library. Parts of this library are summing, integrator and gain blocks. All of the function blocks are modeled by Voltage Controlled Voltage Sources (VCVS) in SPICE environment. These components are listed in Table 3.2.

Table 3.2. Components of SPICE model of accelerometer

Symbol	SPICE netlist	Function
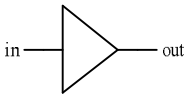	.subckt amp in out E1 out 0 in 0 {Ao} .param Ao={gain} .ends	Simple gain factor
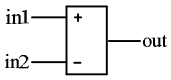	.subckt dif in1 in2 out E1 out 0 value={V(in1)-V(in2)} .ends	Difference module
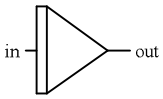	.subckt int2 in out E1 out 0 value={sdt(V(in))} .ends	Integrator module
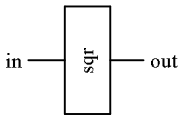	.subckt sqr in out E1 out 0 value={V(in)*V(in)} .ends	Square module
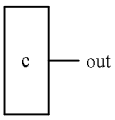	.subckt const out V1 out 0 {Ao} .param Ao={gain} .ends	Constant module
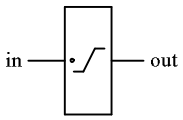	.subckt limit in out .param limit={gain} E1 out 0 value=+ {if(V(in)>{limit}, {limit}, + if(V(in)<{-limit}, {-limit}, V(in)))} .ends	Physical limiter for the mechanical structure

3.4.2. Evaluation of SPICE model

Parameters of closed and open loop accelerometers are used in an SPICE model to solve the deflection of seismic mass. SPICE model of the open loop MEMS accelerometer is illustrated in Figure 3.18. Capacitive pick-off circuit is neglected to reduce simulation time.

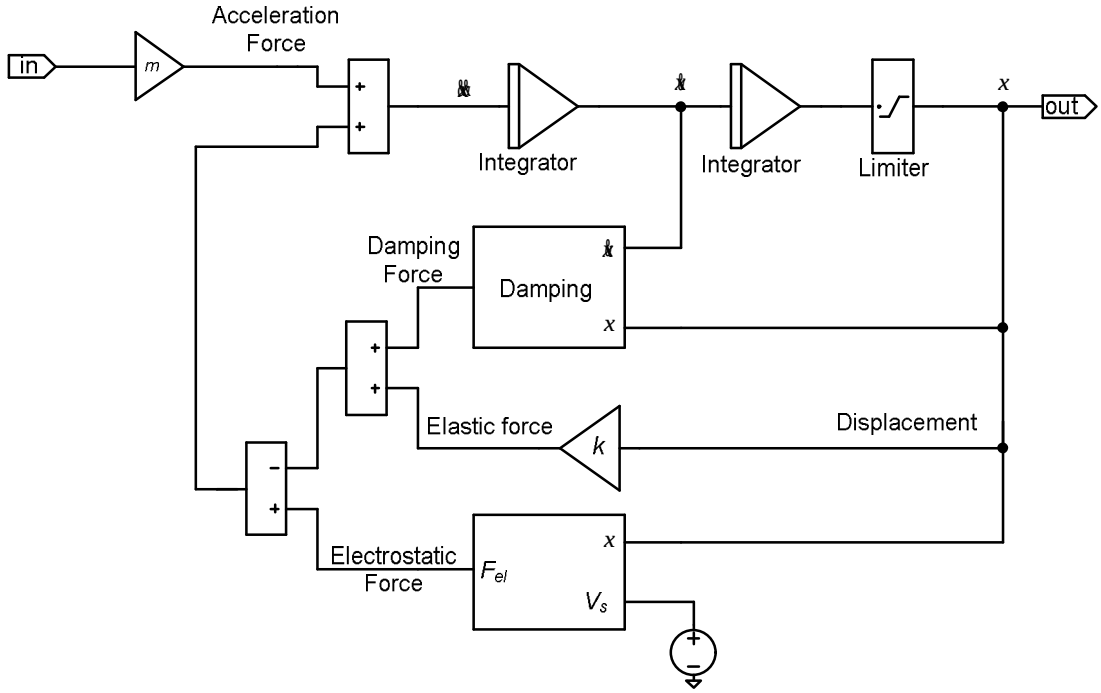

Figure 3.18. SPICE model of an open loop accelerometer

A set of simulation were performed for step shaped and sine wave accelerations for the open looped accelerometer. Response of the accelerometer to the sine wave accelerations with various amplitudes are given in Figure 3.19.

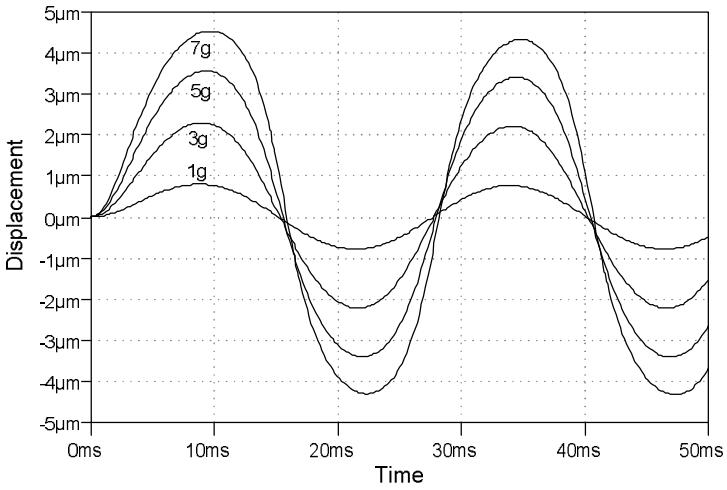

Figure 3.19. Response of the open-loop system for sine inputs

Figure 3.20 shows response of the open looped accelerometer to the step shaped accelerations with 1g, 3g, 5g and 7g, respectively.

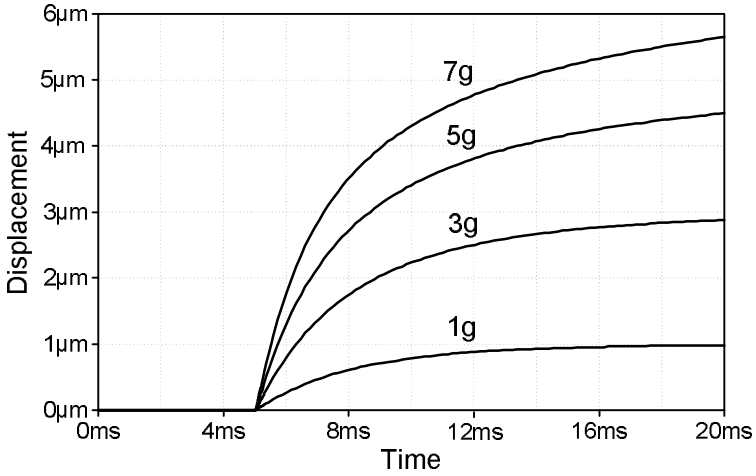

Figure 3.20. Step response of the open loop accelerometer

A step shaped 3g acceleration signal is applied to the open looped accelerometer. Forces that are acting on the seismic mass are illustrated in Figure 3.21. Acceleration force (F_i), damping force (F_a) and spring force (F_e) and electrostatic force (F_{el}) are represented with respect to time for an interval of 25ms. In open looped accelerometers source of the electrostatic forces is excitation voltage of the capacitive pick-off system. This voltage holds as low as possible to minimize

nonlinear electrostatic force. Because of this F_{el} is given with 10^3 gain factor in Figure 3.21.

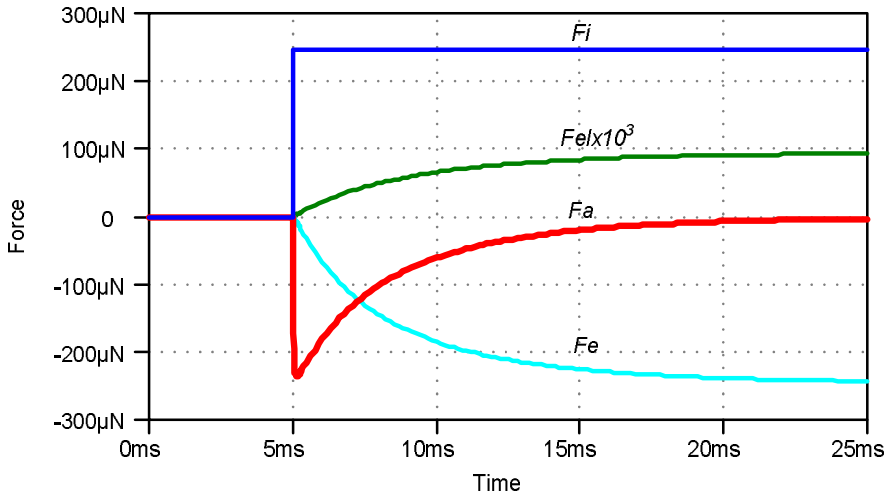

Figure 3.21. Graphics of the forces that acts on seismic mass

Simulation results for the closed loop accelerometer are given in Figure 3.22. Capacitive pick-off circuit is replaced with a simple gain block to reduce simulation time. Such model contains Proportional Integral Derivative (PID) controller for the compensation (Kraft, 1997).

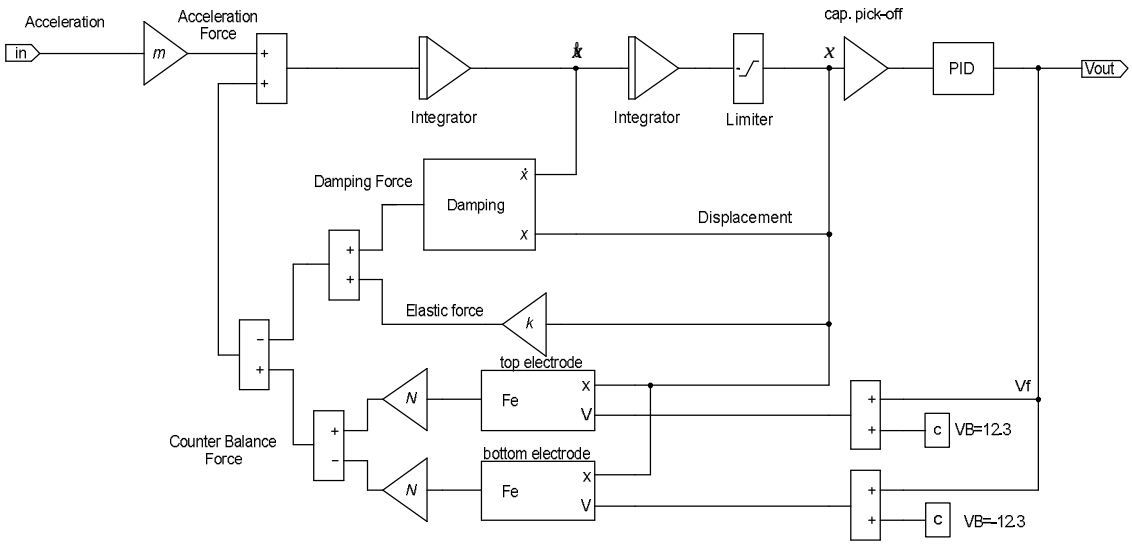

Figure 3.22. SPICE model of a conventional closed loop accelerometer

In first simulation sine wave acceleration signal applied to the conventional closed loop accelerometer with 1, 3, 5 and 7g, respectively. Figure 3.23a shows generated electrostatic counter balance force, Figure 3.23b shows deflection of the seismic mass and Figure 3.23c shows output signal of the accelerometer.

As seen on Figure 3.23, all signals are truly sinusoidal and nonlinear effects such as damping and nonlinear electrostatic force are minimized. For the applied accelerations seismic mass is stayed very close to its rest position. Figure 3.23b, clearly shows that maximum deflection was about 0.11µm for 7g acceleration. It is almost 1/10 of the open loop displacement.

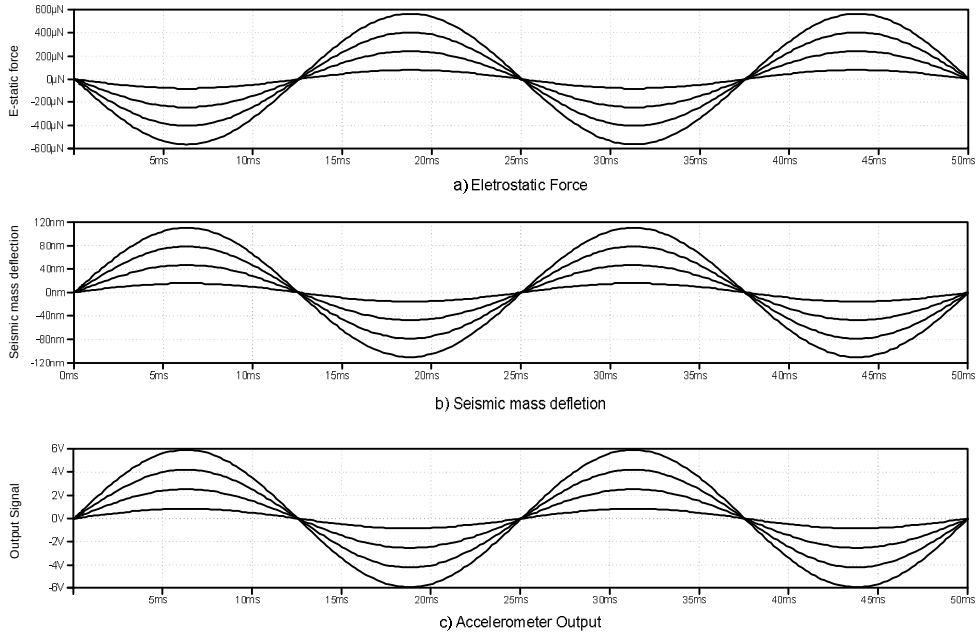

Figure 3.23. Response of closed loop accelerometer to sine wave

In second simulation, step shaped acceleration signals are applied to the conventional closed loop accelerometer with 4g, -3g, 0g and 1g amplitudes. Response of the closed loop accelerometer is depicted in Figure 3.24.

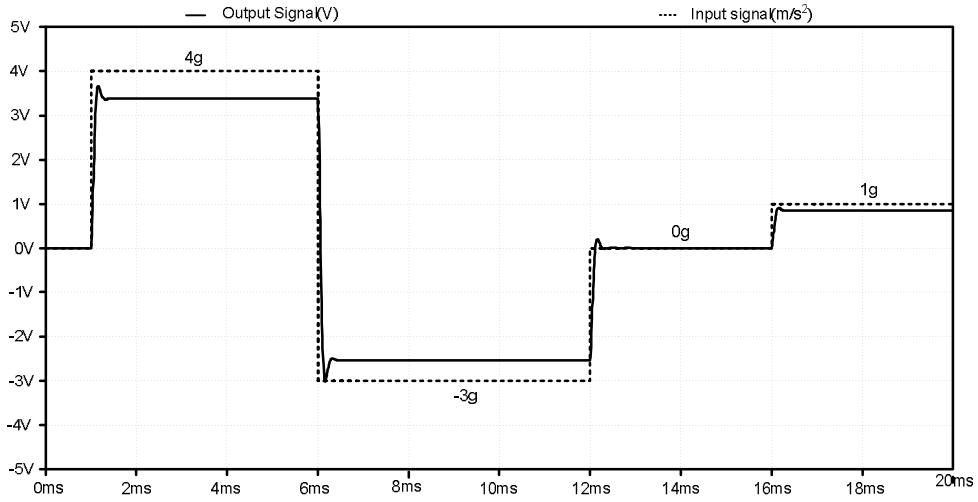

Figure 3.24. Response of closed loop accelerometer to step

As seen on Figure 3.24 conventional accelerometer closely follows the input acceleration with over-shoot. According to simulation results shown in chapter 3.1 MATLAB/Simulink and SPICE results was matched. Thus, closed loop controller for the MEMS accelerometer can be designed with proposed SPICE model.

3.5. Methods

In contrast to the conventional control techniques such as PID, fuzzy logic formulates the control action in terms of linguistic rules. On the other hand, it needs heavy computation burden to translate the fuzzy rules to a control action. A neural network is a nonlinear algorithm which, unlike fuzzy logic, it can be easily worked out because it's mathematical rather than linguistic nature. Moreover, a neural network system can work as nonlinear function approximator. In this way neural network can able to approximate any control relationship of practical interest to learn such a relationship through a training process (Buja & Todesco, 1994).

In this work, neural network control method for closed loop control of MEMS accelerometer is proposed. This method employs and extends techniques of artificial neural network. It is used as a solution of implementing the input-output relationship of an FLS. NN is proposed to ease the control of the computation

burden. Simplified block diagram of the proposed accelerometer is given in Figure 3.25.

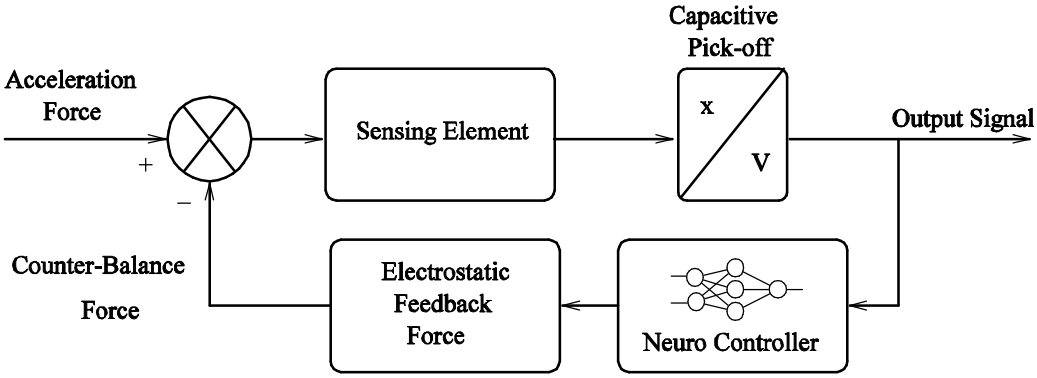

Figure 3.25 Block diagram of proposed accelerometer

Detailed model of the proposed accelerometer is illustrated in Figure 3.26.

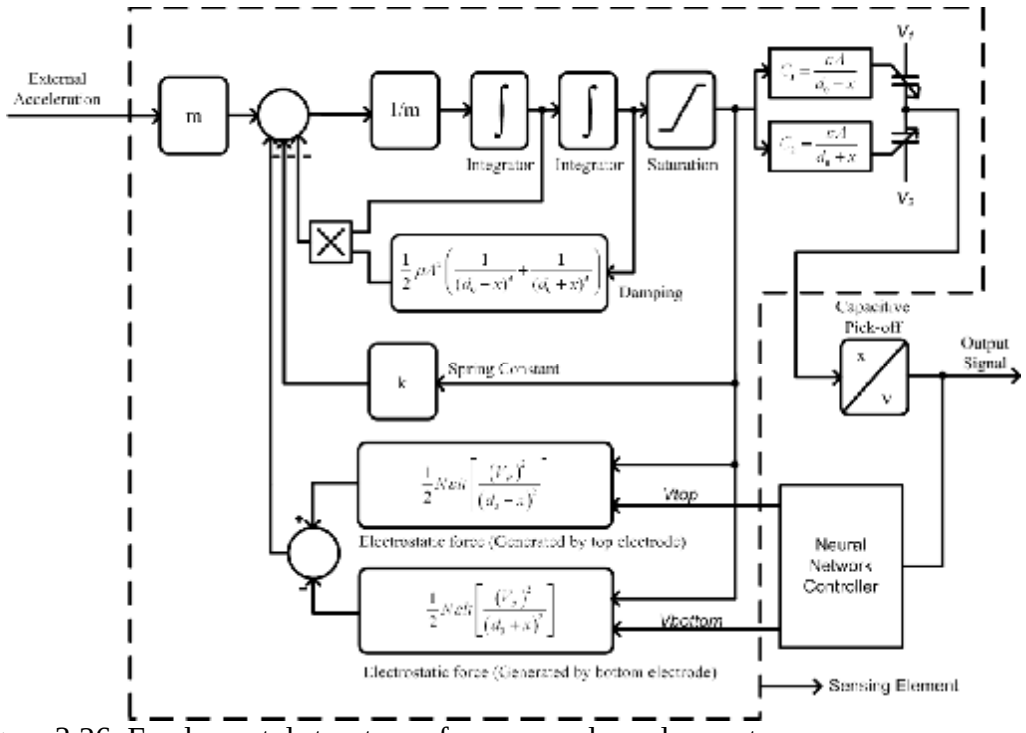

Figure 3.26. Fundamental structure of a proposed accelerometer

It can be seen from the model that illustrated in Figure 3.26 the electrode voltages are generated by neural network controller. Voltage exertion is achieved by applying voltage to the electrode furthest from the seismic mass, the other electrode is grounded. The selection of the energized electrode is done by polarity of the displacement of the seismic mass. In this way only one electrostatic force is

generated on the seismic mass which pulls it back to the central position. Thus negative feedback action is produced even though the forces employed are always attractive. Proposed neural network mimics the behavior of the ∑ΔM controller with fully analog system.

3.5.1. Fuzzy Logic System Design

In recent years, Fuzzy logic has gained much popularity in many control applications. It provides an effective means of capturing the approximate, inexact nature of the real world. Fuzzy Logic System (FLS) is a set of linguistic control rules. It is closer to human thinking and language than the simple logic. In essence, the FLS provides an algorithm which can convert the linguistic control strategy based on expert knowledge into an automatic control strategy (Lee, 1990). The FLS can be designed without the exact model of the system (Kumar et al., 2008).

A short list of applications of FLS includes: Aircraft control, subway operation, automobile cruise control, automatic transmission, space shuttle docking, elevator scheduling, stock market analysis, TV picture adjustment, handwriting recognition, video image stabilizer (Mendel, 1995).

The purpose of designing and applying FLS is to control ill-described and complex plants and processes that can hardly be handled by classical systems theory, classical control techniques, and classical two-valued logic. The fuzzy logic controller directly performs the control actions and thus completely replaces a conventional control algorithm (Chen, 2001).

The majority of FLS is knowledge-based systems in that either their fuzzy models or their fuzzy logic controllers are described by fuzzy *IF-THEN* rules, which have to be established based on expert's knowledge about the systems. Moreover, the introduction of input-output intervals and membership functions are more or less subjective, depending on the designer's experience and the available information (Chen, 2001).

Fuzzy logic has limitations and domains of applicability. As other control system solutions, the fuzzy logic solution may not be always the best solution for any problem.

Limitations of fuzzy logic from a control engineering point of view include:

- Fuzzy logic cannot solve problems that have no known solution. Fuzzy logic requires the knowledge of an expert for generating exact results. It is very useful when there is an expert of system who can map the input set and output set, although there is no mathematical model to follow. If there is no acknowledge solving the problem, fuzzy logic principles cannot be applied.
- Fuzzy logic algorithms do not have the ability to learn membership functions or rules during or after problem solving.
- Extensive verification and validation are required, especially where safety is a key factor (Ibrahim, 2004).
- Computation process of FLS is a complex task that requires heavy computation time and memory (Barsoum, 2000)

Proposed FLS detects displacement of seismic mass and exerts proper electrode voltages. The FLS has the role of providing a linear relationship between the displacement and the electrostatic feedback force.

The Mamdani fuzzy controller has been designed with one input and two outputs. Membership functions and rules are obtained from an understanding of nonlinear behavior of electrostatic feedback force and are modified and tuned by simulation performance. Rules table and the stability of the fine tuned system with simulation performance are justified using the approach in reference (Yi & Chung, 1994).

Fuzzy logic uses linguistic variables instead of numerical ones. The process of converting a numerical variable into a linguistic variable is called Fuzzification. Linguistic fuzzy sets for input of proposal FLS is illustrated in Figure 3.27.

The input has eleven membership functions: NVB, NB, N, NM, NS, Neu, PS, PM, P, PB, and PVB. The N represents negative values, and the P represents positive values. Neu simply means it a neutral value or near zero. If a S,M,B,VB precedes P

or N it means that it is ”small”, ”medium”, ”big”, and ”very big” values, respectively.

The reverse of fuzzification is called defuzzification. The FLC produces the required output in a linguistic variable. According to real world requirements the linguistic variables have to be transferred to crisp output. The defuzzification technique used in this fuzzy controller is a centroid method. It is one of the most commonly used defuzzification strategies in the design of FLS.

This method determines the center of the gravity of the combined membership function. It is also known as center of gravity or center of area defuzzification. This technique was developed by Sugeno in 1985 (Rao & Saraf, 1996).

Figure 3.28 shows the membership functions for outputs. Each of the outputs has six membership functions: Neu, PS, PM, PB, PVB, and PVVB as shown in Figure 3.28. Neu simply means it a neutral value or near zero. ”P” stands for positive. If a S,M,B,VB and VVB precedes P it means that it is ”small positive”, ”medium positive”, ”big positive”, ”very big positive” and ”very very big positive” respectively. Proposed FLS is designed and simulated in MATLAB/Simulink environment with eleven rules. The core of the rule set of the FLS is given in Table 3.3.

Table 3.3. Rule set of FLS

Rule 1: If input is PVB then (V_{top} is PVVB) and (V_{bottom} is Neu)
Rule 2: If input is PB then (V_{top} is PVB) and (V_{bottom} is Neu)
Rule 3: If input is P then (V_{top} is PB) and (V_{bottom} is Neu)
Rule 4: If input is PM then (V_{top} is PM) and (V_{bottom} is Neu)
Rule 5: If input is PS then (V_{top} is PS) and (V_{bottom} is Neu)
Rule 6: If input is Neu then (V_{top} is Neu) and (V_{bottom} is Neu)
Rule 7: If input is NS then (V_{top} is Neu) and (V_{bottom} is PS)
Rule 8: If input is NM then (V_{top} is Neu) and (V_{bottom} is PM)
Rule 9: If input is N then (V_{top} is Neu) and (V_{bottom} is PB)
Rule 10: If input is NB then (V_{top} is Neu) and (V_{bottom} is PVB)
Rule 11: If input is NVB then (V_{top} is Neu) and (V_{bottom} is PVVB)

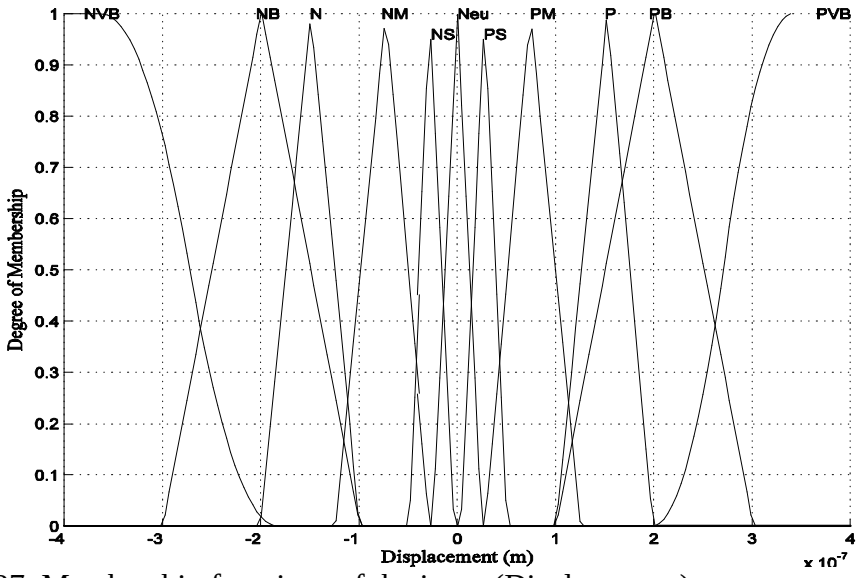

Figure 3.27. Membership functions of the input (Displacement).

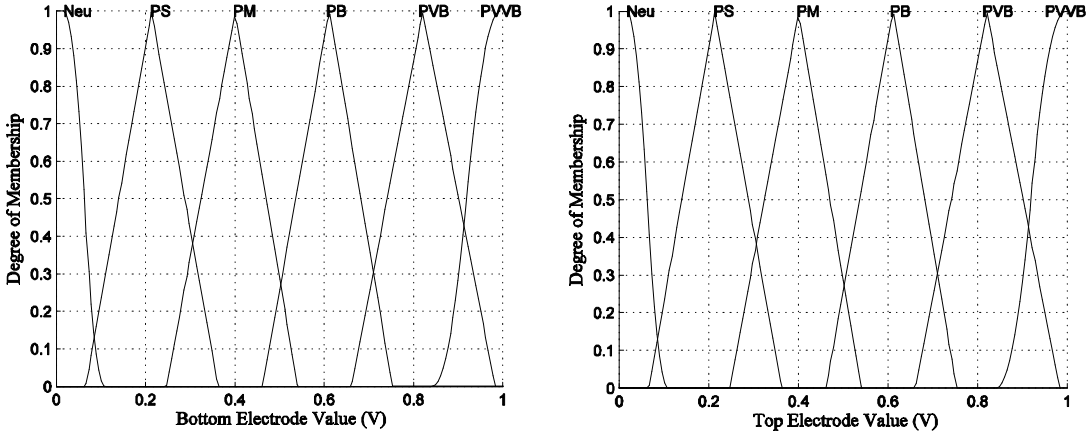

a) Bottom Electrode b) Top Electrode

Figure 3.28. Membership functions of bottom and top electrodes.

According to the fuzzy rule base of input and output, control surfaces are described. The control surfaces are shown in Figure 3.29 and legends V_{top} and V_{bottom} are stand for top electrode voltage and bottom electrode voltage, respectively.

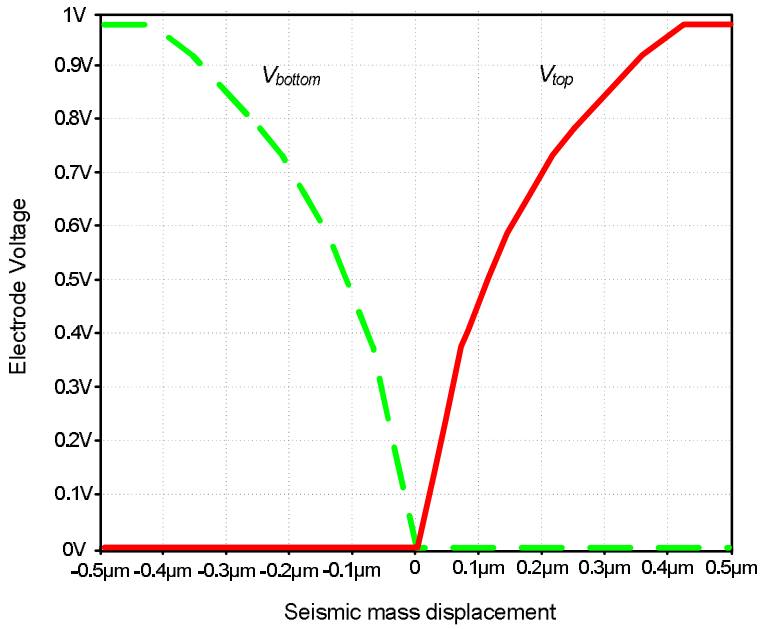

Figure 3.29. Control surfaces of the FLS

As seen on Figure 3.29, at a time only one electrode is active and other is held at zero potential. In other words, only the electrode further away from the seismic mass is excited, the other one is grounded. Proposed accelerometer uses this control method and it is similar to the ∑ΔM.

Consider the accelerometer electrode structure shown in Figure 3.30 in which the movable electrode is suspended by a spring (for simplicity spring is not shown in figure). When no acceleration is applied, the electrodes are separated by a gap d_0.

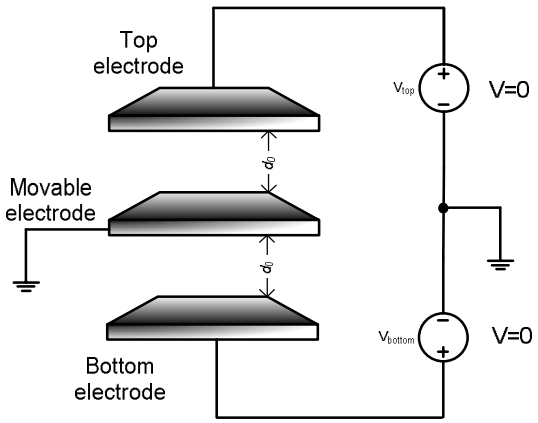

Figure 3.30. Illustration of the electrodes (in rest position)

As the acceleration increases, an electrostatic force is generated and it pushes the movable electrode to its rest position as given in Figure 3.31. Movable electrode is always held electrically ground potential by the mechanical anchors. The force on the electrodes will become very high as the gap is reduced and drops off rapidly as the gap is increased. The force acting on the plates will be inversely proportional to the square of the gap. So, applied voltages have to be nonlinear as given in Figure 3.29.

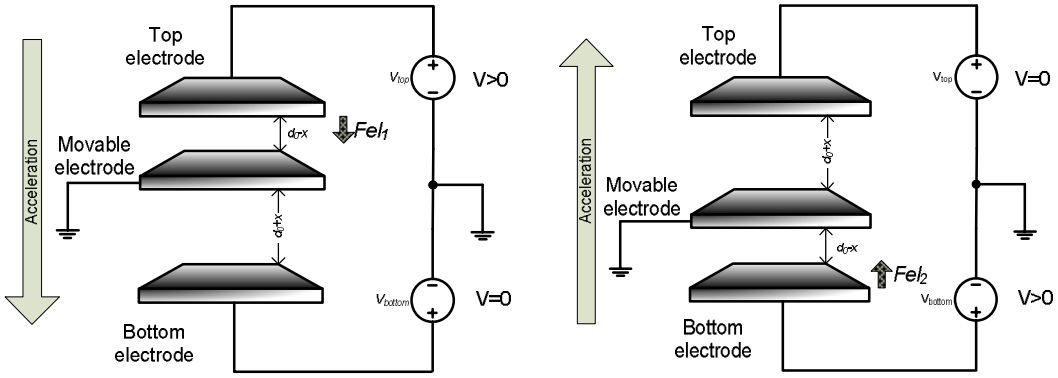

a) Positive displacement b) Negative displacement

Figure 3.31. Illustration of the electrodes in acceleration condition

3.5.2. Neural Network Implementation

In recent years, fuzzy logic and neural networks have received much attention in the control applications. Fuzzy logic is therefore an attractive technique for control of an ill-defined or parameter-variant plant (Buja & Todesco, 1994). On the other hand, computation process of FLS is a complex task that requires heavy computation time and memory (Barsoum, 2000). It has been found that the computation burden in the FLS can be reduced if it could be implemented in an ANN (Kumar et al., 2008). So, from the designed FLS, training patterns are generated and these are used to train the ANN to be a controller (Buja & Todesco, 1994; Kumar et al., 2008).

Artificial Neural Networks (ANNs) are well known systems with their function approximation and system control abilities. ANNs can be used for the identification and control of dynamical systems, mapping the input–output

representation of an unknown system with its control law. ANNs can be implemented in pre-trained mode on hardware. Only transferring weight and bias values of each neuron into memory of controller hardware is required for forward calculation. ANNs can predict the transfer function of a system using input and output data sets.

ANNs are generally realized by simulation programs running on computers. On the other hand both these methods have some disadvantages. Since ANNs are naturally analog and inherently more suited for analog implementation. The analog approach is an attractive alternative for nonlinear signal processing. It provides parallel processing with a speed limited only by the delay of signals through the network. Processing speed of an analog element is much smaller compared to an element in digital ones (Lehmann, 1994).

3.5.3. Artificial Neural Network Model

In engineering point of view the human brain can be seen as an analog computer with huge memory capacity. Human being can recognize faces and understand speech very rapidly and accurately. It is much better than that of any digital computer. For example, it takes about 100-200 msec for the brain to recognize a familiar face on a photograph.

A human brain contains approximately 100 billion (10^{11}) neurons with about 1,000 to 10,000 connections each (resulting in a total of 10^{14}-10^{15} interconnections). A biological neuron is shown in Figure 3.32. Each neuron receives its input from neighboring neurons over special nerve fibres, called dendrites. Their sum builds up an electrochemical potential inside the cell body of the neuron. When this potential exceeds a certain threshold the neuron fibres send signals along the output fibre, called as axon. Although, the axon normally is quite short, it can reach several meters in length. It ends in synapses. These are the connections to the dendrites of another neuron or directly to another neuron (Chible, 1997).

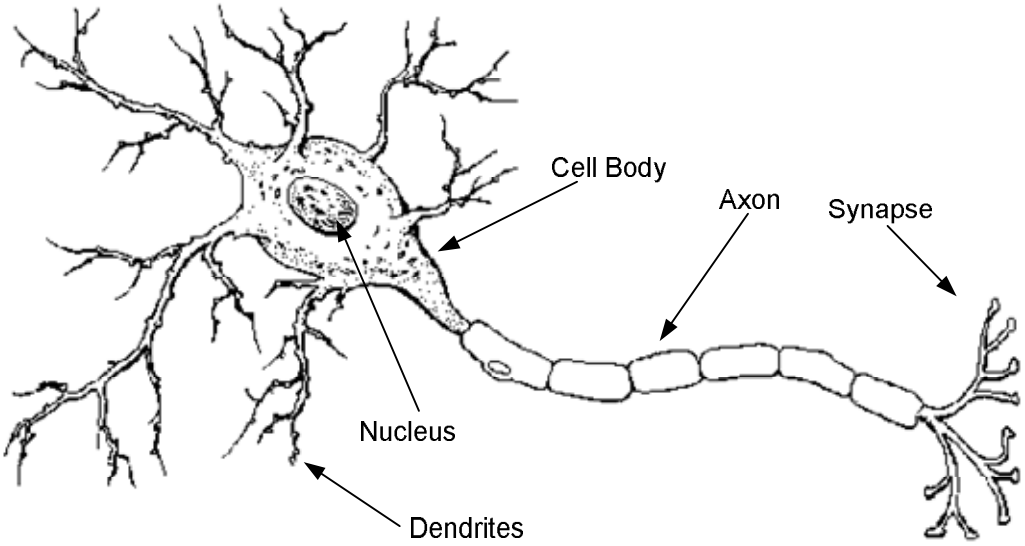

Figure 3.32. A biological neuron

The behavior of an ANN is inspired from the behavior of a real neuron in human nervous system. The ANNs are also called neuro-computing or parallel distributed processing. Neural computing is an alternative to programmed computing (Nascimento Jr, 1994).

Perhaps the greatest advantage of ANNs is their ability to be used as an arbitrary function approximation mechanism learning from observed data. There are many desirable characteristics of human brain which are not presented by von Neumann or modern parallel computers. These include

- massive parallelism,
- learning ability,
- adaptivity,
- fault tolerance.

Modeling a biological nervous system using ANNs also increases our understanding of biological functions. The transmission of signals in biological neurons through synapses is a complex chemical process in which specific neurotransmitter substances are released.

The synapses of the neuron are characterized by weights which are the strengths of the connections between a neuron and an input. Learning occurs in a neural network by adjustment of these connections. Figure 3.33 shows the model for an artificial neuron.

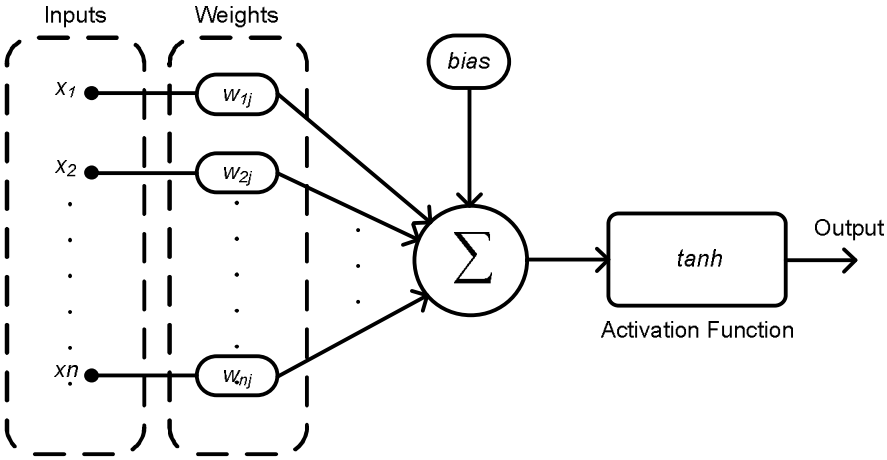

Figure 3.33. McCulloch-Pitts model of a neuron

In the next step, an adder sums up all the weighted input signals. This combination is a linear operation. Finally, the sum of the weighted input signals is passed through the Activation Function (AF) which is typically nonlinear (Haykin, 2006). The given model of artificial neuron was firstly introduced by McCulloch et al. (McCulloch & Pitts, 1943). Originally the neuron activation function in McCulloch-Pitts model was threshold function; however linear, sigmoid and tangent hyperbolic functions are also widely used nowadays.

This artificial neuron computes a weighted sum of its input signals, generates an output. Mathematical, expression for artificial neuron with tangent hyperbolic function is given in Eq. (3.15).

$$y = tanh\left(\sum_{j=1}^{n} w_j x_j\right) \tag{3.15.}$$

where *tanh* is activation function of neuron, w_j is the connection strength or weight of synapse associated with the jth input and x_j is the neuron input.

The intent of the activation function is to model the nonlinear behavior of the cell where there is no output below a certain value of the argument (Sarangapani, 2006). Depending on each particular application a number of these simplified neurons are connected together in different ways. These neurons are arranged in a layered structure to form a network.

The network has a capability to perform massively parallel computations and called as multi layer perceptron neural network. Simplified view of a multi layered neural network is illustrated in Figure 3.34.

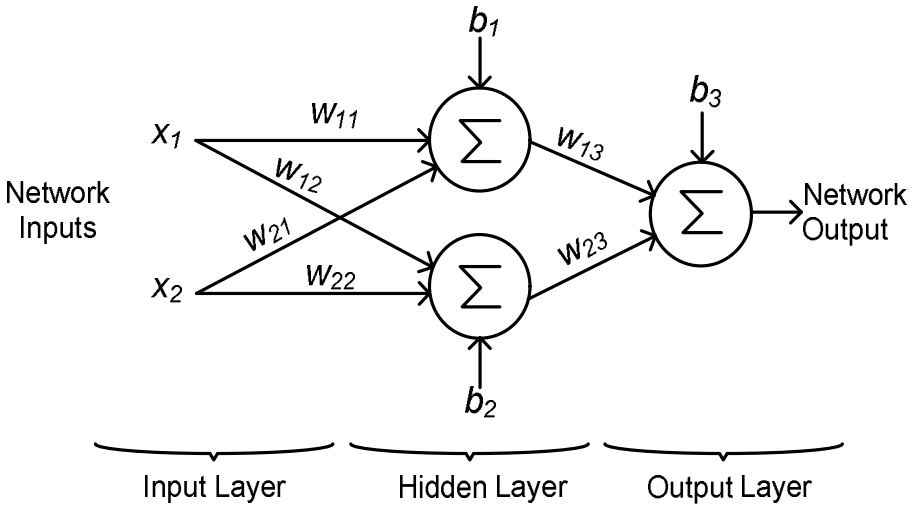

Figure 3.34. Simplified view of a feed forward ANN

The learning problem consists of finding the optimal combination of network weights, so that the network function approximates a given function as closely as possible. There are three different types of learning methods for ANNs. These are supervised learning, unsupervised learning and reinforcement learning. The supervised and unsupervised networks are widely used for function approximation in many fields of control (Haykin, 2006). Proposed neural network in this thesis uses supervised learning algorithm.

The objective in supervised learning is to predict the target values from the input values. The supervised neural network reads the input and output values in the training data set and makes changes on the weight values to reduce the difference between the predicted output and target output values. This is repeated in much

iteration until the neural network reaches specified level of accuracy. Training of proposed ANN is stopped when error goal of less than required i.e. 10^{-4} is reached.

Back propagation, or propagation of error, is a common training method of teaching ANNs to perform a given task. Such learning algorithm looks for the minimum of the error function in weight space. The combination of weights which minimizes the error function is considered to be a solution of the learning problem. Illustration of the learning process is depicted in Figure 3.35.

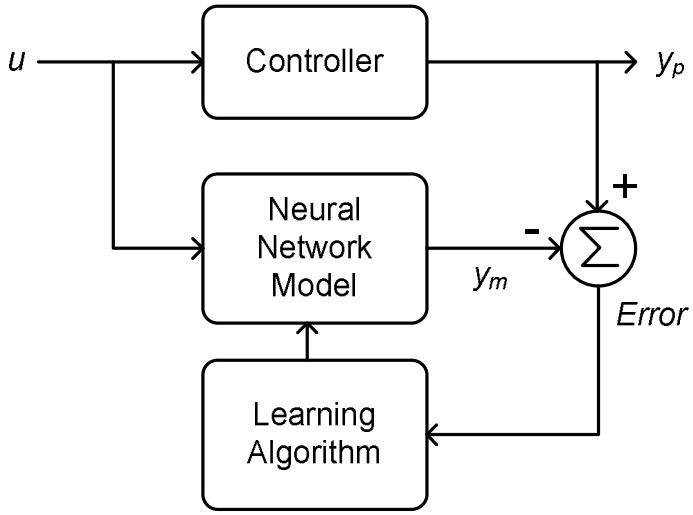

Figure 3.35. Learning process of ANN

Training data set of ANN is obtained from input-output relation of FLS. The controller consists of one input, two outputs and one hidden layer with six hidden neurons. Activation functions of the hidden layer neurons are tangent hyperbolic sigmoid and that of the output neurons are pure linear. Role of the controller is detecting the mass displacement and applying proper electrode voltages.

Block diagram of proposed accelerometer is given in Figure 3.36. The neural network implementation is chosen due to its compatibility in design and implementation with IC technology.

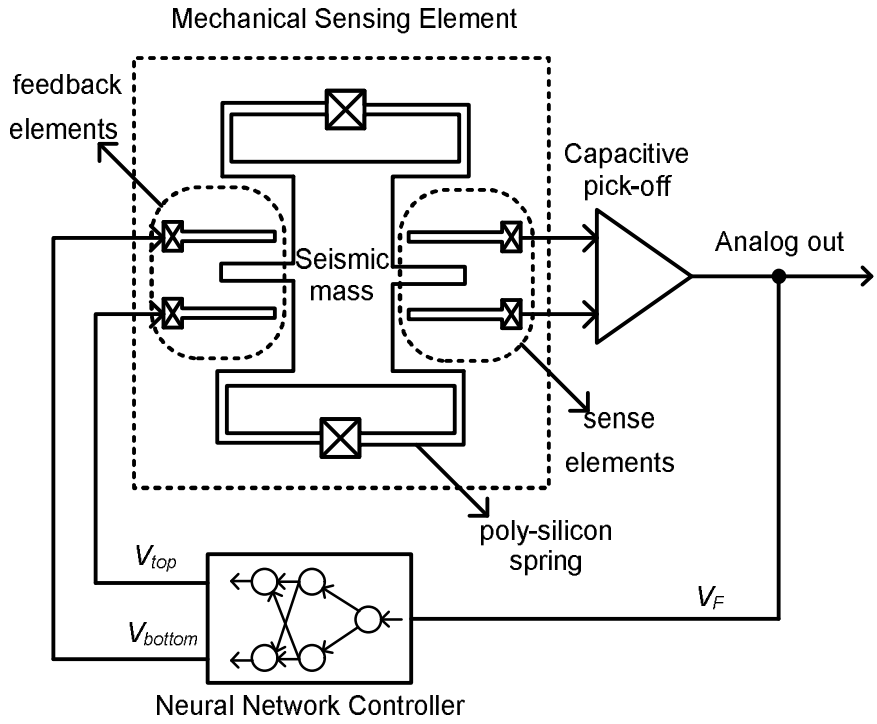

Figure 3.36. Block diagram of proposed accelerometer

Proposed NNC can be implemented with the same die area of mechanical sensing element accelerometer. In addition to closed loop operation of the MEMS accelerometers electrostatics forces is utilized. This force is generated by applying DC voltage to the capacitive electrodes. Some control methods use double sided excitation for generating electrostatic forces. Proposed NNC exerts excitation voltage only one electrode at a time where, the other one is grounded. Applied bias voltages to the electrodes eliminate the nonlinear effects of electrostatic characteristics.

Proposed NNC aims to generate a counter balance force against to inertial force. A reason for the counter balance force is the limiting the displacement of the seismic mass. Advantages of the limited displacement are listed as follows (Beeby et al., 2004).

- Differential change in capacitance is only proportional to displacement for small seismic mass motion.
- Damping mechanism is based on squeeze film effects, only for small seismic mass motion, the damping constant can be assumed as constant

- Suspension system can be assumed as linear only for small seismic mass motion.
- Electrostatic force due to electrical excitation signals can be neglected only for small seismic mass motion.

3.6. Neural Network Hardware

Neural networks are often limited to software, although, they can be implemented on different types of hardware such as Digital Signal Processors (DSP), Field Programmable Gate Arrays (FPGA), Personal computers (PC) and dedicated digital or analog hardware. Hardware realization of neural networks with their generalization capability is useful for numerous signal processing and control applications. Neural networks require a lot of computing time to be simulated on a computer resulting a great difficulty to investigate the behavior of large neural networks and to verify their ability to solve problems. ANN hardware integration has the advantage of achieving signal processing directly.

Digital Signal Processors (DSP) need A/D and D/A circuits to interface with sensors and actuators. This, increases the energy and silicon area budget. From this perspective, dedicated analog implementations can compete for speed and size with DSPs.

The ANN system solves complicated problems by parallel operation of neurons. They allow the neural network to converge at a higher speed than software-based counterparts. Many applications require real time or fast operation. This is possible only with dedicated neural network hardware. Due to the inherently parallel nature of neural networks, they are suitable for VLSI implementation (Bayraktaroglu, 1999).

Every designer has own method and approach which is the most appropriate for their need and resources. Many VLSI neural network implementations can be found in the literature. These implantations can be classified in three groups:

Digital Implementation: In a digital NN implementation, synaptic weights are stored in digital memories such as shift registers and latches. There are standard cell

libraries for arithmetical operations. Merits of the digital implementation are simplicity, high signal-to-noise ratio, easily achievable cascadability and cheap fabrication. Demerits of the digital implementation are conversion of the digital representations. Most of the real world applications required analog forms input since usually input patterns are available in analog form and control outputs also often required to be in analog form.

Analog Implementation: In an analog neuron weights are usually stored using capacitors and floating gate EEPROMs. Activation functions used in software ANN implementations, cannot be easily implemented in VLSI. Some approximation functions are instead considered to act as AFs. Analog elements are generally smaller and simpler than their digital counterparts. On the other hand, obtaining consistently precise analog circuits, especially to compensate for variations in temperature and control voltages, requires sophisticated design and fabrication.

In analog modeling, signals are typically represented by currents and/or voltages which work with real numbers. The main challenges for analog designs are the synapse multiplier over a useful linear range and the storage of the synapse weights.

An analog implementation is usually efficient in terms of chip area and processing speed, but this comes with the price of a limited accuracy of the network components. In a digital implementation, on the other hand, accuracy is achieved at the cost of efficiency. This amounts to a trade-off between the accuracy of the implementation and the efficiency of its performance.

Hybrid VLSI implementation: Hybrid design attempts to combine the analog and digital techniques. Typically, the external inputs/outputs are digital to facilitate integration into digital systems, while internally some or all of the processing is done in analog or vice versa.

In this section, the design, development and simulation of the artificial neural network controller based on the analog implementation technology are discussed in detail. The design library has been implemented in AMI C5N 0.6μm technology and the simulations have been carried out in LTSPICE IV with Level-49 MOS model description. This chapter also includes definitions of fundamental processing

elements of neural network and its peripheral circuits. Also hardware topologies and circuits are discussed.

Proposed neural network controller contains analog and digital components. Analog function blocks are Activation Function (AF) block and multiplier. AF block performs tangent sigmoid hyperbolic function. Hybrid function block is Digital to Analog Converters (DAC). Weight and bias values are stored digitally in EEPROM units. Processing elements such as multipliers and activation functions are analog. For this reason digital to analog conversion is needed. DAC job is achieved by 9+1 bit precision current mode units. Digital Blocks are EEPROM memory cell and its sensing amplifier. Simplified block diagram of ANN is given in Figure 3.37. Detailed explanations of the modules are given following sections.

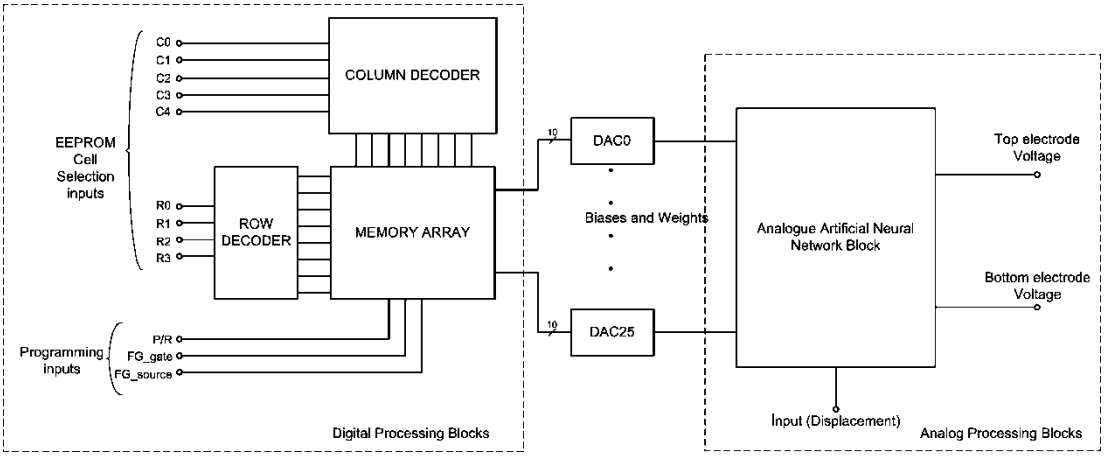

Figure 3.37. Block diagram of Analog ANN

As previously stated above, neural processing elements of proposed NNC are pure analog. Arithmetical operations are realized with voltage input, current output analog blocks. During a neuron operation, the input of the neuron is multiplied by weight matrix; the resultant output is summed and passed through an AF.

In order to neural calculations summing is essential. Specially weighted inputs are summed before passing to the activation function. Current mode output analog multipliers are very beneficial for summing by connecting desired currents together.

In this dissertation, the synapse and neuron circuitry is designed using current mode analog circuits. Current mode signal processing offers several advantages

when used in neural circuits. One of the most apparent advantages is that the summing of many signals is most readily accomplished when these signals are current. In the current domain the summing of analog signals is simply done by connecting the wires. Arithmetic operations, such as summation, subtraction and scaling, are typically difficult to implement and it is often area and power consuming in a voltage mode system.

Other advantage of the current mode implementation is increased frequency of operation due to use of low-impedance internal nodes. The ANN is composed of analog subcircuits such as multiplier and sigmoidal circuits. Activation function block accepts input values as voltage. Current to voltage conversion is a necessity, for this reason a current to voltage converter opamp circuit is designed.

3.6.1. Analog Multiplier

Analog multipliers are useful circuit blocks found in wide area of applications such as modulator, variable frequency filter, oscillator and neural network hardware. Numerous diverse types of integrated multiplier circuits were methodically categorized in reference (Sawigun & Mahattanakul, 2006).

Analog multipliers are easily implemented in CMOS VLSI technology. Many analog multipliers have been proposed in literature (Hollis & Paulos, 1990). Properties of realized multiplier are voltage input, current output, minimum component and capability of making four quadrant multiplications.

These properties make the multiplier very suitable for use in the hardware implementation of ANNs, especially towards modular design. Analog multiplier blocks multiplicities the input data with its corresponding weight.

Since the multiplier is voltage in current out, output of the multiplier can be easily summed. The output currents are summed simply by connecting them to the same node.

Next stage after multiplier is activation function unit. Output range of multiplier must maintain the input range of activation function. Neuron activation

function is generally bipolar value and accepts bipolar valued accepting. This indicates that ANN implementation needs four quadrant multiplier.

This multiplier is termed a four quadrant multiplier because both inputs can be either positive or negative. The ideal output of the multiplier is related to the inputs by

$$I_o = K_m V_{in1} V_{in2} \tag{3.16.}$$

where K_m is multiplier gain . Symbolic view of voltage input current output multiplier is illustrated in Figure 3.38.

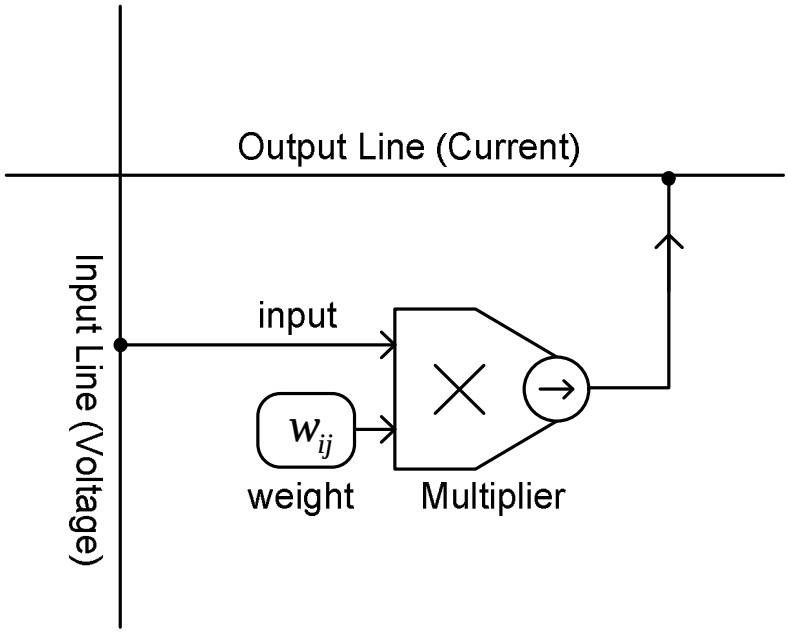

Figure 3.38. Typical electronic synapse

The simplified schematic of CMOS four quadrant multiplier shown in Figure 3.39 is used (Liu, 1994). It has single ended voltage mode inputs and current mode output. Principle of operation of such multiplier is based on the well known identity:

$$(V_1 + V_2)^2 - V_1^2 - V_2^2 = 2V_1V_2 \tag{3.17.}$$

Squaring is achieved using the square relationship between the gate to source voltage and drain current on an MOS transistor in saturation. Simplified circuit

diagram of multiplier is presented in Figure 3.39. Multiplier consists of simply two current mirrors and five MOS transistors. It is required; such five transistors are in working saturation region. According to square law characteristics of saturated MOS transistor, drain currents of M_1 and M_2 are given by:

$$I_1 = K\left(V_{in1} - V_b - V_T\right)^2 \tag{3.18.}$$

$$I_2 = K\left(V_{in2} - V_b - V_T\right)^2 \tag{3.19.}$$

where V_{in1} and V_{in2} are inputs to the multiplier, V_b is bias voltage, V_T is the threshold voltage of the MOS transistors and k_n is the transconductance parameter of MOS transistor.

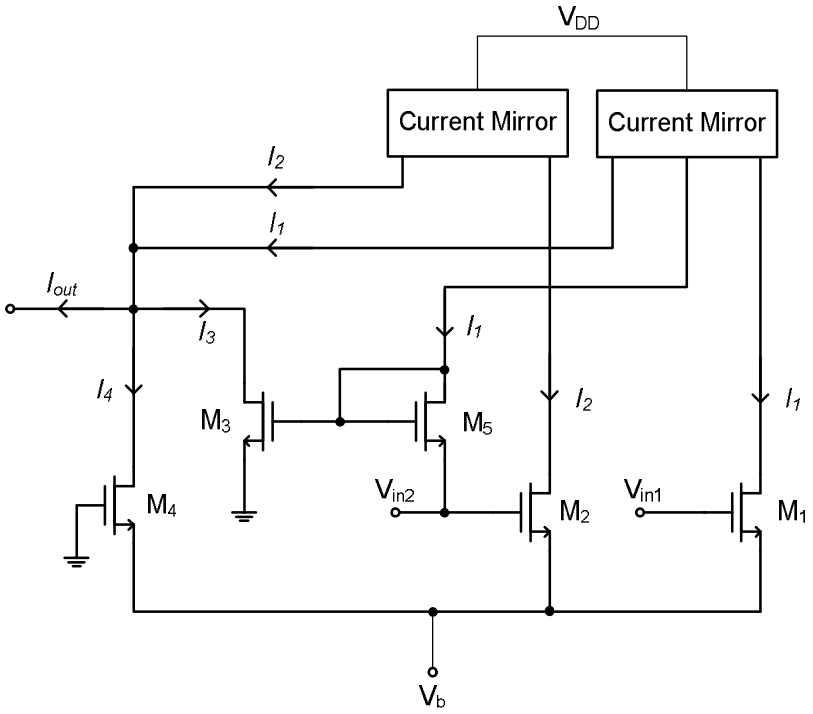

Figure 3.39. Simplified view of four quadrant multiplier

Current mirror keeps the drain currents of M_1 and M_5 in the same value. Since all other parameters are same for these two transistors, the gate source voltages must be equal.

$$V_{GS1} = V_{GS5} \tag{3.20.}$$

$$V_{in1} - V_b = V_{G3} - V_{in2} \tag{3.21.}$$

$$V_{G3} = V_{in1} + V_{in2} - V_b \tag{3.22.}$$

where, V_{G3} is the gate voltage of M_3. The drain currents of M_3 and M_4 are given by:

$$I_3 = k_n \left(V_{in1} + V_{in2} - V_b - V_T \right)^2 \tag{3.23.}$$

$$I_4 = k_n \left(-V_b - V_T \right)^2 \tag{3.24.}$$

Current mirrors feed currents onto the output node. Thus the output current is given by:

$$I_{out} = I_1 + I_2 - I_3 - I_4 \tag{3.25.}$$

Result of this equation gives four quadrant multiplications for single ended inputs as given in Eq.(3.26)

$$I_{out} = -2k_n V_{in1} V_{in2} \tag{3.26.}$$

The (W/L) ratios of MOS transistors used in SPICE simulations are given in Table 3.4.

Table 3.4. (W/L) ratios of the MOS transistors used to realize the multiplier

Device	W/L(μm)
M_1, M_2, M_3, M_4, M_5	4/20
M_6, M_7, M_8, M_9, M_{10}	8/1

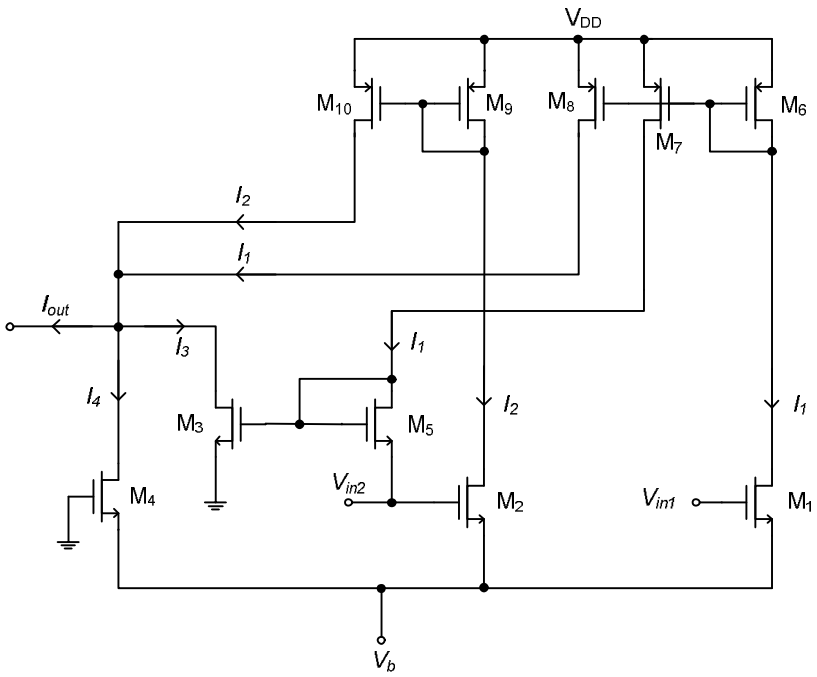

Figure 3.40. Detailed view of four quadrant multiplier circuit

The VLSI layout was produced using Electric VLSI Design System loaded with the MOSIS process design rules. VLSI layout of the four quadrant multiplier is depicted in Figure 3.41.

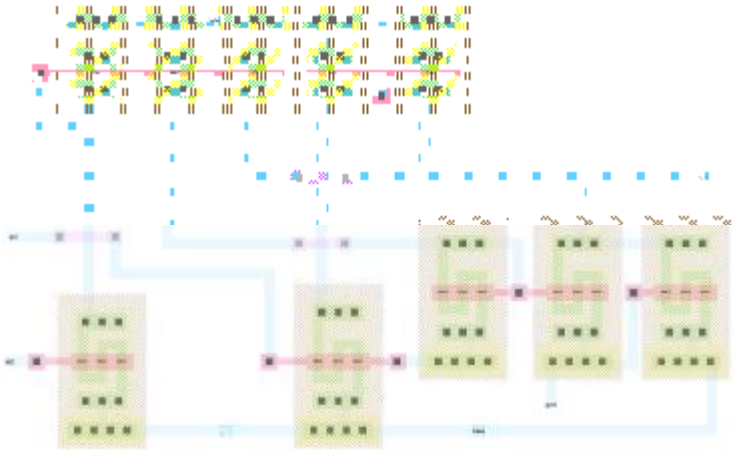

Figure 3.41. Four quadrant multiplier layout

Simulation results show that for a 5V power supply and -2.4V bias, the linear range of the single ended multiplier is more over than ±1V range. Results show that proposed multiplier is good enough for analog neural network implementation.

V_{in1} and V_{in2} are stand for input voltages of multiplier. For range detection purpose, these voltages are swept from -1 to +1 Volt. Performance of multiplier circuit has been evaluated using SPICE and transfer characteristic of analog multiplier is given in Figure 3.42.

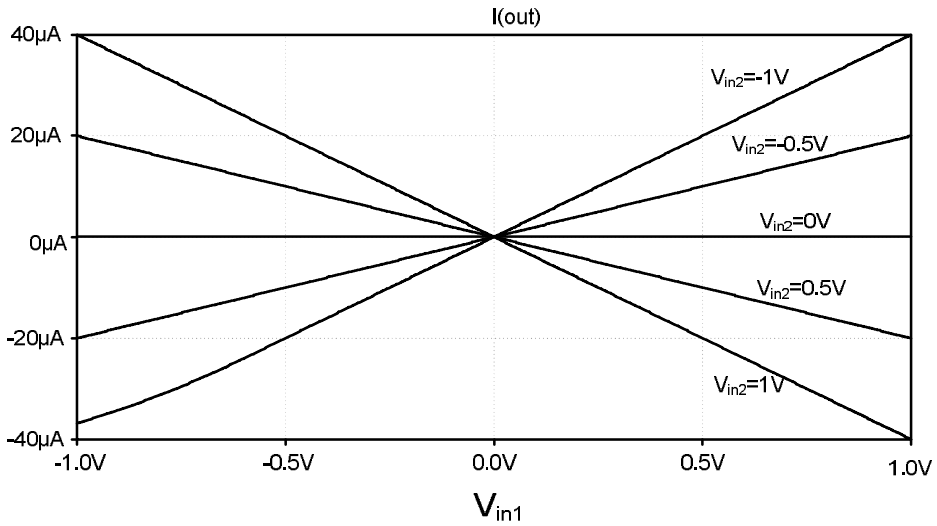

Figure 3.42. DC sweep response of four quadrant multiplier

Behavior of multiplier as a modulator is investigated by feeding it with a sinusoidal voltage of 2 kHz frequency and peak to peak voltage of 500mV amplitude at one input and another sinusoidal voltage of 50 kHz frequency and peak to peak voltage of 100mV amplitude. Figure 3.43 shows the SPICE simulation of multiplier as a modulator.

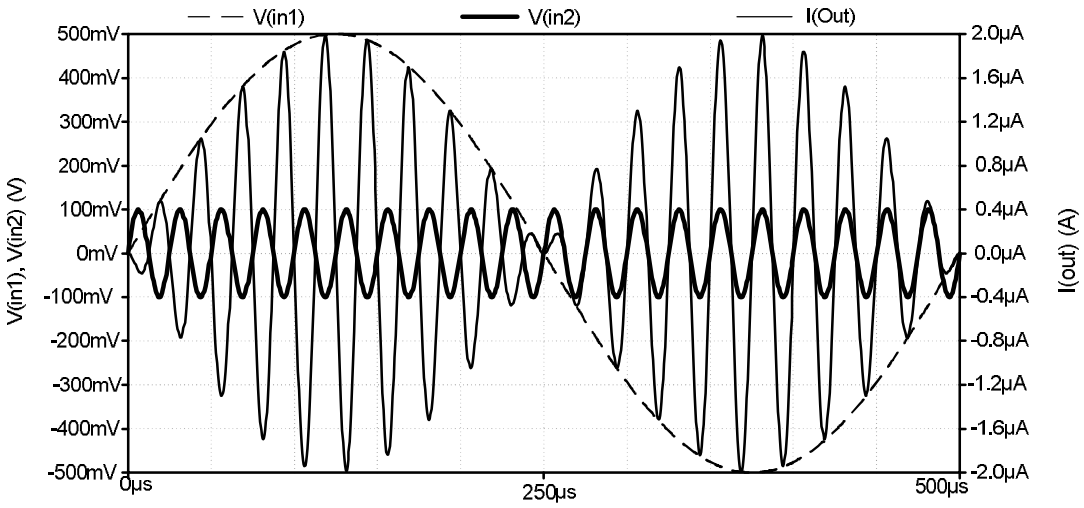

Figure 3.43. SPICE simulation of multiplier as a modulator

Behavior of four quadrant multiplier as a squarer is investigated by applying same input to both input terminals. Figure 3.44 shows the SPICE simulation of multiplier as a squarer.

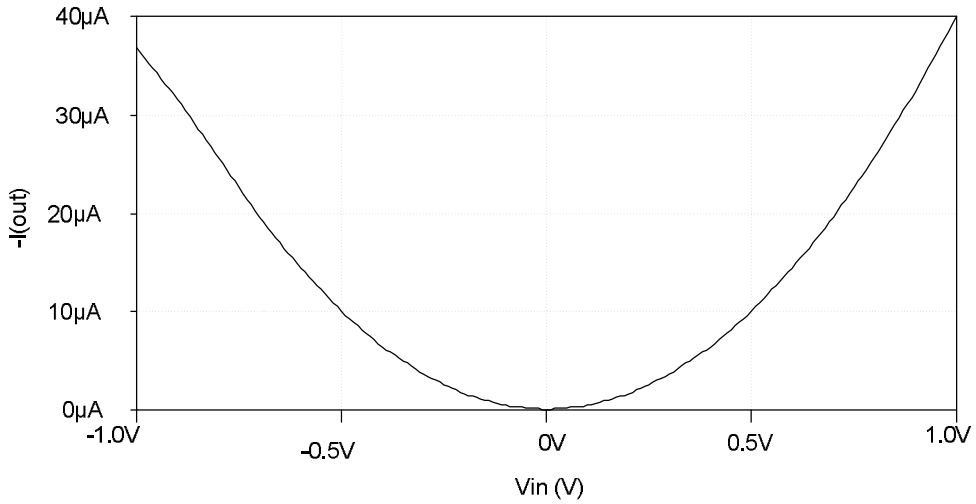

Figure 3.44. Plot of multiplier as squarer

3.6.2. Analog Activation Function

Nonlinear activation functions are essential for neural network operations. The AF of a neuron can be simple limiter, a continuous sigmoid function or linear threshold activation. If the sum of the signals at the input of the neuron exceeds a certain threshold the neuron fires, according to type of the activation function.

An important property of the AF is that a continuous derivative exists, which is desirable when performing back propagation based learning. In conventional feed forward neural networks the most commonly used AFs are sigmoid and tangent hyperbolic (*tanh*). Tangent hyperbolic function is defined in Eq. (3.27) and illustrated in Figure 3.45.

$$\tanh x = \frac{e^{2x}+1}{e^{2x}-1} \tag{3.27.}$$

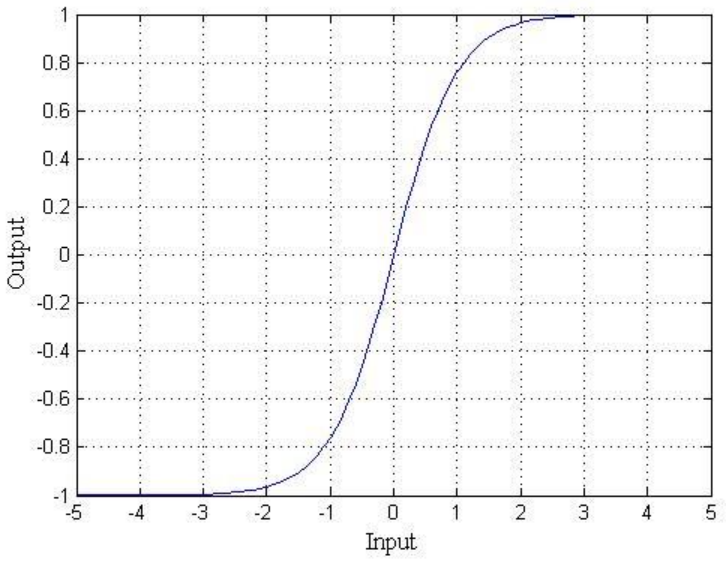

Figure 3.45. Transfer characteristic of an ideal *tanh*

Sigmoid is the one of the widely used neural AFs. It has a wide range of applications in Hopfield networks in addition to being employed in multilayer perceptrons. There are two major variants of sigmoid function. They are the logistic

and the hyperbolic functions. A logistic sigmoid function, also known as a log-sigmoid function, is given by the relationship:

$$s\ (t) = \frac{1}{1 + e^{-b\,t}} \tag{3.28.}$$

The sigmoid functions is similar to the step function, but with the addition of a region of uncertainty. Sigmoid functions in this respect are very similar to the input-output relationships of biological neuron. Graphic of the sigmoid function is given in Figure 3.46.

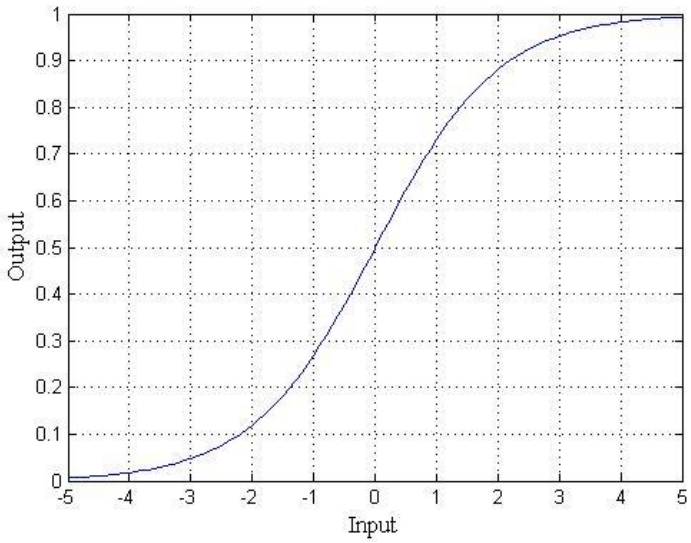

Figure 3.46. Graph of a sigmoid function

An AF can easily be implemented in VLSI without the need of resistors is demonstrated in Figure 3.47. This activation function is made up CMOS differential pair. The MOS differential pair circuit has been widely used as a fundamental building block in most of the analog implementations of neuron circuits.

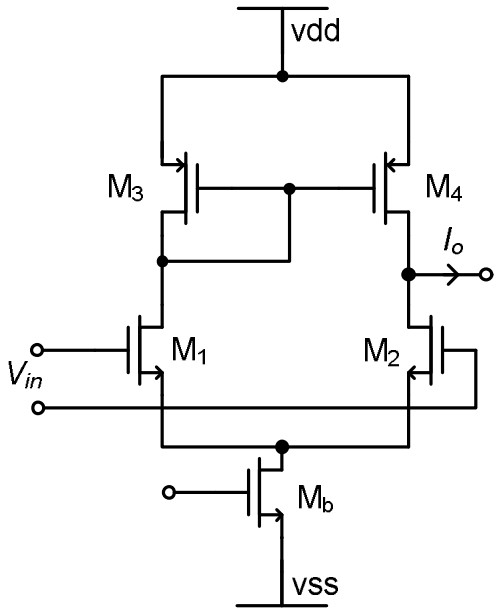

Figure 3.47. Simple MOS differential pair

Much neural network implementation uses some approximation of *tanh.* One of the approximations is digital hardware implementation of the hyperbolic tangent sigmoid function. Digital implementation employs a piecewise linear approximation using a lookup table (Namin et al., 2009). Also there are high accuracy analog examples of such approximations (Al-Ruwaihi, 2002). The proposed circuit is a single circuit that can be programmed to realize different activation functions.

A sigmoid circuit introduced in (Al-Ruwaihi, 2002) is used to generate the activation function on ANN. The design is basically a variation of the differential amplifier. This circuit is used to generate the activation function for the neuron. Circuit diagram of the sigmoid generator and the VLSI layout are given in Figure 3.48 and Figure 3.49, respectively.

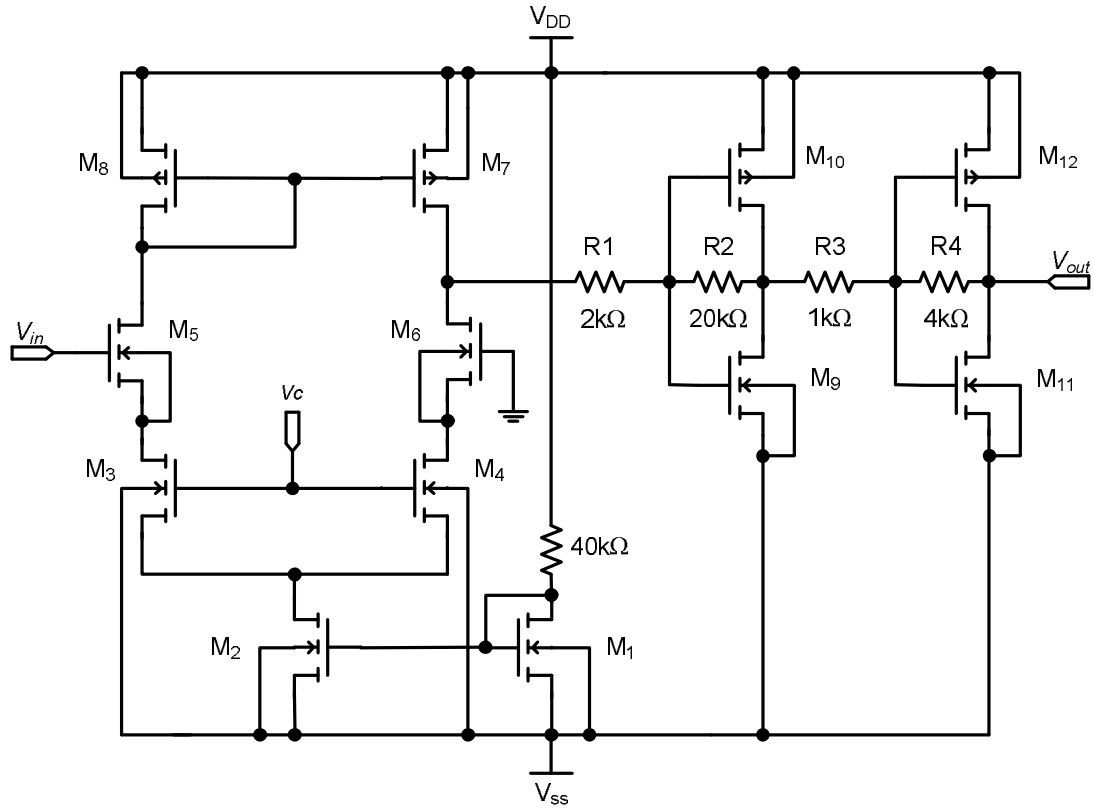

Figure 3.48. Activation Function Circuit

The (W/L) ratios of MOS transistors used in SPICE simulations are given in Table 3.5.

Table 3.5. (W/L) ratios of MOS transistors

Device	W/L(μm)
M_1, M_2, M_{10}, M_{12}	5/2
M_3, M_4, M_9, M_{11}	2/2
M_5,M_6	20/2
M_7,M_8	20/3

Layout of the ativation function circuit is depited in Figure 3.49.

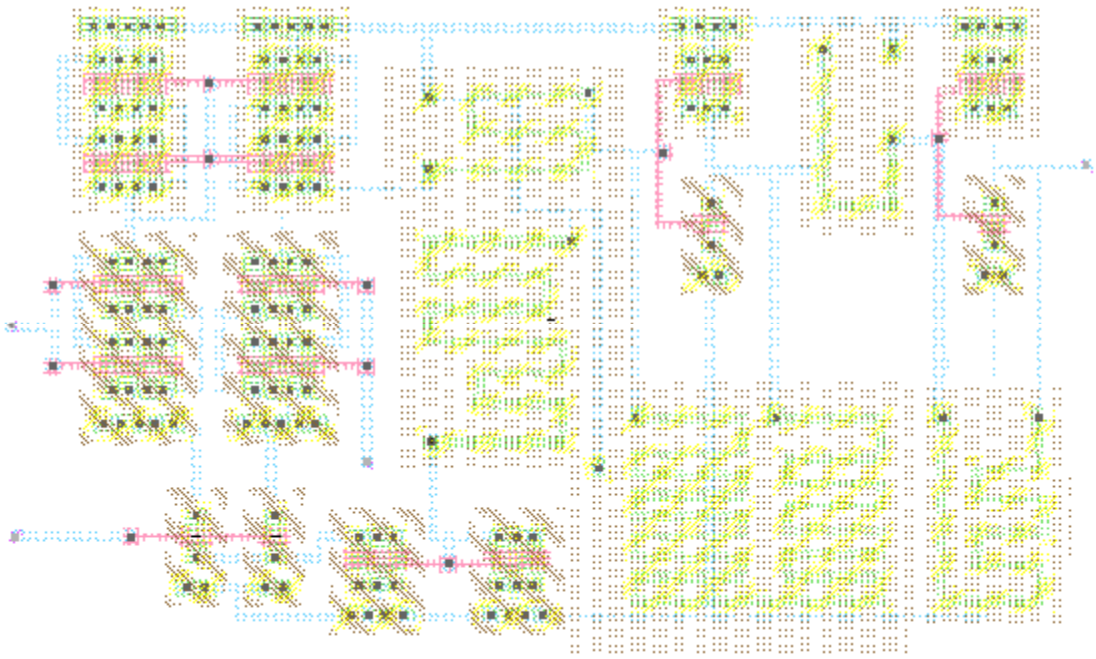

Figure 3.49. Layout of the activation function circuit

Transfer characteristic of the sigmoidal circuit is plotted in Figure 3.50.

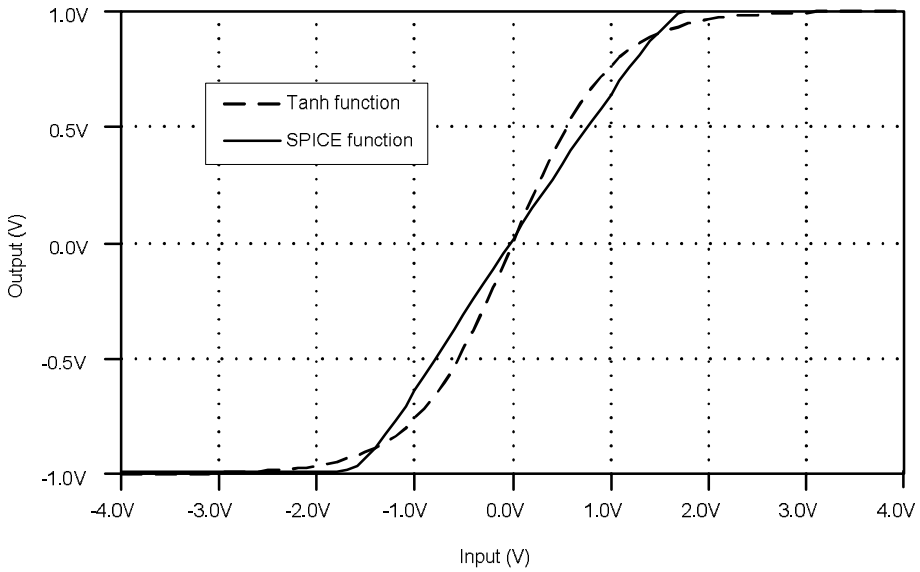

Figure 3.50. Voltage transfer characteristics of activation function.

Hardware implementation of the sigmoid function tends to deviate from ideal function such as the *tanh* function. It becomes necessary to compute the derivative of function actually being implemented which cannot have a simple function form.

As seen on Figure 3.50, characteristic of proposed analog tangent hyperbolic function shows some differences from ideal tangent hyperbolic sigmoid function. CMOS neural network has an activation function different than ideal function so, an approximation function needs to be developed. After that approximation, this function has to be used to train the ANN. The polynomial curve fitting used to approximate the activation function is given in Eq. (3.29)

$$P(x) = P_1 x^5 + P_2 x^4 + P_3 x^3 + P_4 x^2 + P_5 x + P_6 \qquad (3.29.)$$

Coefficients of a polynomial *P(x)* are given in Table 3.6. Polynomial curve fitted function and the original characteristic of differential pair circuit are given in Figure 3.51.

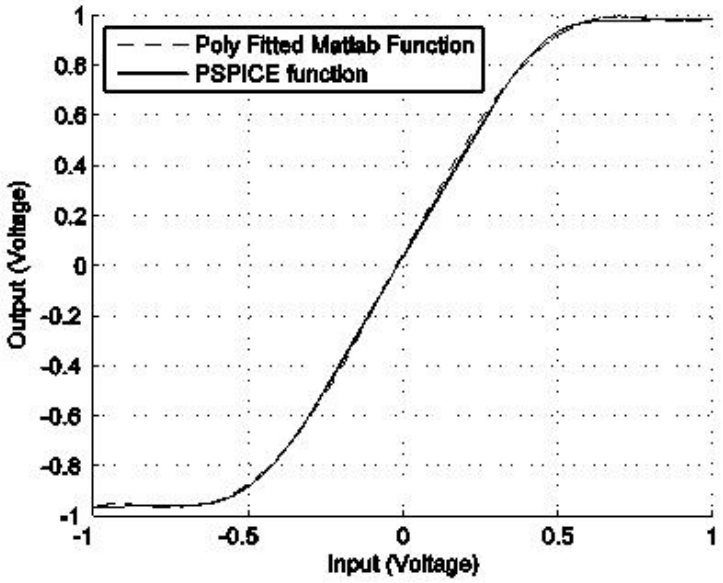

Figure 3.51. MATLAB poly fitted and tangent hyperbolic functions

Table 3.6. Coefficients of a polynomial p(x)

Polynomial Coefficient	Value
P_1	1.0795
P_2	0.0355
P_3	-2.4387
P_4	-0.0560
P_5	2.3379
P_6	0.0308

3.6.3. EEPROM

Storage of synaptic weights and bias values is major concern for analog ANN implementations. Generally, these weight and bias values are stored in analog or digital memories. Analog memories have some advantages over digital ones such as smaller area, lower power consumption and higher dynamic range. As a disadvantage, programming of the analog memory requires longer time and to guarantee the writing of the correct value a precise control circuit is required. Details of this control circuit are given following titles.

Floating Gate MOS (FGMOS) devices are frequently used in analog and digital circuits. Such devices can be easily implemented in 2 poly CMOS processes. Generally, FGMOS devices contain more than one input and can apply different transconductance parameters to such inputs due to layout design. This is advantage of the FGMOS devices over the traditional MOS transistor. Applying different weights to different inputs is the imitating the McCulloch-Pitts neuron model (Kesilmis et al., 2006).

Electrically Erasable Programmable Read-Only Memory (EEPROM) and is a type of non-volatile memory. In this work, the weights and bias values are stored in FGMOS based EEPROM (Diorio et al., 1997).

FGMOS memory devices are useful because of their ability to store an electrical charge for extended periods of time. Today the main market of FGMOS memories is portable equipments, and the applications span from set top boxes, cars, games, computers and other peripherals. One of the greatest advantages of FGMOS

devices is that it is CMOS process compatible. This allows the processing of a single chip containing both a processor and a memory array (Pavan et al., 2004).

The first report of a FGMOS was made by Kahng et.al. This device can store charge between the high impedance gates (Kahng & Sze, 1967). The current interest in FGMOS circuits started from developing large-scale computations in neural systems, which are inherently analog. In 1989 Intel employed the FGMOS as an analog nonvolatile memory element in its ETANN (An Electrically Trainable Artificial Neural Network) chip (Holler et al., 1989).

Circuit symbol and the simplified VLSI layout of the FGMOS are shown in Figure 3.52. FGMOS is the same as the regular MOSFET with an additional gate added. The new gate gets places just above the original gate. The new gate is named as control gate.

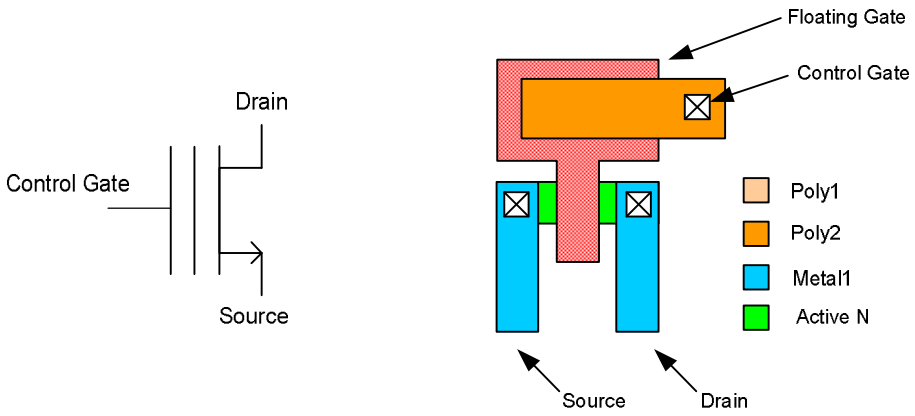

a) Circuit symbol of FGMOS b) Simplified layout of the FGMOS

Figure 3.52. Symbol and layout of the FGMOS

FGMOS devices can be modeled as a MOSFET and capacitors used to couple control voltages to the floating gate as shown in Figure 3.53. Resistance and capacitance values are obtained from reference (Sinencio, 2010). Control gate surrounds the floating gate, so after the programming charge trapped on the floating gate remains there. In Figure 3.53, V_{FG} value represents the threshold variation after the programming.

The charge stored on the floating gate can be modified by applying voltages to the source; drain and control gate terminals, such that the fields result in phenomena like Fowler-Nordheim tunneling and hot carrier injection.

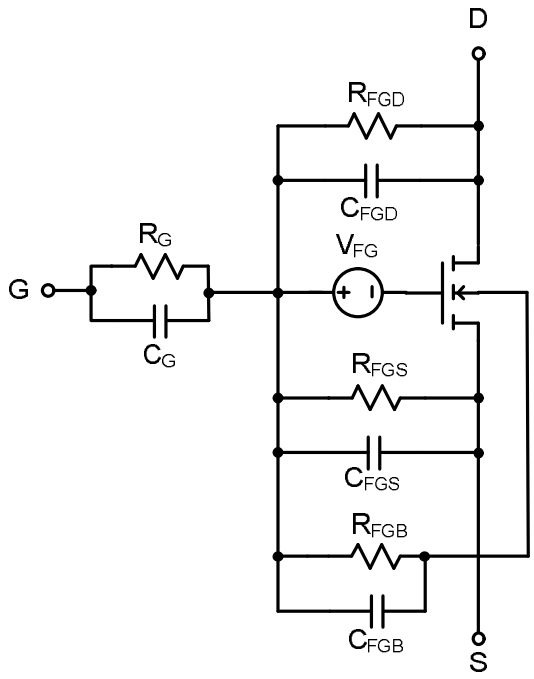

Figure 3.53. Equivalent circuit model of a FGMOS

Cross-section view of the FGMOS is depicted in Figure 3.54. As previously decelerated, purpose of the floating gate is to trap electrons behind the gate area. Since the gate is electrically isolated from the other components electrons can neither enter nor leave this region under normal operating conditions. This phenomenon is allows the FGMOS to be used as non-volatile memory.

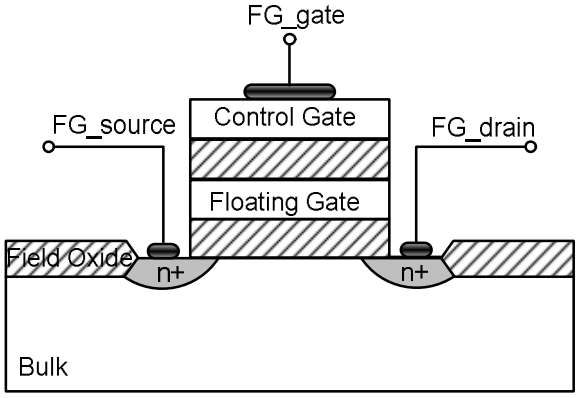

Figure 3.54. Floating Gate MOSFET

Programming of FGMOS device is realized by Fowler-Nordheim tunneling effect. Thomsen and Brooke were firstly demonstrated use of electron tunneling in a FGMOS that allowed without requiring access to specialized fabrication processes (Thomsen & Brooke, 1991). Programming of the FGMOS is rather simple. A 12V potential at the control gate forces electrons in the substrate to tunnel through the dielectric and be deposited in the floating gate. Programming method of FGMOS is illustrated in Figure 3.55.

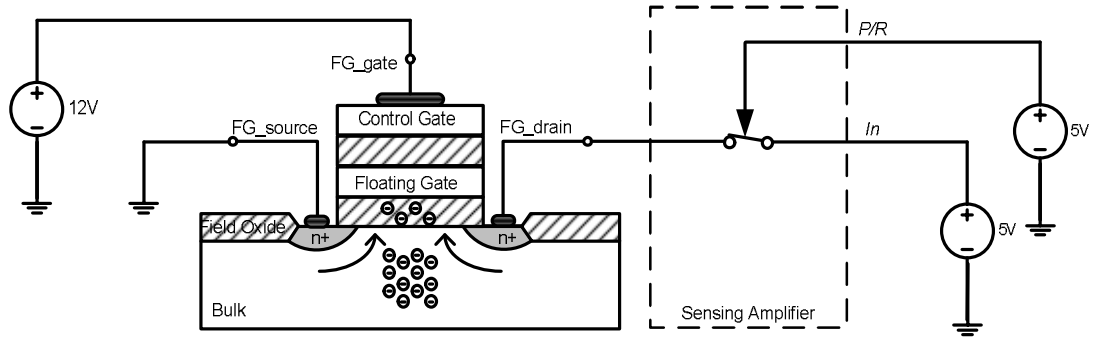

Figure 3.55. Programming of a FGMOS

In order to an erase operation the control gate is grounded and a 5V voltage applied to the source. This forces the electrons trapped in the floating gate to move to the substrate as shown in Figure 3.56.

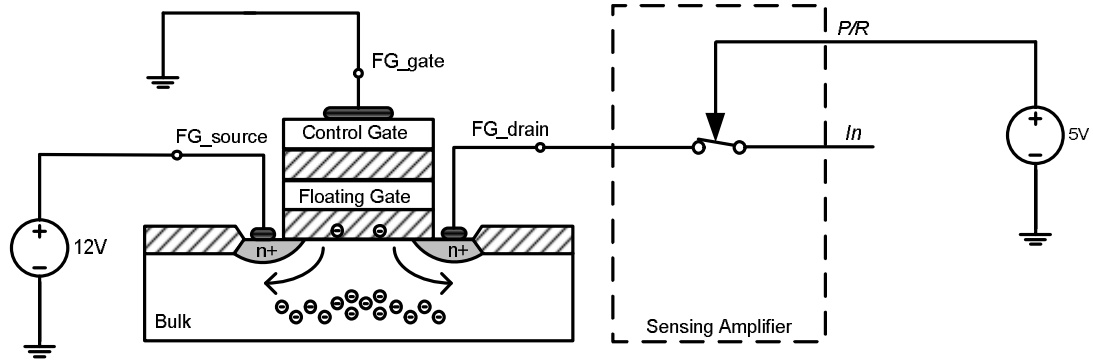

Figure 3.56. Erasing of a FGMOS

3.6.4. Sensing Amplifier

In order to erasing, writing and charge sensing operations of FGMOS cell sensing amplifier circuit is utilized. Circuit diagram of sensing amplifier is shown in Figure 3.57. Sensing amplifier consists of three NOT gates, two transmission gates and a diode connected MOS. Sensing amplifier contains five input/ouput ports. These are *P/R* for mode selection, *In* for programming, *output* to supply ADC modules with bit values, *FG_gate* and *FG_source* for applying various voltage values in order to writing and erasing modes.

The *P/R* input is a mode selection input that selects between reading and writing modes. Applying a logic "1" value to *P/R* input activates the writing mode. Also, applying a logic "0" value activates the reading value. The other input *In* is programming input that provide 5V while system is in programming mode. All *In* pins of the FGMOS memory units are directly connected together. In programming mode desired memory cell can be easily selected by using address decoder circuit. Outputs of the FGMOS cells directly connected to the ADC modules. In working mode, sensing amplifiers produces corresponding bit values without need of the row or column decoders.

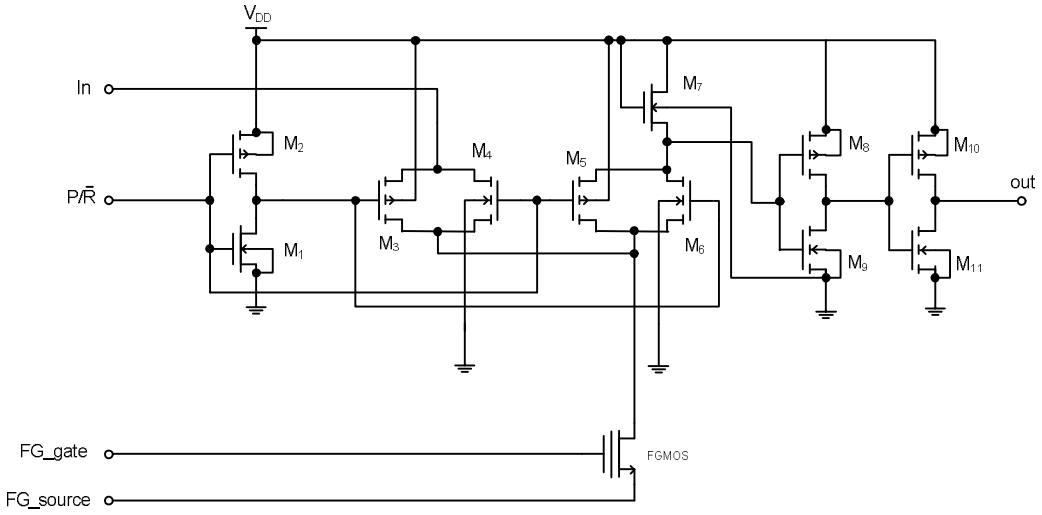

Figure 3.57. Sensing amplifier Circuit

Layout of the sensing amplifier circuit with FGMOS is given in Figure 3.58.

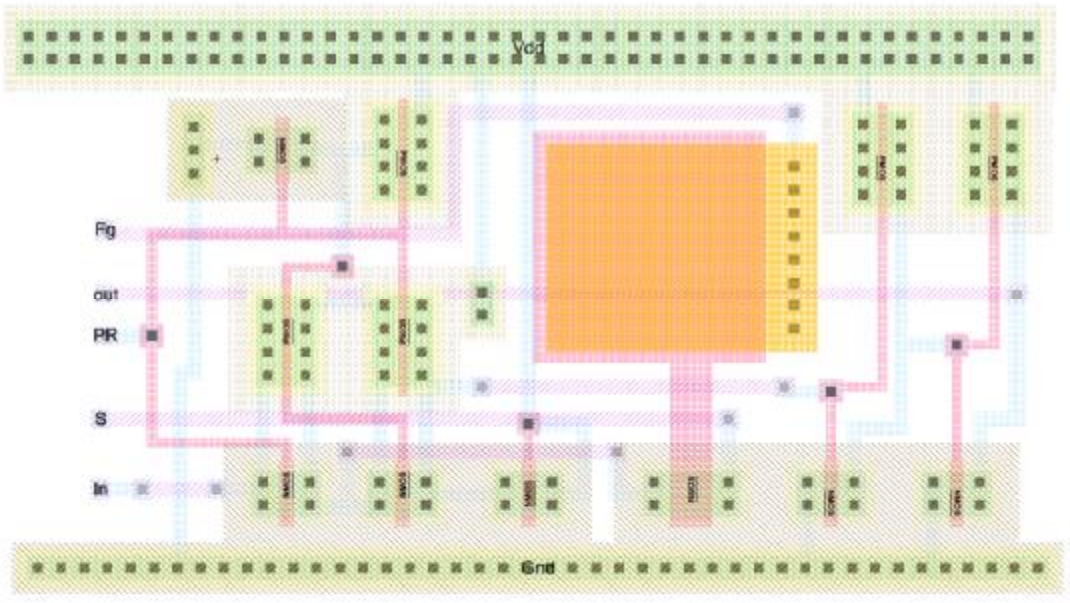

Figure 3.58. Layout of the sensing amplifier

Block diagram of the sensing amplifier with FGMOS cell is given in Figure 3.59. Sensing amplifier has got two modes, one is detecting the charge of FGMOS and other is writing the bit value.

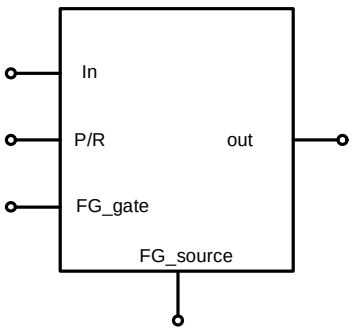

Figure 3.59. Block diagram of the sensing amplifier

A simulation has been done to obtain charge detection ability of the sensing amplifier and result is depicted in Figure 3.60. Programmed FGMOS holds some charge between floating gate area and this charge can be deleted by using sense amplifier. It can be clearly seen from Figure 3.60 charges above the 1.5V range is assumed as logic “1” by the sensing amplifier.

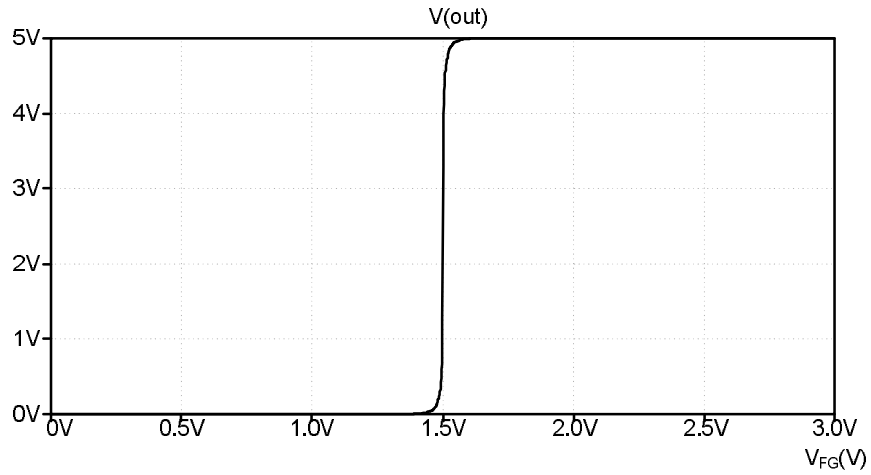

Figure 3.60. Voltage Transfer characteristics of sensing amplifier

3.6.5. Address Decoder Circuits

Address decoder circuits are specially designed for writing process of the EEPROM. For this purpose 4x10 (column) and 5x26 (row) decoder circuits have been designed. By using decoders, all of EEPROM memory array can be easily selected and programmed. EEPROM modules have been designed to hold 10 bit data but one bit is reserved for sign bit. So, EEPROM array holds 9 bit data and one sign bit for the neural calculations. Sign bit represents negative or positive value of the data. DAC modules generate positive or negative output according to sign bit.

AND gates are essential for the decoder circuit design. For the assembly of the decoder structure two, four and five input AND gates are designed. Circuit symbol and the detailed schematics for the two input AND gate are illustrated in Figure 3.61.

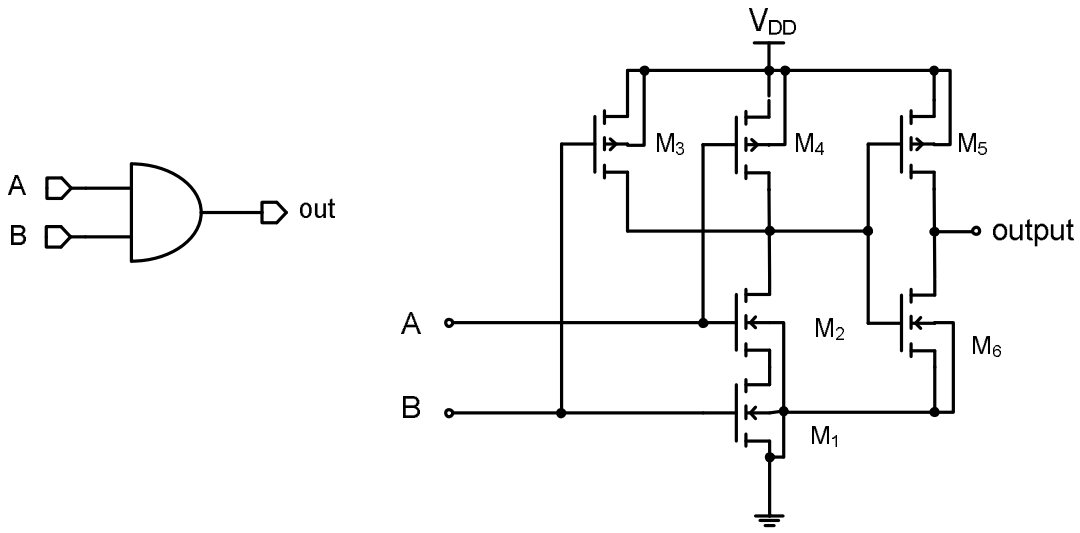

a) Symbol b) Schematic

Figure 3.61. Two input AND gate

Layout of the two input AND gate circuit is depicted in Figure 3.62.

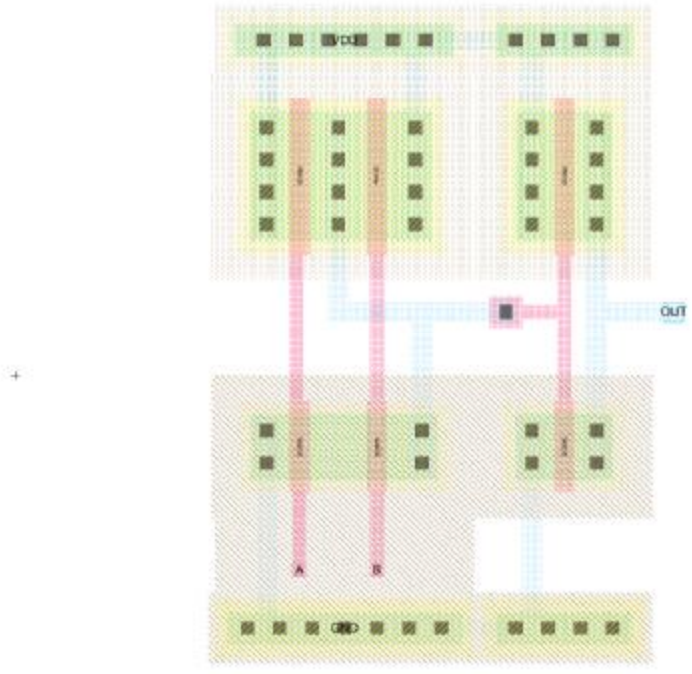

Figure 3.62. Layout of the two input AND gate

Circuit symbol and the detailed schematics for the four input AND gate are illustrated in Figure 3.63

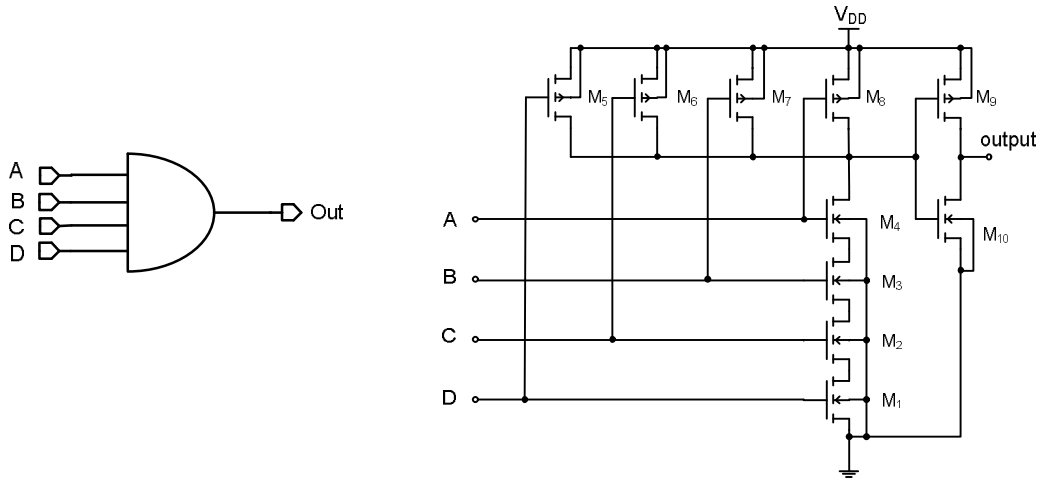

a) symbol b) Schematic

Figure 3.63. Four input AND Gate

Layout of the four input AND gate is depicted in Figure 3.64.

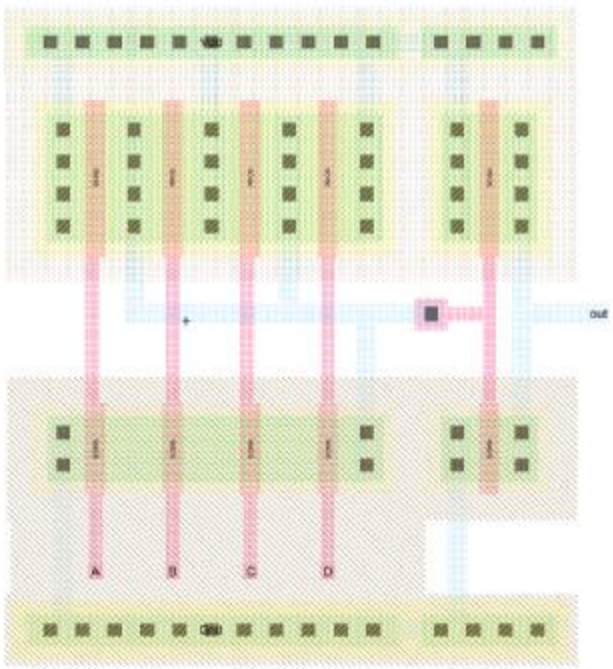

Figure 3.64. Layout of the four input AND gate

Circuit symbol and the detailed schematics for the five input AND gate are illustrated in Figure 3.65

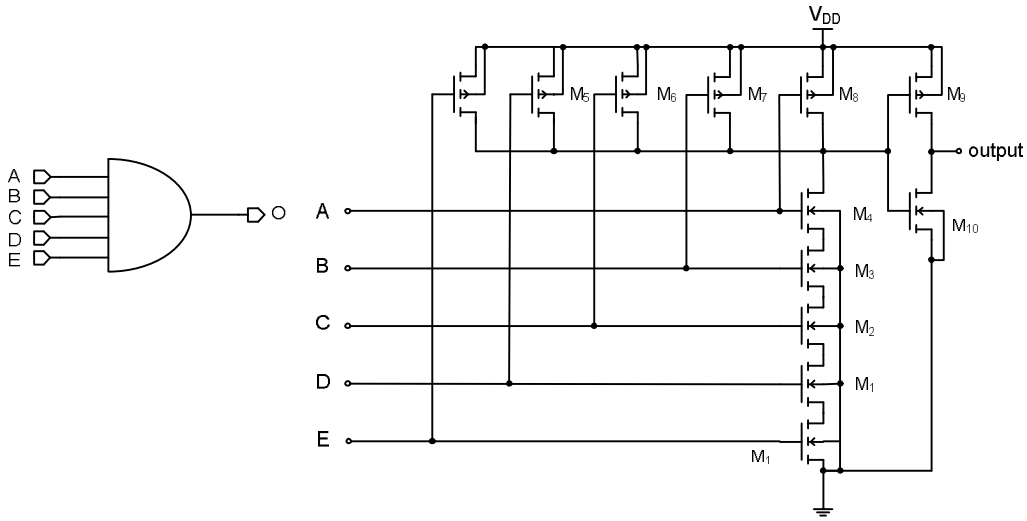

c) symbol d) Schematic

Figure 3.65. Five input AND gate

VLSI layout of the five input AND gate is depicted in Figure 3.66.

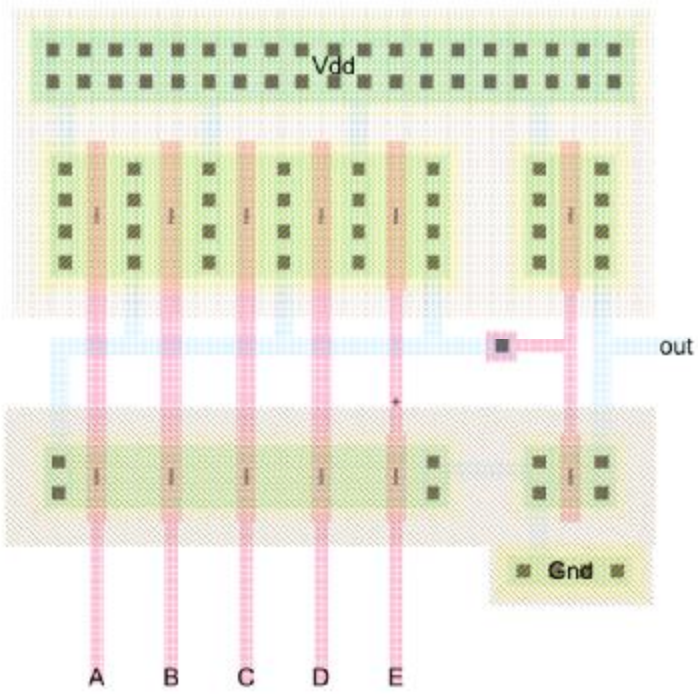

Figure 3.66. Layout of the four input AND gate

As previously stated, address decoders are enables the selection of the EEPROM memory cells in programming. 4x10 decoder 5x26 decoder use four and five input AND gates, respectively. Block diagram of the 4x10 and 5x26 address decoder circuits are illustrated in Figure 3.67. Detailed circuit diagram of the 4x10 address decoder is given in Figure 3.68.

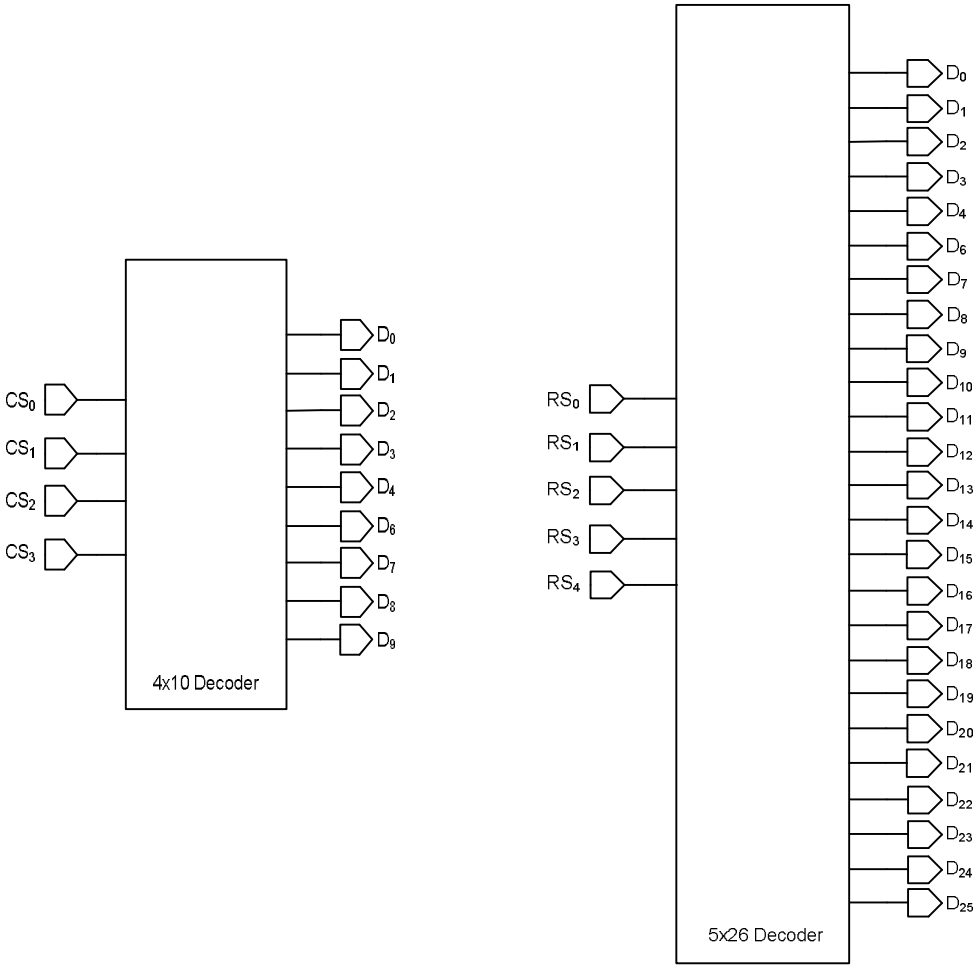

a) 4x10 Decoder b) 5x26 Decoder

Figure 3.67. Block diagrams of decoders

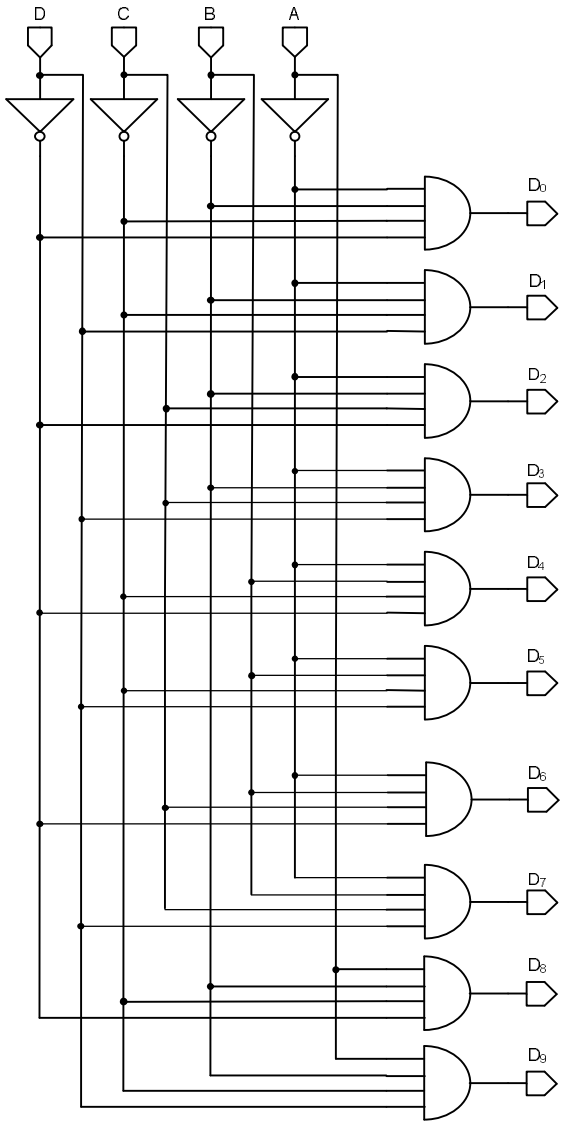

Figure 3.68. Row decoder block

Layout of the row decoder block is given in Figure 3.69.

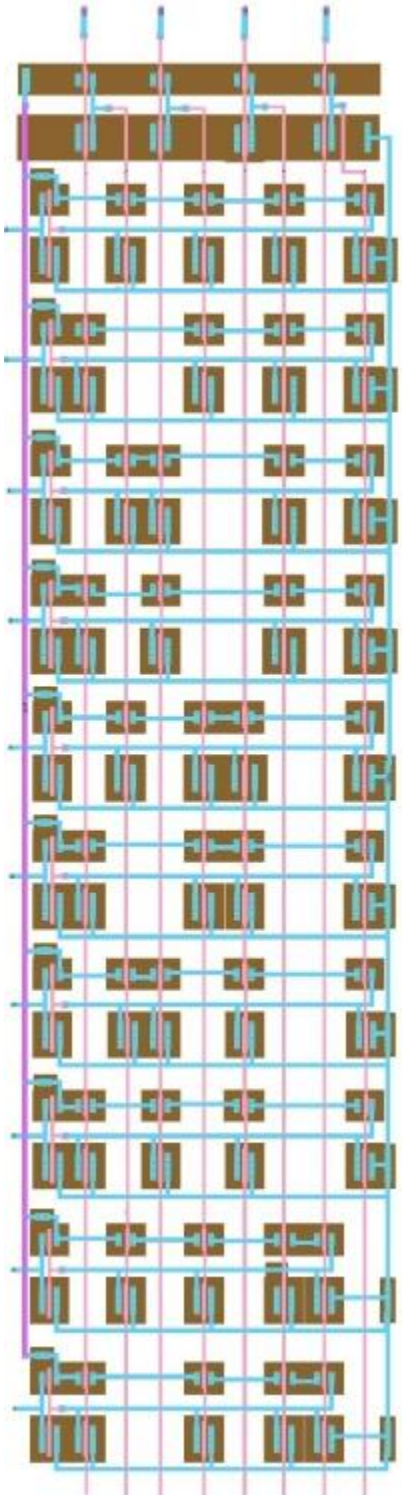

Figure 3.69. Layout of row Decoder

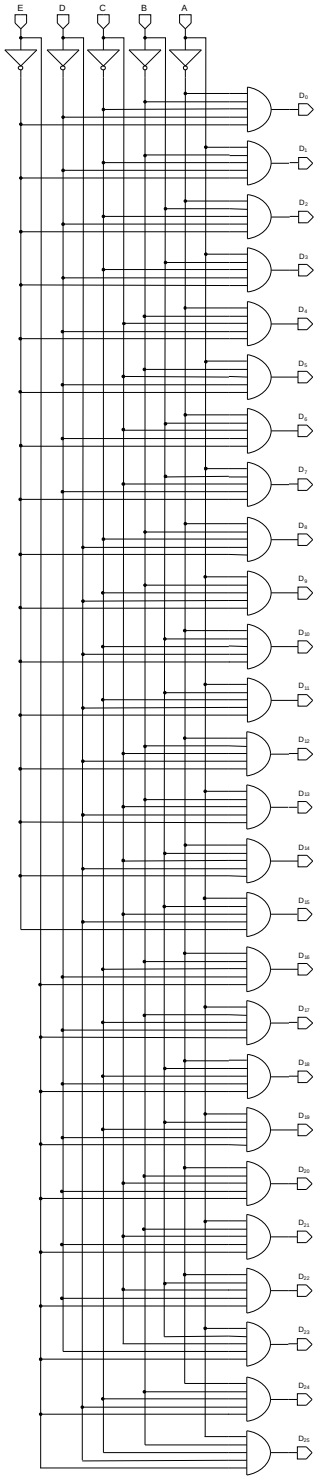

Figure 3.70. Column Decoder

VLSI layout of the column decoder block is given in Figure 3.71.

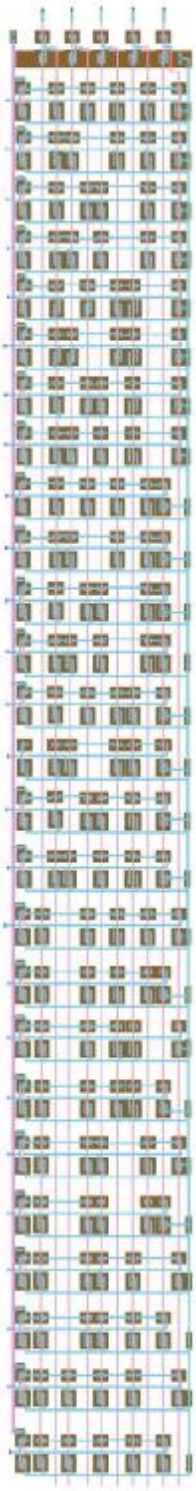

Figure 3.71. Layout of column decoder

Simplified block diagram of the 10bitx26 EEPROM modules is given in Figure 3.72. As seen on figure EEPROM module consists of 4x10, 5x26 decoders and FGMOS cells. Outputs of the FGMOS directly connected to the corresponding ADC modules.

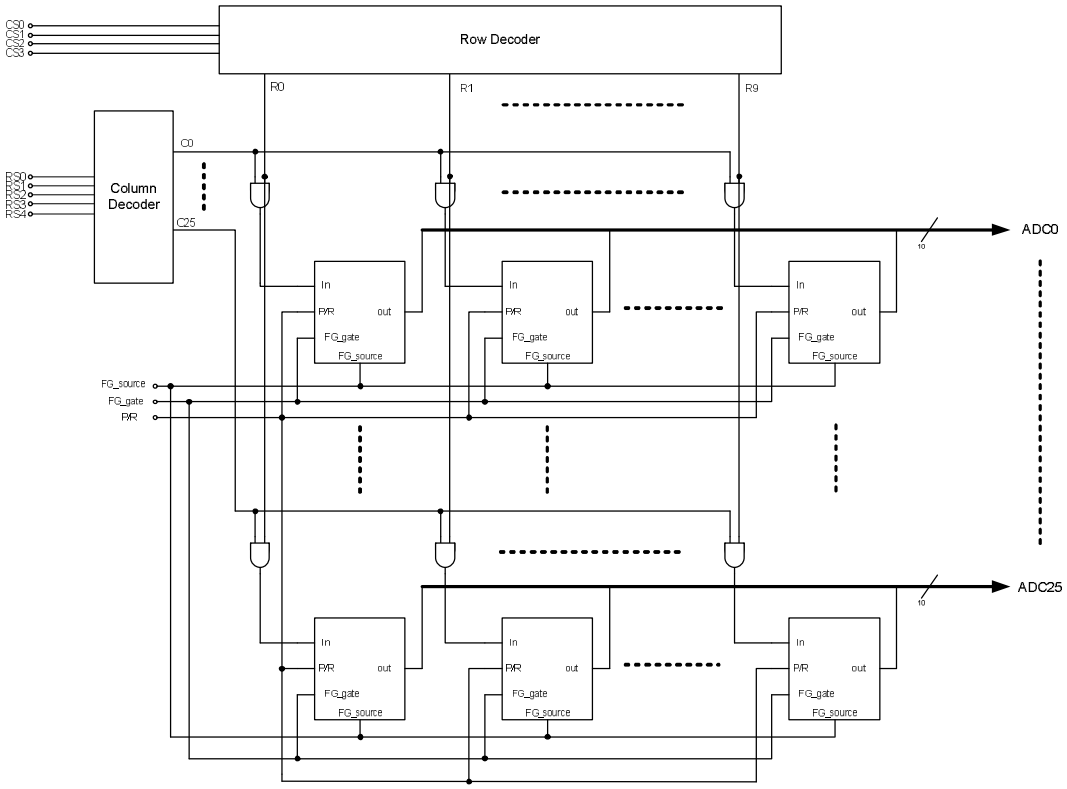

Figure 3.72. Block diagram of the EEPROM

3.6.6. Digital to Analog Converter

Weight and bias values of the proposed neural network are digitally stored in EEPROM. Current mode Digital to Analog Converter (DAC) circuits utilized to convert these values to analog. Such DAC is designed as binary weighted. Illustration of simplified current mode binary weighted DAC is shown in Figure 3.73. An n-bit DAC of this type consists of n-weighted current sources (which may simply use current mirrors) in the ratio $1:2:4:8\ldots2^{n-1}$. (Zumbahlen, 2008).

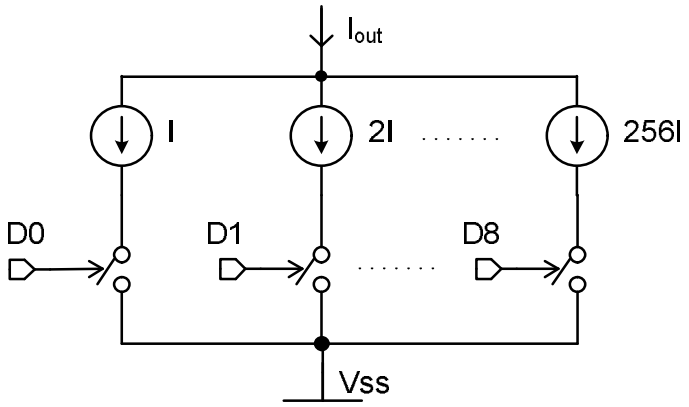

Figure 3.73. Current-mode binary-weighted DACs

Schematics of a nine bit DAC with a sign bit depicted in Figure 3.74. Proposed DAC is consists of 9 bit binary weighted current sources. *W/L* ratios of the MOS transistors M_1-M_9 are 1/1, 2/1, 4/1, 8/1, 16/1, 32/1, 64/1, 128/1, 256/1 (μm). Such DAC is programmed via EEPROM cell array to generate nine bit resolution weight and bias values. The sign bit controls the direction of the output current and is turned on for a negative current output. When the sign bit is turned on, the drain current of the M_{11} is copied to that of M_{13} and M_{14}. By pulling down the drain current of M_{11} with twice as much using M_{13} and M_{14}, the direction of the output current becomes opposite compared to a positive output current. Consequently a negative weight or bias value can be produced. An op amp based circuit is added to perform the current-to-voltage (I/V) conversion. This implementation generates weight and bias voltages in range of +1,-1V. (Ota & Wilamowski, 1994)

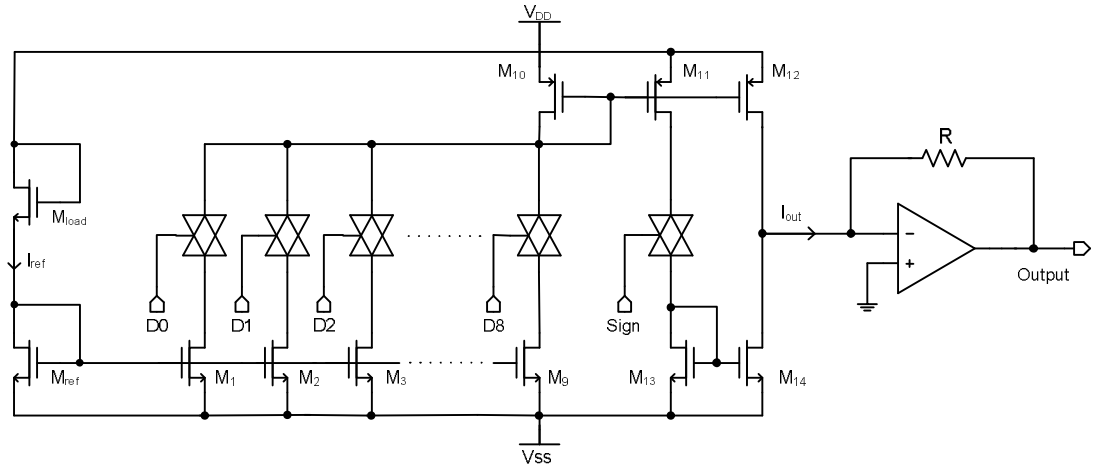

Figure 3.74. 9 bit DAC with 1 sign bit

During the working mode of neural network circuitry weights and bias values remain constant.

3.6.7. Operational Amplifier

The operational amplifiers (OPAMP) are fundamental building block of analog circuits. Analog circuits can perform many types of signal filtering, arithmetic operation and current to voltage conversion. OPAMPs are commonly used for these tasks as well as for generic derivative, integrator and gain circuits especially in PID controller. Designed OPAMP is used to realize current to voltage conversion. Circuit symbol of the OPAMP and detailed design are illustrated in Figure 3.75 and Figure 3.76, respectively.

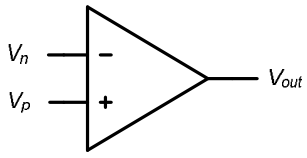

Figure 3.75. Circuit symbol of the OPAMP

Such OPAMP consists of differential amplifier, gain stage and output buffer stage. Operation range of the OPAMP circuit is [-1V, +1V]. Voltage transfer characteristic of the OPAMP as an inverter is given in Figure 3.78. Output current of the proposed OPAMP is varies from -1.15mA to 1.13mA. Simulation results show that OPAMP circuits have good performance.

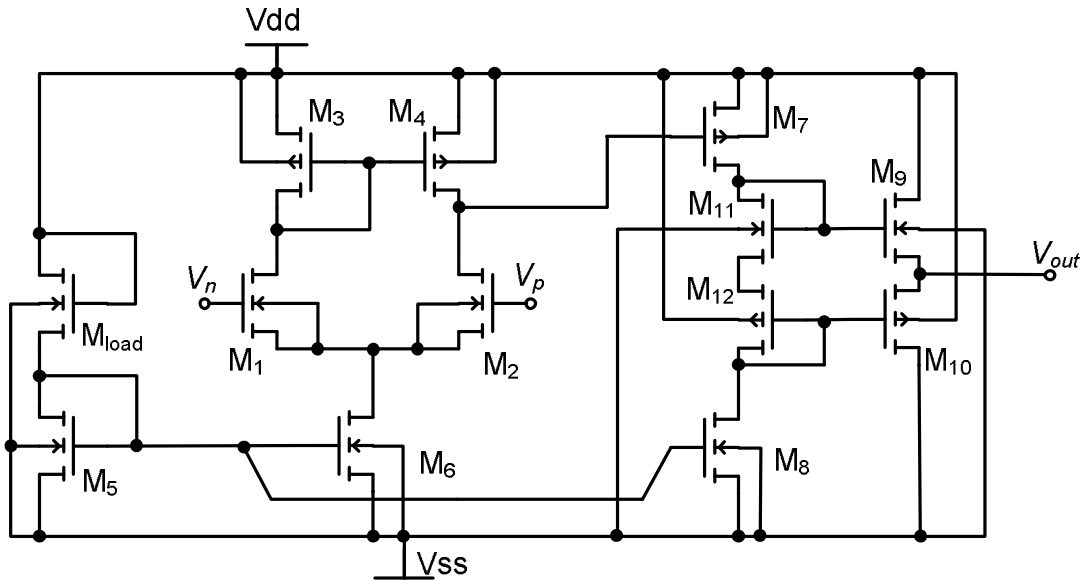

Figure 3.76. Schematic of Operational amplifier

Layout of the OPAMP circuit is depicted in Figure 3.77.

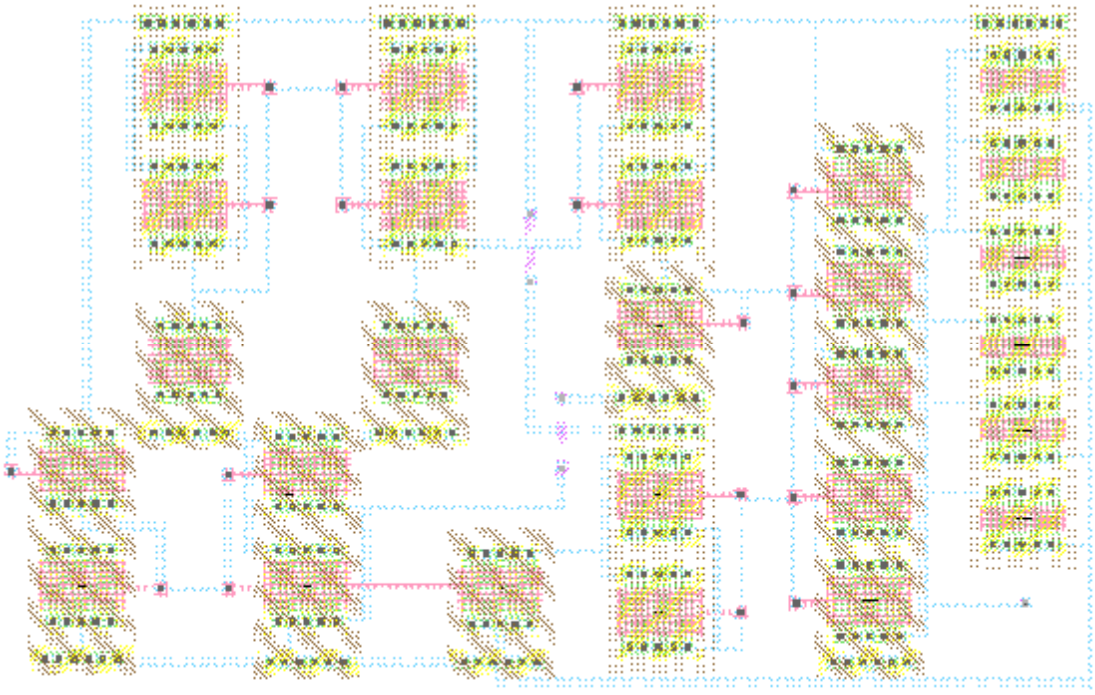

Figure 3.77. Layout of the OPAMP

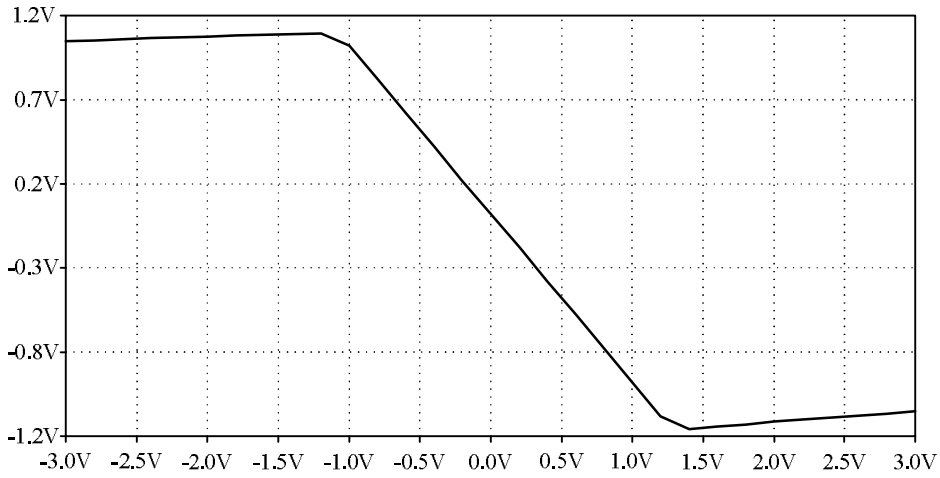

Figure 3.78. Voltage Transfer Characteristic of OPAMP

Frequency response of the OPAMP is illustrated in Figure 3.79.

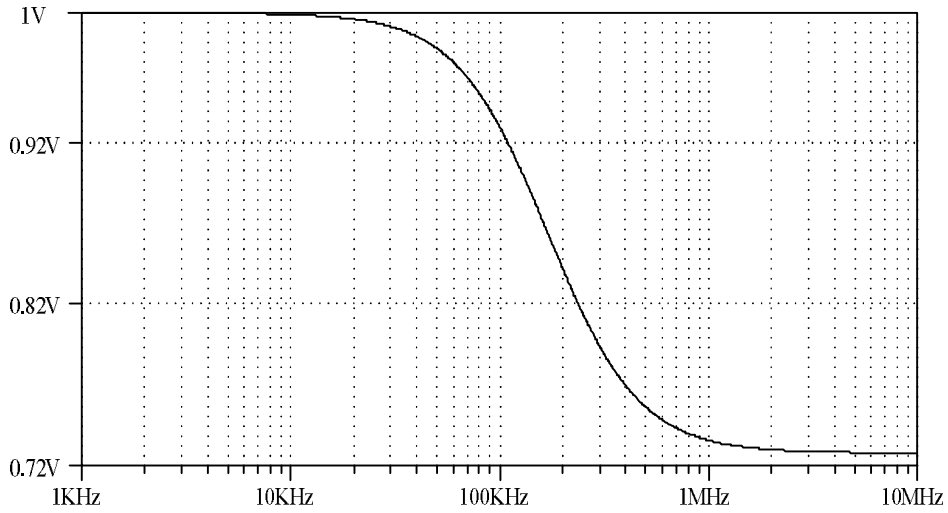

Figure 3.79. Frequency Response of OPAMP

Table 3.7. (W/L) ratios of MOS transistors

Device	W/L(µm)
M_1,M_2,M_{11}	15/2
M_3,M_4,M_7	70/5
M_5,M_8	15/5
M_6	30/5
M_9	150/2
M_{10}	300/2
M_{12}	30/2

3.7. Training of Neural Network

ANNs are typically thought of as black boxes trained to a specific task on a large number of data sets. The ANN training algorithm reads the input and output values in the training data set and makes changes to the weight values to reduce the difference between the predicted output and target output values.

There are three approaches to train neural network hardware. These are offline, online and chip-in-the-loop training. Taking into account all three implementations, the minimal size hardware implementation seems to be offline learning implementation. Using the first implementation approach, if the model of the hardware analog neural network perfectly matches the real neural network, this implementation will be the superior one. An almost perfectly matching model can be the SPICE model of the analog network. MATLAB software can easily be used for training as well.

The back propagation algorithm based on gradient descent, algorithm is used for the training of the proposed neural network (Rumelhart et al., 1986). Main aim of this work is designing a neural network controller for batch production sensor. Proposed controller is an application specific system not a general purpose controller. In this work offline learning technique is the best selection.

3.8. Evaluation of Proposed Analog Neural Network

It is possible to construct a multilayer feed forward neural network implementation using multiplier and activation function circuits. Figure 3.80 shows two inputs, two hidden unit, one output feed forward VLSI neural network for XOR realization. A neural network with weights appropriately chosen to implement the XOR function is illustrated in Figure 3.80. The inputs and the weight values for the network and neuron outputs are chosen to [0, 1] V.

Weight and bias values for the actual circuit is given in

Table 3.8. A LTSPICE simulation was done on the actual circuit using these weight and bias values and the outputs were seen to be correct XOR outputs.

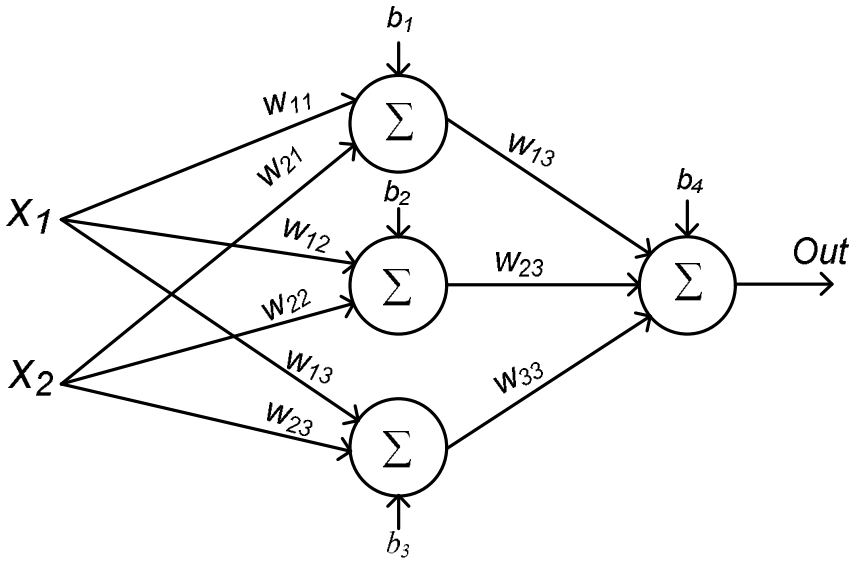

Figure 3.80. Neural Network for implementing XOR

Table 3.8. Synaptic weights and biases of XOR implementation

Hidden Layer				Hidden to Output Layer			
w11	-0,443	b1	2,954	w13	-0,312	b4	0,222
w21	0,3975						
w31	0,5049	b2	-4,374	W23	-0,586		
w41	0,3239						
w51	-0,581	b3	1,336	W33	-0,770		
w61	-0,185						

A VLSI implementation of neural network for XOR is illustrated. Analog multipliers and digital weight storage are used. The neural network is able to accept digital inputs and provide analog outputs. Analog neural network circuitry is trained off-line. A gradient descent learning algorithm is used to train neural network on two input XOR gate. Good training results were shown for training of two inputs, one hidden layer and one output analog neural network. Many of sub circuits and techniques are borrowed from pervious designs, but overall system architecture

design is novel. SPICE simulation results depicted in Figure 3.81, voltages V(x1) and V(x2) denotes inputs and V(out) denotes output of the XOR.

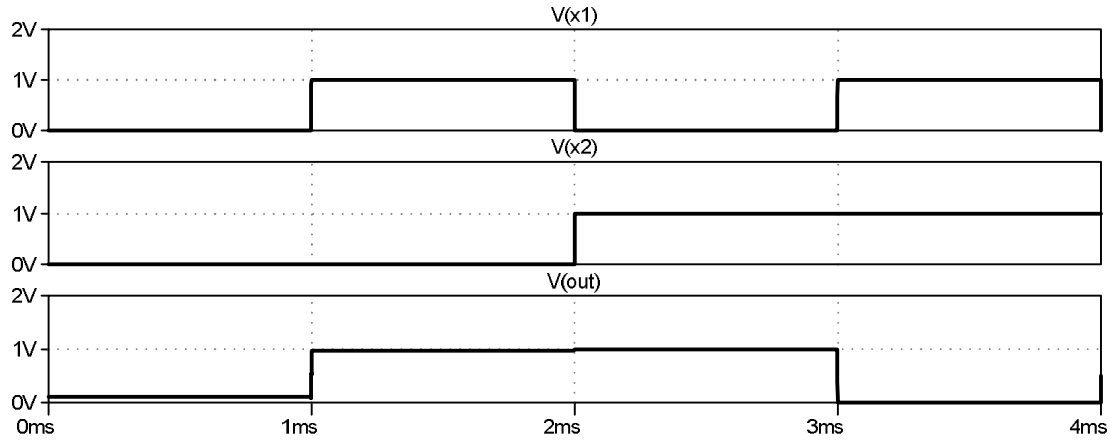

Figure 3.81. XOR approximation of the proposed ANN

3.9. Artificial neural network based MEMS accelerometer

As outlined above, open loop accelerometers have disadvantages such as nonlinear damping and electrostatic force. Analog and digital closed loop accelerometers are proposed to eliminate these nonlinearities. An alternative approach is to employ an ANN based controller that can compensate the nonlinearities of the accelerometer. The current work presents neural network based control method for the MEMS accelerometer.

Sensing element of the proposed accelerometer is the same as the open and conventional closed loop accelerometer. As previously stated, capacitive pick-off block gives conversion of the deflection of the seismic mass into voltage and assumed as simple gain block in SPICE simulations.

Neural network hardware can be implemented using analog or digital systems. Digital neural network implementations necessitate the use of ADC and DAC blocks that use extra chip area and power. Analog circuits can be chosen due to high speed, low power consumption and small chip area. That is reason why analog implementation has been chosen for NNC design.

The proposed NNC consists of one hidden layer with six neurons and one output layer with two neurons. It is fully analog in order to avoid analog-digital

conversions. The number of neurons in the hidden layer has been chosen in order to supply good approximation ability. Figure 3.82 shows the multi layer view of proposed the NNC.

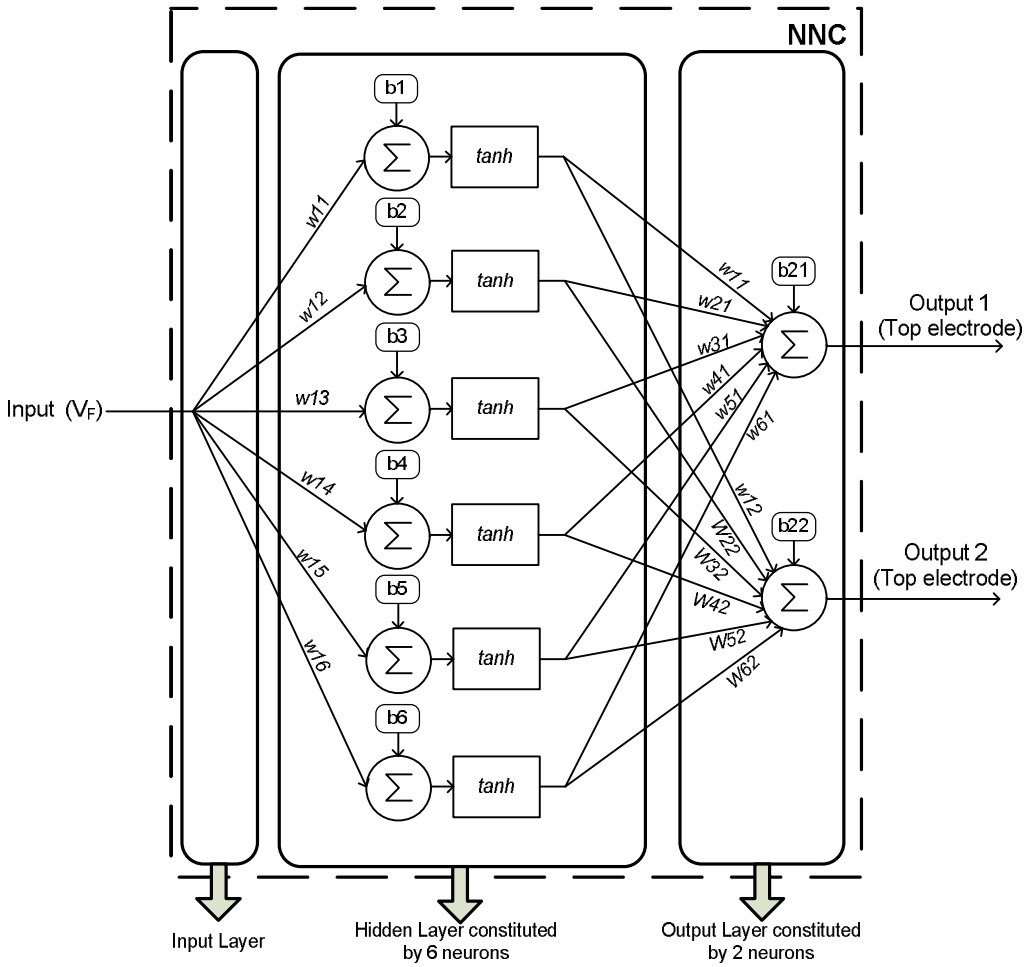

Figure 3.82. MLP structure of the proposed NNC

Number of neurons has been kept as small as possible for simplicity in hardware implementation. The chosen training method is back propagation with simple gradient descent algorithm. Training work is carried out in MATLAB and optimum weight and bias values have been found. The synaptic weight and bias values for the proposed NNC are given Table 3.9.

Table 3.9. Synaptic weights and biases of NNC

Input to Hidden Layer			
w_{11}	-0,144	b_1	-0,780
w_{21}	0,506	b_2	0,034
w_{31}	1,000	b_3	0,019
w_{41}	-1,000	b_4	0,020
w_{51}	0,506	b_5	-0,033
w_{61}	-0,144	b_6	0,780

Hidden to Output Layer			
w_{11}	-0,005	b1	0,597
W_{21}	0,223		
W_{31}	0,234		
W_{41}	0,242		
W_{51}	-0,233		
W_{61}	0,045		

Hidden to Output Layer			
W_{12}	0,045	b_2	0,597
W_{22}	0,233		
W_{32}	0,242		
W_{42}	0,235		
W_{52}	0,223		
W_{62}	0,005		

In this section it is intended to show a neural network based nonlinear controller. Proposed NNC is designed with AMI C5N 0.6µm technology in MOS transistor level. Subcomponents of the proposed NNC are given previous chapter. SPICE model of the neural network based MEMS accelerometer is depicted in Figure 3.83.

Input of the NNC is directly connected to the capacitive pick-off block and output is connected to OPAMP amplifiers. Hardware implementation of the ANN has some limitations such as range of the multipliers and AFs, for this reason, neural calculations are realized in [-1 +1] V. Range of electrode voltages are [0, 5] V, in order to maintain electrode voltages, output of the NNC has to be widened by de-normalize block. Such block consists of simple OPAMP circuit with voltage gain of 5. AF block of the hidden layer is *tanh* and detailed modeling is given in previous section.

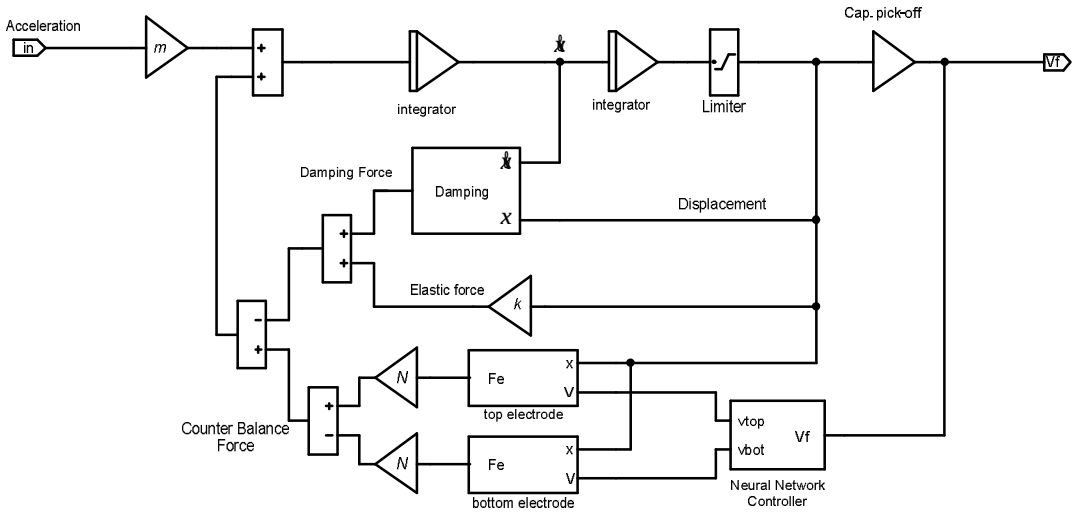

Figure 3.83. SPICE model of the ANN based accelerometer

In this section the hardware design of the proposed NNC is described. Such controller consists of one input one output neuron circuit, AF circuit and six input one output neuron circuit. Block diagram of the one input neuron is depicted in Figure 3.84. Role of the neuron model amplify the input the proportional to the respective weight value and add bias value, and to apply nonlinear AF to the processed signal. Thus a neuron circuit should consist of an analog multiplier and analog adder and activation function. The neuron is identical to one of six designed in parallel in the neural network. It is composed by multiplier cell followed by adder.

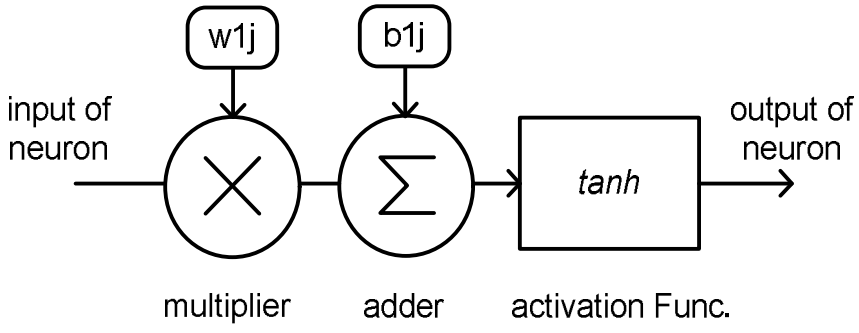

Figure 3.84. Functional blocks of a neuron

Electronic circuit simulations have been achieved with LTSPICE software. SPICE blocks of the one input one output neuron is illustrated in Figure 3.85. Multiplication range of the proposed multiplier is [-1, 1] V however, MATLAB training program generates weight values in range of 10. Therefore, a summing amplifier circuit is designed with gain factor of to 10. Proposed neuron consists of four quadrant multiplier (Liu, 1994). Such multiplier has been chosen for its simplicity and it ability to accepting single ended voltages as input.

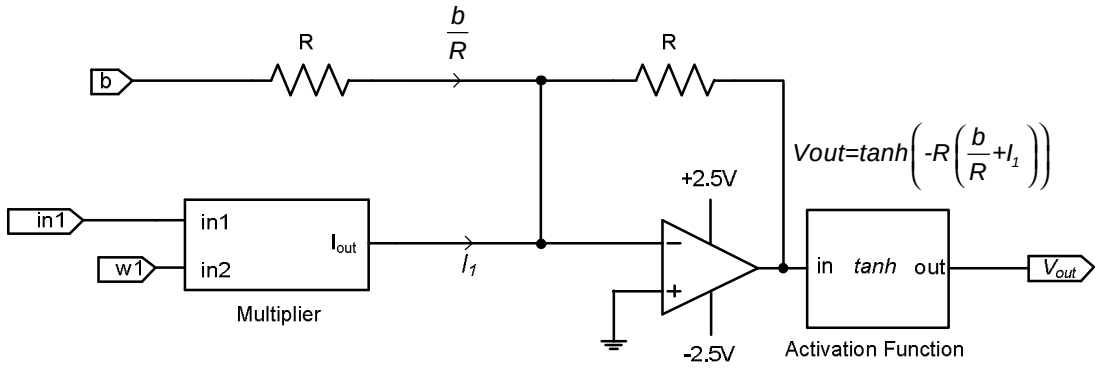

Figure 3.85. One input one output neuron circuitry

Construction of the output layer neurons is similar to the hidden layer neurons. SPICE blocks of the six input and one output neuron without AF is illustrated in Figure 3.86. The neuron is identical to one of two designed in parallel in the neural network.

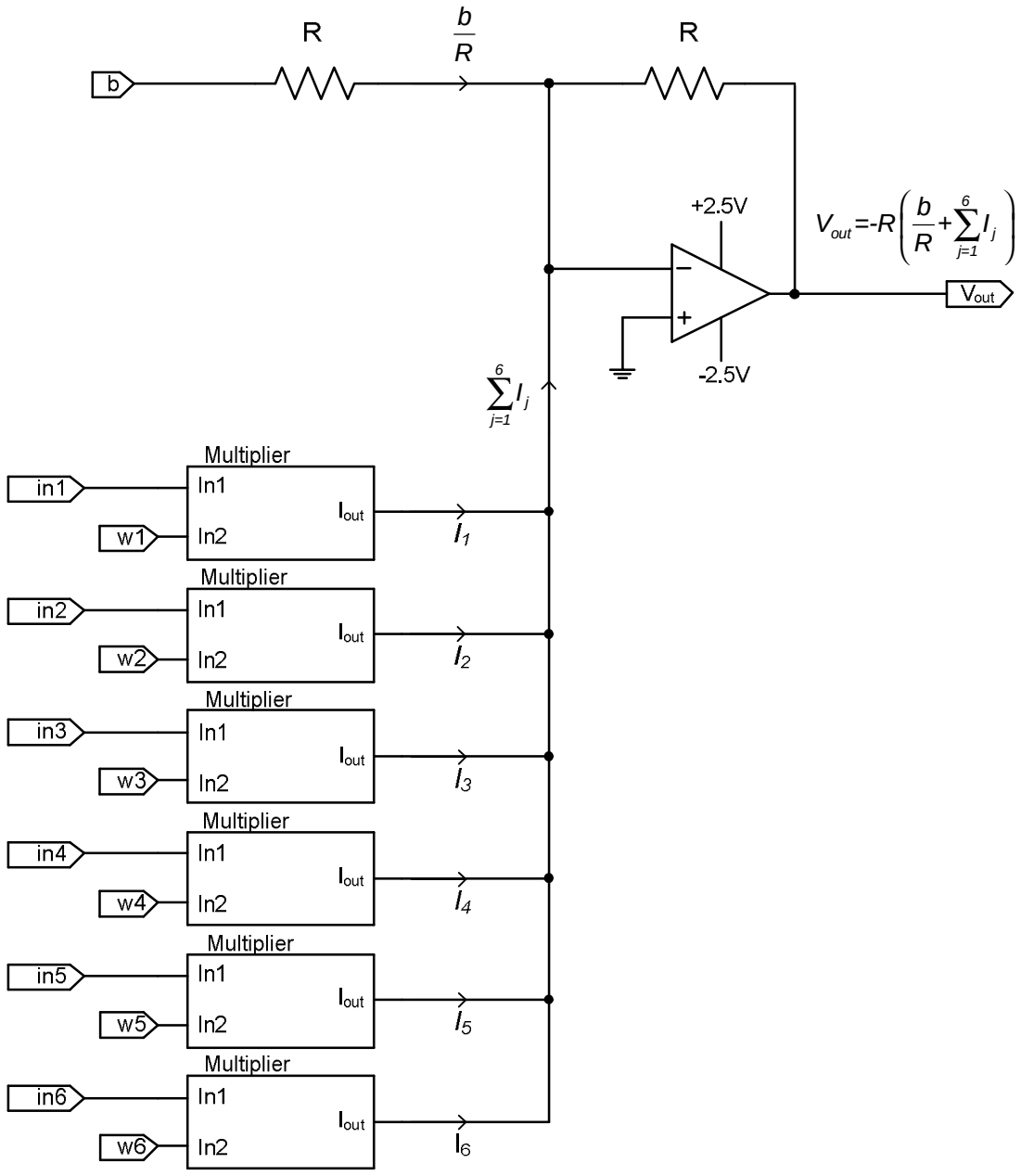

Figure 3.86. Six input one output neuron circuitry

4. RESULTS AND DISCUSSIONS

The main aim of the thesis is to design a neural network controller for MEMS accelerometer. Neural network training is the major problem during design of NNC. For this purpose, a fuzzy logic system is designed. The fuzzy system achieves the generating proper electrode voltages to eliminate nonlinear effects of electrostatic feedback force. This fuzzy system is also used for obtaining training data set of proposed analog neural network. Data of the nonlinear input output relation of fuzzy system is utilized for training of neural network controller in manner supervised learning. Designing and learning processes of the NNC is implemented in MATLAB environment where realization and testing of the NNC is done in SPICE environment.

Developed analog controller is using analog neural network hardware for capacitive MEMS accelerometer. It consists of multipliers, tangent hyperbolic activation functions and memory units. These blocks are simulated together with mechanical MEMS element in SPICE environment. All of proposed blocks are designed in transistor level with AMI C5N 0.6μm technology parameters. Performance of the each component of analog neural network hardware is given Chapter 3. Analog neural network hardware is designed for one input and two output topology. Input of proposed controller is displacement of seismic mass and outputs are required electrode voltages to control. Such neural network consists of one hidden layer with 6 hidden neurons.

The neural network implementation is chosen due to its compatibility in design and implementation with IC technology. Proposed NNC can be designed and implemented with same die area of MEMS part. MEMS accelerometers are controlled by voltage excitation to their electrodes. Proposed NNC exerts excitation voltage only one electrode at a time, the other one is grounded. Applied voltages to the electrodes eliminate the nonlinear effects of electrostatic characteristics. Proposed NNC minimizes the displacement of seismic mass from its rest position.

4.1. Simulation Results

As previously mentioned in chapter 3, simulations of the open, closed and proposed accelerometer have been performed in LTSPICE environment. Sine shaped acceleration signals with frequency of 40Hz applied to open loop accelerometer model and result are depicted in Figure 4.1. Nonlinear effects of the system can be easily noticed on this case. Displacement of the seismic mass is like a sine wave for smaller magnitudes, however for larger magnitudes it gets slightly deformed.

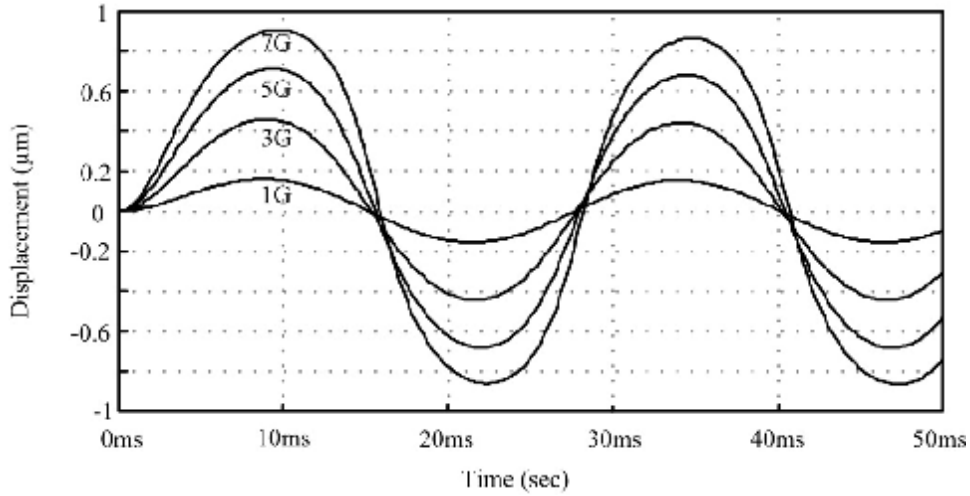

Figure 4.1. Response of conventional analog accelerometer

Simulation of the open loop accelerometer shows that such accelerometer can work linearly in ±3g range. Nonlinear effects of the damping and electrostatic force increases with deflection of the seismic mass. Limited performance of the open loop accelerometer shows that designing of a closed loop system is not a trivial task. To obtain higher range from same accelerometer, it is necessary to closing its loop and limiting the displacement of the seismic mass.

Comparative simulations have been made for a conventional and the proposed accelerometer. PID gain settings are K_P=-6, K_I=-0.6 and K_D=0 and a bias voltage V_B is set to 12V. Normalized transfer characteristic of the two accelerometers over the ±38g range depicted in Figure 4.2. The responses due to the proposed and PID controller are depicted with solid and dotted curves, respectively.

It can be seen from figures that dynamic range of the proposed accelerometer is wider than conventional one. Also hysteresis effect is almost eliminated. NNC shows a better performance in the response specification as compared to the PID controller.

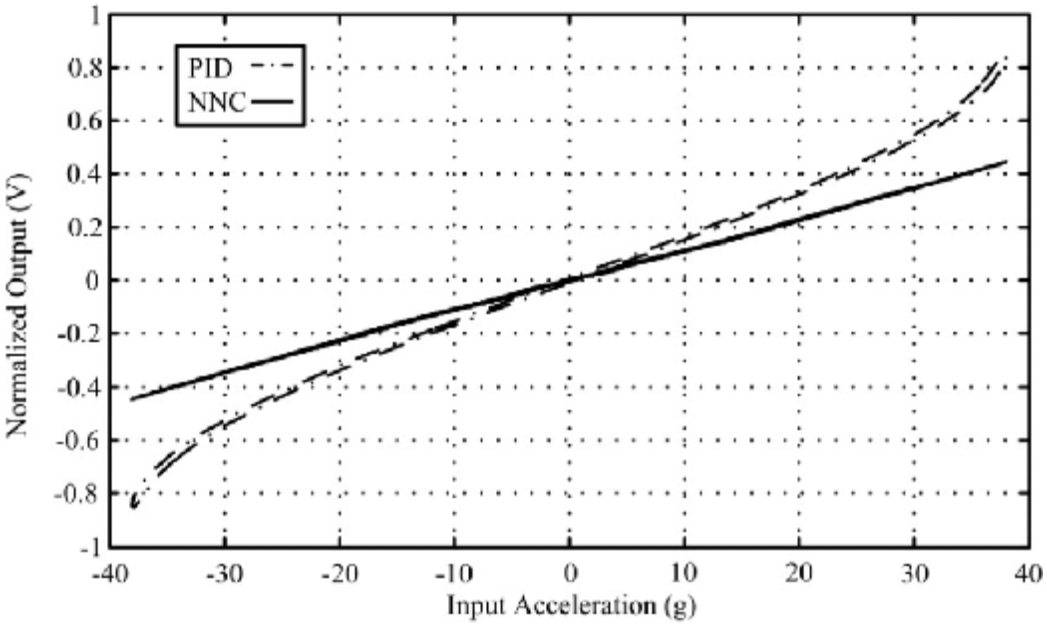

Figure 4.2. Transfer characteristics of the PID and NN based accelerometers

Normalized responses of conventional (dashed line) and proposed accelerometers (solid line) to the step shaped accelerations are depicted in Figure 4.3. According to given figure, the proposed controller has faster than in settling time response in comparison with the PID controller.

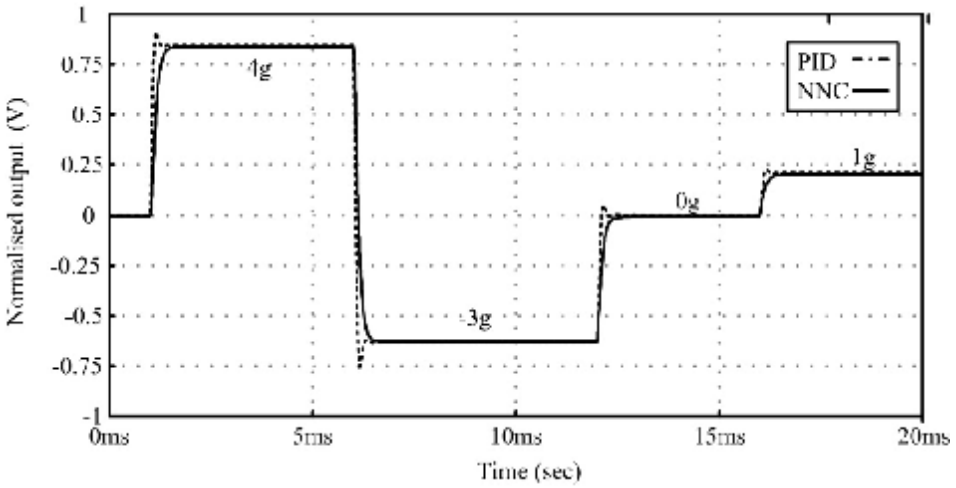

Figure 4.3. Response to the step shaped acceleration

Responses of the open and closed loop accelerometers are depicted in this section. When open loop and closed loop cases of the accelerometer are compared, it can be easily seen that response of the close loop is much faster than open loop. From the results of the closed loop cases one can easily notice that output is much closer to the input acceleration. Table 4.1 compares the performance of closed loop controllers. Settling time of the conventional closed loop and neural network based accelerometers are 0.5ms and 0.25ms respectively. The NNC is producing zero steady state error.

Table 4.1. Comparisons between PID and NNC

Controller	Overshoot	Rise Time	Setting Time
PID	6.8%	0.1ms	0.5ms
NNC	0	0.2ms	0.25ms

When closed loop cases of the accelerometer are compared to each other, the proposed controller has smooth, non-oscillatory transient response without overshoot. Conventional and proposed controllers are compared with several criteria, such as response time, linearity and range. Results shows performance of the proposed NN based controller is better than conventional accelerometers.

5. CONCLUSIONS

This work focused on the design of a neural network based active control system to improve linearity of MEMS accelerometer. More importantly, it reduces the displacement of the seismic mass to reduce nonlinear effects. Simulation results have demonstrated the effectiveness of the proposed approach for improving range of accelerometer. Results also show that response of the proposed controller is better than conventional one.

Proposed controller is fully analog and it eliminates the need of the digital to analog conversion. Proposed neural network uses analog synapses and neurons with a digital weight bus. The neural network is trained with off line data. The weights and biases are stored digitally in FGMOS memory. In order to realize such controller, a fuzzy logic system is designed to generate proper electrode voltages to eliminate nonlinear electrostatic force effect. Fuzzy logic needs heavy computation burden to translate the fuzzy rules to a control action. In this way neural network is utilized to approximate control surface of the fuzzy logic system through a training process. All the simulations indicated that the best results are obtained by the proposed fuzzy logic system and neural network system.

There are various analog implementation examples of neural network in literature. These examples show that neural networks are well suitable systems for analog VLSI implementation from its analog nature. Finally, according to simulation results the best of control of capacitive MEMS accelerometer is obtained with the proposed analog neural network controller. According to the author's knowledge, the analog ASIC implementation for the MEMS accelerometer is reported for the first time with this work.

REFERENCES

ACAR C., SHKEL A. 2003. Experimental evaluation and comparative analysis of commercial variable-capacitance MEMS accelerometers. Journal of Micromechanics and Microengineering , vol. 13, no. 634.

AL-RUWAIHI K. 1997. CMOS analogue neurone circuit with programmable activation functions utilising MOS transistors with optimised process/device parameters. Circuits, Devices and Systems , vol. 144 no. 6, pp. 318-322.

AL-RUWAIHI K., QAMBER I. 1999. Novel behavioral macromodeling using SPICE and its applications to high-voltage engineering education. Computer Applications in Engineering Education , vol. 7, no. 3, pp. 155-161.

ANALOG DEVICES. 1996. Analog Devices: http://www.analog.com/en/obsolete/adxl05/products/product.html

BAO M. 2005. Analysis and Design Principles of MEMS Devices. Shanghai: Elsevier.

BAO M., Yang H. 2007. Squeeze film air damping in MEMS. Sensors and Actuators A: Physical , vol. 136, no. 1, pp. 3-27.

BARSOUM N. 2000. Artificial neuron controller for DC drive. IEEE Power Engineering Society Winter Meeting, pp. 398-401. Singapure.

BAYRAKTAROGLU I. S. 1999. ANNSyS: an Analog Neural Network Synthesis System. Neural Networks , vol. 12, no. 2, pp. 325-338.

BEEBY S., ENSELL G., KRAFT M., & WHITE, N. 2004. MEMS mechanical sensors. Artech House.

BOSER B., HOWE R. 2002. Surface micromachined accelerometers. IEEE Journal of Solid-State Circuits , vol. 31, no. 3, pp. 366-375.

BRYZEK J., ROUNDY S., BIRCUMSHAW B., CHUNG C., CASTELLINO K., STETTER, J. 2006. Marvelous MEMS. IEEE Circuits and Devices Magazine , vol. 22, no. 2, pp. 8-28.

BUCH P., NARAYAN A., NEWTON A., SANGIOVANNI-VINCENTELLI, A. 1997. Logic synthesis for large pass transistor circuits. IEEE/ACM International Conference on Computer-Aided Design, pp. 663-670. San Jose.

BUJA G., TODESCO F. 1994. Neural network implementation of a fuzzy logic controller. IEEE Transactions on industrial electronics , vol. 41, no. 6, pp. 663-665.

CHARLOT B., MIR S., PARRAIN F., COURTOIS B. 2001. Generation of electrically induced stimuli for MEMS self-test. Journal of Electronic Testing , vol. 17, no.6, pp. 459-470.

CHEN G. A. 2001. Introduction to fuzzy sets, fuzzy logic, and fuzzy control systems. CRC Press.

CHOWDHURY S., AHMADI M., MILLER W. 2005. A closed-form model for the pull-in voltage of electrostatically actuated cantilever beams. Journal of Micromechanics and Microengineering , vol.15, pp.756.

CHU, P., PISTER S. 1994. Analysis of closed-loop control of parallel-plate electrostaticmicrogrippers. IEEE International Conference on Robotics and Automation, 1, pp. 820-825. San Diego.

COLINET E., JUILLARD J., NICU L., BERGAUD C. 2005. Digital self-calibration method for MEMS sensors. IEEE Transactions on Instrumentation and Measurement , vol. 54, no. 4, pp. 1438-1443.

CORTÉS-PÉREZ A., HERRERA-MAY A., AGUILERA-CORTÉS L., GONZÁLEZ-PALACIOS M., TORRES-CISNEROS M. 2010. Performance optimization and mechanical modeling of uniaxial piezoresistive microaccelerometers. Microsystem Technologies , vol. 16, no.10.

DIORIO C., HASLER P., MINCH A., MEAD, C. 1996. A single-transistor silicon synapse. IEEE Transactions on Electron Devices , vol. 43, no.11, pp. 1972-1980.

DIORIO C., HASLER P., MINCH B., MEAD C. 1997. A complementary pair of four-terminal silicon synapses. Analog Integrated Circuits and Signal Processing , vol. 13, no. 1, pp. 153-166.

FUJITA H. 2007. Two decades of MEMS from surprise to enterprise. IEEE 20th International Conference on Micro Electro Mechanical Systems, pp. 1-6.

FUTANE N., CHOWDHURY S., CHOWDHURY C., SAHA, H. 2010. ANN based CMOS ASIC design for improved temperature-drift compensation of piezoresistive micro-machined high resolution pressure sensor. Microelectronics Reliability , vol. 50, no.2, pp. 282-291.

GAURA E. 2000. Neural network techniques for the control and identification of acceleration sensors. Coventory University .

GAURA E. 2001. Neural-network compensation methods for capacitive micromachined accelerometers for use in telecare medicine. IEEE Trans. on Information Technology in Biomedicine , vol. 5, no. 3, pp. 248-252.

GAURA E., KRAFT, M. 2002. Are neural network techniques the solution to measurement validation, monitoring and automatic diagnosis of sensor faults? Proceedings of the 41st SICE Annual Conference, pp. 2052-2057. Osaka.

GAURA E., RIDER R., STEELE N. 2000. Closed-loop neural network controlled accelerometer. Proceedings of the Institution of Mechanical Engineers, Part I: Journal of Systems and Control Engineering, pp. 129-138.

GIBSON D., PURDY C. 1999. Extracting behavioral data from physical descriptions of MEMS for simulation. The Journal of VLSI Signal Processing , vol. 22, no. 2.

GIBSON D., PURDY C., HARE A., BEYETTE F. 1999. Design automation of MEMS systems using behavioral modeling. Ninth Great Lakes Symposium on VLSI, pp. 266-269.

HASSANI F. P. 2010. Design of a smart MEMS accelerometer using nonlinear control principles. Smart Structures and Systems , vol. 6, no.1, pp. 1-16.

HAYKIN S. 2006. Neural networks: a comprehensive foundation. NJ: Prentice Hall.

HOLLER M., TAM S., CASTRO H., BENSON R. 1989. An electrically trainable artificial neural network (ETANN) with 10240 `floating gate' synapses. International Joint Conference on Neural Networks, 2, pp. 191-196. Washington, DC.

HOLLIS P., PAULOS J. 1990. Artificial neural networks using MOS analog multipliers. IEEE Journal of Solid-State Circuits , vol. 25, no.3, pp. 849-855.

HOLLOCHER D., MEMISHIAN, J. 2003. Patent No. 6530275. United States.

HORSLEY D., HOROWITZ R., PISANO, A. 1998. Microfabricated electrostatic actuators for hard disk drives. IEEE/ASME transactions on mechatronics, pp. 175-183.

HUNG E., SENTURIA S. 1999. Extending the travel range of analog-tuned electrostatic actuators. Journal of Microelectromechanical Systems , vol. 8, no. 4.

IBRAHIM A. 2004. Fuzzy logic for embedded systems applications. Newnes.

IEEE. 2007. IEEE Standard for Inertial Sensor Terminology. IEEE.

JUDY J. 2001. Microelectromechanical systems (MEMS): fabrication, design and applications. Smart materials and Structures , vol.10, pp.1115.

KAHNG K., SZE S. 1967. A floating gate and its application to memory devices. IEEE Transactions on Electron Devices , vol. 14, no. 9, pp. 629-629 .

KESILMIS Z., AVCI M., AKSOY M. 2006. Yüzen geçit MOS transistorlarda parametrik saçılma analizi. ELECO 2006. Bursa.

KORVINK J., PAUL O. 2006. MEMS: a practical guide to design, analysis, and applications. Norwich: William Andrew.

KRAFT M. 1997. Closed loop digital accelerometer employing oversampling conversion. Coventry University.

KRAFT M. 2000. Micromachined inertial sensors: state-of-the-art and a look into the future. Measurement and Control , vol. 33, no. 6, pp. 164-168.

KRAFT M., Lewis C. 1998. System level simulation of a digital accelerometer. Proceedings of the 1st International Conference on Modeling and

Simulation of Microsystems, Semiconductors, Sensors and Actuators, pp. 267-272, Santa Clara.

KRAFT M., LEWIS C. P., HESKETH, T. 1998. Closed-loop silicon accelerometers. IEE Proceedings-Circuits Devices and Systems , vol. 145 no. 5, pp. 325-331.

KUMAR M. 2010. MEMS:Theory and Usage in Industrial and Consumer Applications. National Conference on Computational Instrumentation, pp. 1-6, Chandigarh, INDIA.

KUMAR N., SADASIVAM V., SUKRIYA H. 2008. A Comparative Study of PI, Fuzzy, and ANN Controllers for Chopper-fed DC Drive with Embedded Systems Approach. Electric Power Components and Systems , vol. 36, no. 7, pp. 680-695.

KUMAR N., SADASIVAM V., SUKRIYA H., BALAKRISHNAN S. 2008. Design of low cost universal artificial neuron controller for chopper fed embedded DC drives. Applied Soft Computing , vol. 8, no. 4, pp. 1637-1642.

LEE C. 1990. Fuzzy logic in control systems: Fuzzy logic controller-part I. IEEE Transactions on systems, man, and cybernetics , vol. 20, no. 2, pp. 404-418.

LEHMANN T. 1994. Hardware Learning in analogue VLSI Neural NEtworks. Ph.D Thesis . Technical University of Denmark.

LEWIS C., KRAFT M. 1996. Simulation of a micromachined digital accelerometer in SIMULINK and PSPICE. UKACC International Conference on Control '96, pp. 205-209.

LIU S. H. 1994. CMOS four-quadrant multiplier using bias feedback techniques. IEEE Journal of Solid-State Circuits , vol. 29, no. 6, pp. 750-752.

LO N., BERG, E., QUAKKELAAR S., SIMON J., TACHIKI M., LEE H. (1996). Parameterized layout synthesis, extraction, and SPICE simulation for MEMS. IEEE International Symposium on Circuits and Systems, 4, pp. 481-484, Atlanta.

LU C., LEMKIN, M., BOSER, E. 1995. A monolithic surface micromachined accelerometer with digital output. IEEE journal of solid-state circuits , vol. 30, no. 12, pp. 1367-1373 .

LU L., WU C. 1994. The design of the CMOS current-mode general purpose analog processor. IEEE International Symposium on Circuits and Systems, 5, pp. 549 - 552. London.

MALUF, N., WILLIAMS, K. 2004. An introduction to micromechanical System engineering. Artech House.

MARCO S., SAMITIER, J., RUIZ O., HERMS A., MORANTE J. 1993. Analysis of electrostatic-damped piezoresistive silicon accelerometers. Sensors and Actuators A: Physical ,vol. 37, no. 1, pp. 317-322.

MCCULLOCH W., PITTS W. 1943. A logical calculus of the ideas immanent in nervous activity. Bulletin of Mathematical Biology , vol. 5, no. 4, pp. 115-133.

MEMSIC. 2011. MEMSIC . http://www.memsic.com

MENDEL J. 1995. Fuzzy logic systems for engineering: a tutorial. Proceedings of IEEE , vol. 83, no. 3, pp.345-377.

NAMIN A., LEBOEUF K., MUSCEDERE R., WU H., AHMADI M. 2009. Efficient hardware implementation of the hyperbolic tangent sigmoid function. IEEE International Symposium on Circuits and Systems, pp. 2117-2120. Taipei .

NASCIMENTO JR C. 1994. Artificial neural networks in control and optimization. PhD thesis Manchester UK: Faculty of Technology, University of Manchester , pp. 8-9.

OTA Y., WILAMOWSKI, B. 1994. VLSI Implementation of a Programmable Current-Mode Neural Network. Intelligent engineering systems through artificial neural networks: proceedings of the Artificial Neural Networks in Engineering Conference, pp. 13-16. Missouri.

PARRI J., RATTI S. 2009. Trigonometric function approximation neural network based coprocessor. Microsystems and Nanoelectronics Research Conference, pp. 148-151. Ottawa.

PAVAN P., LARCHER L. 2004. Floating gate devices: operation and compact modeling. Kluwer.

PAYAM A. H. 2007. Design of a hybrid closed loop control system for a MEMS accelerometer using backstepping principle. Internatonal Conference on Microelectronics, pp. 213-216. Cairo.

PHAN K., MAURITZ, A., HOMBURG F. 2008. A novel elastomer-based magnetoresistive accelerometer. Sensors and Actuators A: Physical , vol. 145, pp.109-115.

PIYABONGKARN D. S. 2005. Travel range extension of a MEMS electrostatic microactuator. IEEE Transactions on Control Systems Technology , vol. 13, no. 1, pp. 138-145.

RAO D., SARAF S. 1996. Study of defuzzification methods of fuzzy logic controller for speed control of a dc motor. International Conference on Power Electronics, Drives and Energy Systems for Industrial Growth pp. 782-787, New Delhi , India : IEEE.

ROJAS R. (1996). Neural networks: a systematic introduction. Berlin: Springer.

ROYLANCE L., ANGELL J. 1979. A batch-fabricated silicon accelerometer. IEEE Transactions on Electron Devices , vol. 26, no. 12.

RUMELHART D., HINTON G., WILLIAMS, R. 1986. Learning representations by back-propagating errors. nature , vol. 323, no. 9, pp.534-536.

SAILE V., WALLRABE U. 2009. LIGA and its applications. Wiley.

SARANGAPANI J. 2006. Neural network control of nonlinear discrete-time systems. Taylor&Francis.

SAWIGUN C., MAHATTANAKUL, J. 2006. A low-voltage CMOS linear transconductor suitable for analog multiplier application. IEEE International Symposium on Circuits and Systems, pp.1543-1546. Island of Kos.

SINENCIO E. 2010. http://amesp02.tamu.edu/~sanchez/

SPANGLER C., KEMP C. 1996. A smart automotive accelerometer with on-chip airbag deployment circuits. Tech. Dig. Solid-State Sensors and Actuator Workshop, pp. 221-214, Hilton Head Island.

T.L. GRIGORIE. 2008. The Matlab/Simulink modeling and numerical simulation of an analogue capacitive micro-accelerometer. Part 1: Open loop. International Conference on Perspective Technologies and Methods in MEMS Design, pp. 105-114. Polyana.

T.L. GRIGORIE. 2008. The Matlab/Simulink modeling and numerical simulation of an analogue capacitive micro-accelerometer. Part 2: Closed loop. International Conference on Perspective Technologies and Methods in MEMS Design, pp. 115-121. Polyana.

TANAKA M. 2007. An industrial and applied review of new MEMS devices features. Microelectronic Engineering , vol. 84, no. 5, pp. 1341-1344.

THOMSEN A., BROOKE M. 1991. A floating-gate MOSFET with tunneling injector fabricated using a standard double-polysilicon CMOS process. Electron Device Letters , vol. 12, no. 3, pp.111-113.

TI. 2005. Accelerometers and how they work. http://www2.usfirst.org/2005comp/Manuals/Acceler1.pdf

VERPLAETSE C. 1996. Inertial proprioceptive devices: Self-motion-sensing toys and tools. IBM Systems Journal , vol. 35, no. 3, pp. 639-650.

WICHT H., BOUCHAUD J. 2005. NEXUS market analysis for MEMS and microsystems III. International newsletter on micro-nano integration , pp. 33-35.

WILAMOWSKI B. B. 2000. VLSI Implementation of Neural Networks. International Journal of Neural Systems, vol. 10, pp. 91-198. Singapore, Teaneck.

YAZDI N. A. 1998. Micromachined inertial sensors. Proceedings of the IEEE , vol. 86, no. 8, pp. 1640-1659.

YI Y. S., CHUNG M. J. 1994. Stability analysis of a fuzzy logic controller for an uncertain dynamic system. IEEE World Congress on Computational Intelligence, pp. 1028-1034. Orlando.

YIN L., LIU X., CHEN W., ZHOU Z. 2011. High resolution interface circuit for closed-loop accelerometer. Journal of Semiconductors , vol. 32, no. 4, pp.1-8.

ZHANG G. 1998. Design and Simulation of A CMOS-MEMS Accelerometer. Carnegie Mellon University.

ZHAO S., ZHOU Q., HOU C., BAI J., YANG G. 2010. A compact micromachined interferometric accelerometer based on the diffraction grating. Advanced Sensor Systems and Applications IV, pp.7853.

ZUMBAHLEN H. 2008. Linear circuit design handbook. Elsevier.

CIRRICULUM VITAE

Zehan KESİLMİŞ received the B.S. degree in Electrical and Electronics Engineering from Sakarya University in 2001 and the M.S. degree in 2004 from Çukurova University, in the field of Electrical-Electronics Engineering. His Master thesis title is "Utilizing ultrasonic in dying process" supervised by Asst. Prof Murat AKSOY. He has worked in several research projects supported by Scientific and Technical Council of Turkey. His research areas are VLSI design, neural network and implementation, embedded system design. He is a member of Turkish Chamber of Electrical Engineers. He is currently working as a research assistant in Department of Electrical Electronics Engineering at Çukurova University.